MODELING THE CREEP BEHAVIOR OF TORSIONAL SPRINGS

by

Ajith Ramesh

A dissertation submitted to the faculty of
The University of North Carolina at Charlotte
in partial fulfillment of the requirements
for the degree of Doctor of Philosophy in
Mechanical Engineering

Charlotte

2009

Approved by:

_____
Dr. Kingshuk Bose

_____
Dr. Kevin Lawton

_____
Dr. David Boyajian

_____
Dr. Shen-En Chen

ABSTRACT

AJITH RAMESH: Modeling the creep behavior of torsional springs
(Under the direction of DR. KINGSHUK BOSE and DR. KEVIN LAWTON)

This dissertation presents a detailed model of the 'overall' behavior of Torsional springs. Torsional springs (also called 'Clock' springs) are a kind of spiral springs which are supposed to provide a certain torque when wound-up to a certain rotation. However, it is observed that the moments that are developed relax when the springs are kept loaded over long periods of time. The research presented here is an attempt to investigate this behavior by identifying the role played by the various influencing parameters.

The dissertation focuses on the development of a detailed component-level finite element model to investigate the instantaneous moment-rotation response as well as the long-term (time-dependant) structural response of a torsional spring. Torsional springs belong to a class of planar spiral springs that are commonly made out of Elgiloy - an alloy of Cobalt, Chromium, Nickel, and Iron. Elgiloy has very high yield strength, and is commonly used as a spring material in analog clocks. In addition, the research also aims at developing a better understanding of the dependence of the response of the spring on the different design parameters that define its geometry and material properties. Frictional contact, large deformations, and nonlinear material behavior (plasticity and creep) are among the major challenges that need to be resolved in order to obtain a thorough understanding of the problem. The modeling effort also focuses on understanding the experimentally-observed hysteresis associated with a cyclic moment versus rotation response, as well as the development of simple analytical models which can approximately describe the structural response of a typical torsional spring.

DEDICATION

To my loving parents, wife, and daughter

ACKNOWLEDGEMENTS

I would like to thank my graduate advisor, Dr. Kingshuk Bose, for his valuable support and guidance throughout this research work. I would like to extend my special gratitude towards him for motivating me in my graduate studies, and benefitting me with his immense professional knowledge and expertise. I would like to thank my co-advisor, Dr. Kevin Lawton, for giving me an opportunity to participate in this research. He has played a major role in providing me with the important experimental data required for the validation of the finite element results. He and his experimental group have been encouraging factors for the overall progress of the research. I would like to thank Dr. David Boyajian and Dr. Shen-En Chen for serving as the dissertation committee members, and for actively participating in the review of my dissertation.

I would like to thank The Lawrence Livermore National Laboratory for the financial support that they rendered for the smooth functioning of the project. I would like to thank my fellow colleagues at the Department of Mechanical Engineering and Engineering Science at UNC Charlotte, for their extended support and motivation throughout my graduate life at UNC Charlotte.

On a personal level, I would like to mention my family who have always stood by me at difficult times, and encouraged me in successfully completing the research.

INTRODUCTION

Torsional springs are typically used to provide a certain amount of resisting torque at a specified rotation. The research presented here is part of a broader program that also has an experimental component [10] for measuring both the instantaneous and long-term responses of the spring. However, current experimental setups cannot measure the stress relaxation response of the spring over extended service lives--of the order of several years or decades. The experiments measure the creep of the spring under a constant applied load, over a relatively short period of time (of the order of months). Furthermore, a large number of experiments would be needed to gain sufficient insight into certain aspects of the complex spring response, such as the dependence of the spring performance on the coefficients of friction between the various contacting parts of the spring. Numerical modeling can provide some of the critical insights in this regard.

It is assumed that the structural response of the spring mechanism is a strong function of the 'base state' of the spring. By the 'base-state' we refer to the state of residual stresses, plastic strains, contact conditions, etc., that the spring material experiences at the end of the spring forming process (i.e., the process of forming the planar spiral spring from a long strip of elgiloy). In order to capture the base-state, the model first tracks the spring forming process; the details of which are discussed in Chapter 2 of this dissertation.

The actual application of the spring system involves winding up the formed spring so as to generate a certain torque at a specified rotation. The model captures the instantaneous moment-rotation response of the spring during such additional wind-ups. This part of the modeling effort is discussed in Chapter 3 of this dissertation. These

springs are also observed to exhibit significant hysteresis when subjected to rotation-controlled loading and un-loading cycles. Chapter 3 also presents the details of modeling the hysteresis response, and correlating it with the experimentally observed behavior.

An important goal of the research is to understand the long-term relaxation response of the spring system from a pre-loaded (i.e., wound-up) state. This is achieved by allowing the loaded (wound-up) spring to relax over long periods of time, of the order of years or a decade. The stress relaxation manifests itself through a corresponding torque drop which is captured by the finite element model. This part of the modeling effort is discussed in Chapter 4 of this dissertation.

Chapter 5 of this dissertation discusses the development of simple analytical models, based on the principles of Statics and Mechanics of Solids, to describe the relaxation response of the preloaded spring. The results of the earlier sections can be utilized to develop a 'torsional creep law' that describes the structural response of the torsional spring, and can be used in a systems-level model to describe the behavior of such a spring using a limited number of degrees of freedom, instead of the more detailed (and computationally expensive) component-level model developed in the earlier sections.

Based on the experience gained from developing the conceptual finite element model, which is discussed in the chapters 2 to 5, a new model is developed which can predict the instantaneous and long-term responses of the torsional spring with relatively better accuracy. This new model, called the "second generation finite element model", is discussed in Chapter 6. The primary goal of this modeling effort is to address any

plausible discrepancies present in the first generation model, and thereby come up with a more accurate, if not an exact numerical replica of the actual torsional spring system.

TABLE OF CONTENTS

CHAPTER 1: INTRODUCTION TO TORSIONAL SPRINGS

1.1 Background

Finite Element models [13] have been used for a few decades now for solving complex linear and non-linear mechanical problems. Solving such problems would be a relatively easier task if they involve small-scale deformations, and if the material response is linear [16]. However, if the response of the system is highly non-linear [5] due to the influence of various factors such as material non-linearity, geometric non-linearity, and boundary non-linearity; solving such problems would not be an easy task and it would involve tackling a number of complexities. One such complex mechanical system is being studied in this research. It involves the development of an appropriate finite element model which can accurately capture the instantaneous as well as the long term structural responses of a torsional spring (also known as a 'clock' spring), which serves as a major structural component in certain mechanical systems and operates by generating a certain torque at a specified value of rotation.

Torsional springs are planar spiral springs made of Elgiloy - an alloy of Cobalt, Chromium, Nickel, Iron, etc. - having unique mechanical properties [2, 3], which, if harnessed effectively can be used for generating significant torques in mechanical systems. The spring mechanism, illustrated in Figure 1.1 (right), comprises of a flat elgiloy strip (wire), an arbor of radius 1 mm onto which the flat wire is wrapped, and a cup with an inner radius of approximately 2.7 mm which houses the entire assembly. The

flat elgiloy strip is 0.1 mm thick, 1 mm wide and 116 mm long, and has 85% cold-work reduction with an associated yield strength of approximately 240 ksi [10] (≈1655 MPa). Approximately 3.5 mm of the strip is annealed and attached onto the centered arbor (concentric with the cup). During the forming process (which takes the configuration from the one shown on the left side of Figure 1.1 to the one shown on the right side), the arbor is rotated so as to pull the strip into a spiral form inside of the cup. Once the entire length of the strip is pulled inside the cup, its rear end is welded onto the cup, as illustrated in Figure 1.1.

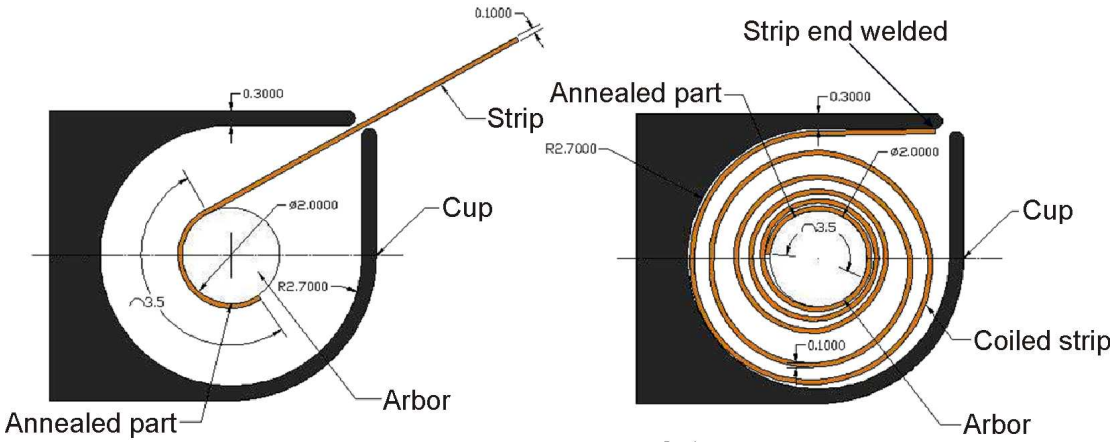

FIGURE 1.1: Schematic of the clock spring assembly before and after spring forming

The springs are required to generate torques of approximately 2.9 ± 0.5 N.mm at 1 revolution, and 4.35 ± 0.55 N.mm at 2.25 revolutions of the arbor.

The material properties of Elgiloy have a key role to play in defining the spring behavior. Elgiloy was originally developed as a spring material for watches and clocks and currently possesses the highest non-magnetic spring characteristics among metallic materials [2]. Table 1.1 (right) shows a comparison of its material properties to that of cold-rolled 302 Stainless Steel. The material has very high yield strength and ultimate

tensile strength, which help in sustaining significantly large deformations of the kind a torsional spring may be subjected to.

TABLE 1.1: Comparison of material properties of Elgiloy with Steel

Materials	Elastic modulus	Poisson's ratio	Yield strength	Ultimate tensile strength
Elgiloy	190 GPa	0.23	1.6 GPa	1.8 GPa
302 Stainless Steel	193 GPa	0.25	1.2 GPa	1.5 GPa

1.2 Related previous work

Remarkably, a literature search has revealed that there is a relatively small amount of recorded work on the finite element modeling of torsional springs. Most of the finite element models [4, 7] that have been developed so far are applicable to springs used in actuation systems for micro-mechanical devices or MEMS. Other published works [8] are confined to the evolution of unique designs for spring systems and/or to experiments to improve the efficiency of actuation. Though spiral springs, having similar geometry as clock springs, do exist, they are made of alloys like steel and are used in motors [7]. Research carried out on the latter has been confined to their manufacturing, and experimental calibration, - for the purpose of bench marking.

Barnes *et al.* [4], at the Sandia National Laboratory developed a new type of surface micro-machined ratcheting actuating system which uses a torsional electrostatic comb drive coupled to an external ring gear through a ratcheting scheme. Low operating voltages (of the order of 18V), minimal rubbing surfaces to reduce friction, and maximized comb finger densities are some of the advantages of this design. This mechanism, known as the 'TRA' or Torsional Ratcheting Actuator, constitutes a large

circular frame which ties the movable banks of the combs together. Four cantilever beams support this frame in its center and act as the frame's spring return. They resist any lateral motion of the frame and allow it only to rotate. The frame is limited to only 2.8º of rotation by stiff spring stops located at its outside edge. The system incorporates two kinds of combs, namely, a stationary kind and a moving one. Actuation is done by applying a periodic voltage signal to the stationary combs. As the voltage signal increases, the torsion frame rotate counter clockwise in response to the electrostatic attraction between the stationary and moving comb fingers. As the frame begins to rotate, the ratchet pawls located along its edge engage the ring gear that surrounds it, with the help of ratchet teeth. The latter is lined along the inside of the ring gear. The ring gear is held to the substrate with the help of four overhanging clips which also constrain it to rotational movement. Any unwanted reverse motion of the gear is prevented by three anti-reverse mechanisms comprising anchored cantilever beams that engage with the ratchet teeth. When the voltage is removed, the central torsion springs force the frame to return to its initial fabricated position, which can be called as the 'spring-back'. During this process, the anti-reverse mechanisms prevent the ratchet pawls from dragging the ring gear along with it. Each of the cantilever beams that make up the torsion springs undergoes an in-plane displacement along with an angular deflection. In addition, as the frame rotates, these individual beams are stretched and thereby they undergo significant linear deformations too. In order to alleviate this strain and generate a linear spring behavior, relief springs were placed at the root of each of the torsion beams. A three-dimensional non-linear finite element analysis was performed to calculate their stiffness due to the complicated spring displacement and geometry involved. The FE model used

was of a single cantilever beam and its strain relief structures. The boundary conditions used were deflection and angle specifications at the free end of the beam and fixed conditions at its base. The total end moment required to deflect the beam to the end conditions was calculated at one degree displacement. Thereby, a torque-deflection relationship was developed for the system. This spring system which was later fabricated and tested was found to agree with the model predictions.

There have been previous research works on spiral springs which are made of metals like steel. They are known as ‘motor springs’ or ‘power springs’. Geometrically they are very similar to clock springs. Carlson [7] discusses such springs which are made of high-carbon, hardened and tempered, cold rolled, or stainless steel. According to their findings, which were corroborated by experiments, they suggest that only for certain ratios of spring length to thickness and/or radius of the arbor to that of the case (or cup); it is possible to accurately compute the relationship between torque and the number of revolutions, for effective actuation. The paper provides bench mark specifications for motor springs with regards to the length to thickness ratio of the strip, material hardness, maximum permissible number of revolutions, ratio of the spring area to that of the case, and the amount of successive winding and unwinding required for controlling torque. The paper also discusses ‘pre-stressed’ motor springs in which the torque is increased by reverse winding that leads to the formation of residual stresses. Such springs can afford to have a larger length-to-thickness ratio, thereby sustaining more number of revolutions before it would reach the tight wound condition. They were found to produce 25 to 50 percent more torque than the regular motor springs. The higher torque capacity, increase in deflection, and fatigue life often justify the increase in the manufacturing cost of such

springs when compared to the regular ones. In both kinds of springs, a large amount of friction was found to be generated, both by the coils rubbing against one another and the spring rubbing against the case. This led to irregularities in torque between the designed values and the actual operating characteristics. Results from the experiments also revealed the fatigue life and torque-deflection characteristics of both the pre-stressed and the regular springs. They were found to exceed about 200,000 cycles when operating at high stresses of the order of 250,000 psi. The results also suggest that reduced stresses can produce longer lives.

Chen *et al.* [8] investigated the spiral profile design of flexure springs. Using analytical techniques and the finite element methods, they showed that the spiral profile is a key factor that can influence the performance of a spring. The involute of a circle, with the Cartesian coordinate system as the basis, was used as the model geometry for the analytical model. A geometrically non-linear static structural analysis was also conducted using the finite element method. Though their work was based on flexure springs and hence, not directly related to the research presented here, their findings still do justify the model geometry of the spring system considered here.

1.2.1 Previous work on elgiloy-based springs

Previous research conducted on elgiloy-based springs focused on measuring the properties of the elgiloy material (including creep) from a material science perspective [2,3] and/or studies conducted on the load relaxation response of elgiloy-based helical coil springs [11]. There is little or no reference in the literature on the mechanical behavior and/or design of torsional springs.

Lawton *et al.* [21] (the experimental group associated with this project) discusses an instrument that they developed for measuring the rotational creep of elgiloy springs. The set-up comprises of two compact linear interferometers which are mounted side by side to measure the displacements of two retro-reflectors (RR). The latter are mounted on a load arm that loads the spiral with the help of hanging masses. The rotational creep of the spring is measured as the ratio of the difference between the linear displacements to the distance between the two beams. The interferometer is considered to be nominally balanced since the distances between the interferometers and the associated retro-reflectors are approximately the same. The principle of operation is as follows: A heterodyne laser source which is part of the set-up generates a beam that is split equally in power by a beam splitter so that half of the beam continues to a mirror and the other half deflects to the first interferometer. The mirror directs its half of the beam to the second interferometer. The beams entering the interferometers are split according to polarizations, by a polarizing beam splitter (PBS). The s-polarization is deflected, which then passes through a quarter-wave plate (QWP), and deflects via the retro-reflector (RR) out to a fiber-optic pickup (FOP). The p-polarization on the other hand, passes through the PBS and QWP, and deflects via the RR back through the QWP to the PBS, and then deflects out to the FOP. The two beams re-combine at the FOP and provide the interference which is detected by the electronics connected to the FOP. The creep that is measured with this instrument is then converted to a corresponding value of stress relaxation using a rigidity modulus.

The results of the finite element model discussed in this dissertation are validated with the experimental results of creep obtained from the above set-up.

1.3 Objectives of the project

The previous section gave a brief overview of some of the related research work in this area. The major factors which make the research presented in this dissertation unique, include, the material used for the system (elgiloy), the investigation into the time-dependant structural response, and most importantly, the systematic modeling of the spring forming process in order to characterize the 'base state' of the spring, and understanding its influence on the subsequent spring response. Given the complexities in the model (alluded to earlier), it cannot be solved using analytical techniques, and hence a finite element-based approach was deemed appropriate.

The overall objective of this project is to develop a detailed finite element model to accurately capture the instantaneous moment-rotation and the long-term time-dependant structural responses of a torsional spring. Specifically, the objectives can be described as follows:

a) Develop a finite element model which will accurately describe the torsional spring system, using the commercial finite element analysis software-Abaqus [1].
b) Model the forming process of the spring (outlined earlier) to capture the state of residual stresses, plastic strains, and contact conditions in the spring coils at the end of the forming process. We believe that the state of the spring at the end of the forming process can have a significant influence on its subsequent nonlinear response.
c) Predict the instantaneous static moment-rotation response for different levels of wind-up.

d) Predict the long-term stress relaxation response and the associated torque drop when the loaded spring is held at a fixed value of rotation.

e) Capture the effects, if any, of a prolonged shelf-life (aging) of the spring - before it is actually used - on its subsequent response.

f) Investigate the influence of the design parameters such as the coefficients of friction and, material plasticity on the performance of the spring.

g) Develop simple analytical models based on the principles of Statics and Mechanics of solids, to verify the trends and order-of magnitudes of the finite element results. The analytical model can be used in the long-term to develop a torsional creep law for the spring, involving the various design parameters.

h) Compare and validate the numerical results with the results from experiments carried out by the other members of the research group [21].

i) Predict the cyclic moment versus rotation response (‘hysteresis’ response) by subjecting the spring to rotation controlled loading-unloading cycles.

j) Develop a second generation finite element model which can capture the instantaneous and long-term responses of the torsional spring with relatively better accuracy than the conceptual first generation model. The new model is meant to address all plausible nuances in the original model, and thereby come up with a more accurate, if not an exact numerical replica of the actual torsional spring system, incorporating even the minute details of the geometry.

1.4 Organization of the thesis

The successive chapters in this thesis follow the project objectives described in the previous section.

Chapter 2 discusses the finite element model for capturing the spring forming process, and outlines the complexities involved in the modeling effort. The end result of this model is an accurate characterization of the 'base-state' of the spring, described by the residual stresses, the plastic strains, and the contact conditions among the coils. It is believed that these factors would have a strong influence on the spring response during the actual application. This chapter also discusses the effects of the 'instantaneous arbor-release' operation, which is considered to be part of the spring forming process, and compares the finite element model profile with the actual spring profile.

Chapter 3 discusses the modeling of the actual application, i.e., the 'wind-ups'. During this modeling effort, the spring is wound-up to various levels of rotation, and the instantaneous moment versus rotation response is captured. The influences of various design parameters such as material plasticity and, friction, on the moment-rotation response are also discussed. The finite element results are compared with the experimental results and the design specifications. The chapter also presents results for the cyclic moment versus rotation response obtained by subjecting the formed spring to rotation controlled loading-unloading cycles.

Chapter 4 discusses the long-term (time-dependant) stress relaxation response of the spring. It starts with a brief description of the uniaxial tension tests used for calibrating the material creep parameters, and focuses subsequently on the stress relaxation response of the spring and the associated torque-drop. The influence of 'aging' (shelf-life of the spring) on the instantaneous as well as the long-term structural responses is discussed as well. In addition, the influences of design parameters such as material plasticity, creep, friction, etc., are also discussed.

Chapter 5 discusses the development of simple analytical models, based on the principles of Statics and Mechanics of solids, to provide a rough verification for the order-of magnitudes and the trends of the finite element results. Such analytical models can be used in the long-term to develop a torsional creep law for the spring. In addition, it also discusses 'rough estimates' made using the linear beam-bending theories in order to get a feel of the finite element results obtained.

Chapter 6 discusses the development of a second generation finite element model for the torsional spring which can capture the instantaneous and long-term responses of the spring with relatively better accuracy than the conceptual first generation model-discussed in chapters 2 to 5. The major goal of this phase of the research is to remove any plausible discrepancies in the original model, and thereby come up with a more accurate, if not an exact numerical replica of the actual torsional spring system, incorporating even the minute details of the geometry. The chapter starts with a detailed investigation on the presence of any nuances in the first generation model in comparison to the actual clock spring, followed by the development of a new design which would address the discrepancies. The material models used for the new model are the same as the ones used for the original model. The chapter advances with a detailed description of the results obtained for the different phases of the spring, which includes: - the spring-forming process, the wind-up application, and the long-term application. The numerical results for the instantaneous and long-term responses are then compared with the design specifications and experimental results.

CHAPTER 2: SPRING FORMING PROCESS

2.1 Objectives

The specific objectives for modeling the spring forming process are capturing the (i) residual stresses, (ii) plastic strains, and (iii) contact conditions, in the spring coils. These quantities describe the "base-state" of the spring at the end of the forming process, and are expected to affect its subsequent performance. The forming process involves large-scale bending deformations of an elgiloy strip that exhibits significant non-linear behavior, along with a significant amount of discontinuous self contact among the different coils of the spring. Hence, there is a need to select a combination of capabilities (elements, material model, contact formulation, etc.) that can effectively capture such a complex process.

2.2 Finite element model

In this section we provide details on the finite element model that was used to model the forming process. The finite element software package, Abaqus, was used for all the simulations.

2.2.1 Element formulation

Two-dimensional plane-strain solid continuum elements, CPE4R [1], were used to model the elgiloy strip. These elements (i) utilize a bi-linear displacement field within the element, (ii) are quadrilateral in shape with 4 nodes located at the four corners, and (iii) use reduced integration for formulating the discretized equations. A typical CPE4R

element is illustrated in Figure 2.1. These elements are particularly suitable for the present problem as they (i) are capable of resisting large distortions, (ii) can prevent volumetric locking that can be a concern when there is an excessive amount of volume-preserving inelastic straining [24], and (iii) have a built-in hour-glass control scheme [1]-provided the mesh is 'sufficiently fine'. We have included 4 elements along the thickness direction of the strip, which is believed to be sufficient enough for suppressing the propagation of the hourglass modes. The presence of large deformations and discontinuous contact in the problem which are not handled well by quadratic elements, and the likelihood of volumetric- and shear-locking with fully-integrated elements justify the use of the first-order reduced-integration elements [1]. The preferences of a two-dimensional model over a three-dimensional one, and reduced-integration elements over incompatible mode fully-integrated elements, were based on lowering the computational cost.

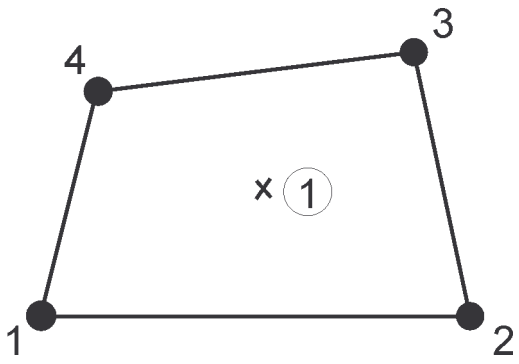

FIGURE 2.1: The 4-node CPE4R element with a single integration point at centroid

The model has approximately 41,300 variables, which includes the degrees of freedom plus the Lagrange multiplier variables. The number of elements used in the

model is approximately18,300, that includes about 9,200 elements generated by the user and about 9,100 internal elements generated for contact.

Though the initial model was generated using beam elements, which are specifically formulated for bending problems, they were found to be not suitable for problems involving self contact and hence were not pursued further.

The arbor and the cup do not undergo any deformation, and hence are modeled as 'rigid bodies'. Generally, stiff components (which do not undergo any deformation) in a mechanical system that are either fixed or undergo large motions are modeled as rigid bodies. A rigid body can be a collection of nodes, elements, and/or surfaces, whose motion is defined by prescribing boundary conditions at a single node (not necessarily part of the body)- called a rigid body reference node. The reference node can have both translational and rotational degrees of freedom [1]. The reaction forces/moments on the rigid body generated due to prescribed motion at the rigid body reference node are available as output quantities. In the current problem, the cup and the arbor are modeled as analytically rigid surfaces. In the absence of any constraints, both the cup and the arbor can have three degrees of freedom defined at their corresponding reference nodes- two translations (in the plane of the model), and one rotation (about a normal to the plane of the model). However, throughout the present analysis, the cup is fixed in all the three degrees of freedom, whereas, the arbor is allowed to rotate and/or translate depending on which stage (or step) of the analysis it is in (refer to the picture of the spring assembly shown in Figure 1.1 of Chapter 1). The torque of the spring system is calculated as the reactional moment at the reference node of the arbor. The primary advantage of using the

concept of rigid bodies is that it enables achieving computational efficiency during the analysis.

2.2.2 Material model

The material model for the instantaneous response is described by an elastic-plastic constitutive law. Figure 2.2 illustrates the response of the elgiloy material, which includes a linear-elastic region denoted by region-I, followed by a plastic region represented by region-II. The material that is loaded and then unloaded in the elastic region will release its acquired strain completely, whereas the material loaded in the plastic region will undergo a permanent deformation with an acquired residual strain-called plastic strain. The current model uses linear hardening for the plasticity response.

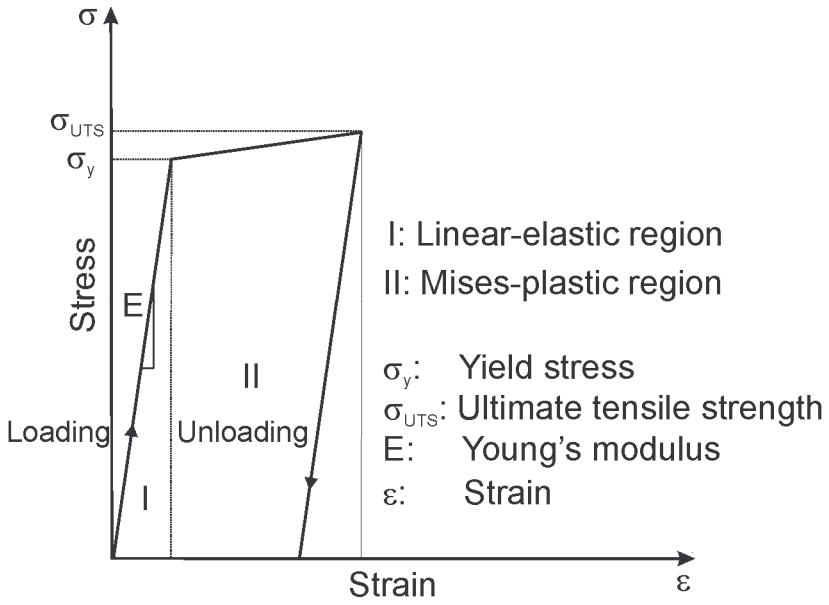

FIGURE 2.2: Instantaneous elastic-plastic response of the elgiloy material

For the case of one-dimensional elasticity, the slope of the linear-elastic curve represents the Young's modulus of elasticity- E. For a generalized three dimensional stress-state, on the other hand, the linear elastic constitutive response is given by [25]:

$$\sigma_{ij} = C_{ijkl}\varepsilon^{el}_{kl}. \qquad (2.1)$$

In the equation above, σ_{ij} refers to the components of the second order Cauchy's stress tensor, C_{ijkl} represents the components of the fourth order elasticity tensor, and ε^{el}_{kl} refers to the components of the elastic strain tensor.

An important ingredient of the plastic response of a material is the yield condition. The present analysis assumes that material yielding is governed by the von Mises yield criterion. As per this condition, a material would undergo yield (or plastic flow) if the effective stress in the material is equal to its yield stress. Generally, the yield condition of a material is based on the definition of its yield surface. The 'yield surface' represents a virtual multi-dimensional surface in stress space. The von Mises yield surface is a circular cylinder of infinite length with its axis inclined at equal angles to the three principal stresses [23, 18]. For an elastic response, the stress-state of a material should lie within the yield surface. When the stress-state lies on the yield surface, the material is assumed to undergo plastic yielding. Mathematically, a general yield surface can be represented by a yield function- $f(\sigma_{ij},\alpha)$, where, σ_{ij} represents the components of the stress tensor, and α is a state variable that is generally referred to as a hardening parameter. For a perfectly-plastic response, the hardening parameter can be omitted from the formulation. Accordingly, the response of a perfectly-plastic material [23] is shown in Equation 2.2. The corresponding associative flow rule [15] is shown in Equation 2.3.

$$f(\sigma_{ij}) = \sigma^{e} - \sigma^{y} \qquad (2.2)$$

$$\dot{\varepsilon}^{pl}_{ij} = \dot{\lambda}\frac{\partial f}{\partial \sigma_{ij}}. \qquad (2.3)$$

In the equations above, σ^e refers to the Mises effective stress, σ^y refers to the initial yield stress of the material, and $\dot{\varepsilon}_{ij}^{pl}$ refers to the plastic strain-rate tensor.

For a linear hardening response, Equation 2.2 can be modified with the inclusion of the hardening parameter, as shown in Equation 2.4 [23, 15]. Generally, the hardening response is modeled by an increase in the yield stress along with an associated plastic straining. Equation 2.5 shows the new expression for the yield stress taking into consideration the hardening parameter.

$$f(\sigma_{ij}) = \sigma^e - \sigma^y(\alpha) \qquad (2.4)$$

$$\sigma^y(\alpha) = \sigma^y + k\alpha. \qquad (2.5)$$

In the equations above, $\sigma^y(\alpha)$ refers to the new value for the yield stress and k is the plastic modulus of the material.

For the Abaqus simulations considered here, the ultimate tensile strength (or, the new value for the yield stress- $\sigma^y(\alpha)$) of the elgiloy material used is $\sigma_{UTS} \approx 1860$ MPa, with the associated plastic strain of $\varepsilon^{pl} \approx 0.014$ [10]. As already mentioned in Chapter-1, the initial yield stress $\sigma^y \approx 1655$ MPa, Young's modulus of Elasticity is 190 GPa, and the Poisson's ratio is 0.23.

Note: The creep material properties of elgiloy are discussed in Chapter-4.

2.2.3 Contact formulation

The forming process of the spring as well as its application involves surface-to-surface contact of the elgiloy strip with the cup and the arbor, as well as self contact of the strip with itself. The built-in node-to-surface master-slave formulation [1] in Abaqus is used for modeling the contact behavior. In this formulation, the surfaces that can

potentially come into contact during the deformation history are classified as master and slave surfaces, respectively [17]. The formulation ensures that the nodes on the slave surface do not penetrate the master surface. Thus, the standard equations of equilibrium are augmented with a number of constraint equations (one for each slave node). The constraints are enforced using either a Lagrange multiplier or a penalty-based approach.

2.2.3.1 Surface behavior in the normal direction

The "constitutive behavior" of the contact formulation in the normal (to the master surface) direction is defined in terms of its pressure versus overclosure relationship, and can be broadly classified into two categories:

(a) Hard contact

The default hard contact algorithm in Abaqus, shown in Figure 2.3a, assumes that the pressure is zero when a slave node is not in contact with the master surface, while it can take on any value when the slave node is in contact. Thus, the use of a hard contact algorithm for the normal behavior may potentially lead to sharp discontinuities in contact pressures across a contact patch. Figure 2.3b illustrates such a behavior using a two-dimensional contact patch.

The spikes (shown in Figure 2.3b) correspond to non-zero pressure at slave nodes that are in contact, while the pressure is zero at slave nodes that are not in contact. In addition, at any slave node that changes the contact status from iteration to iteration, the contact force changes abruptly from a zero to a potentially high non-zero value. This abrupt change in contact pressure can lead to convergence difficulties: a phenomenon that is referred to as contact chattering. The present problem is contact intensive, and during

the initial stages of our modeling effort, the simulation showed evidence of being potentially affected by such discontinuous behavior.

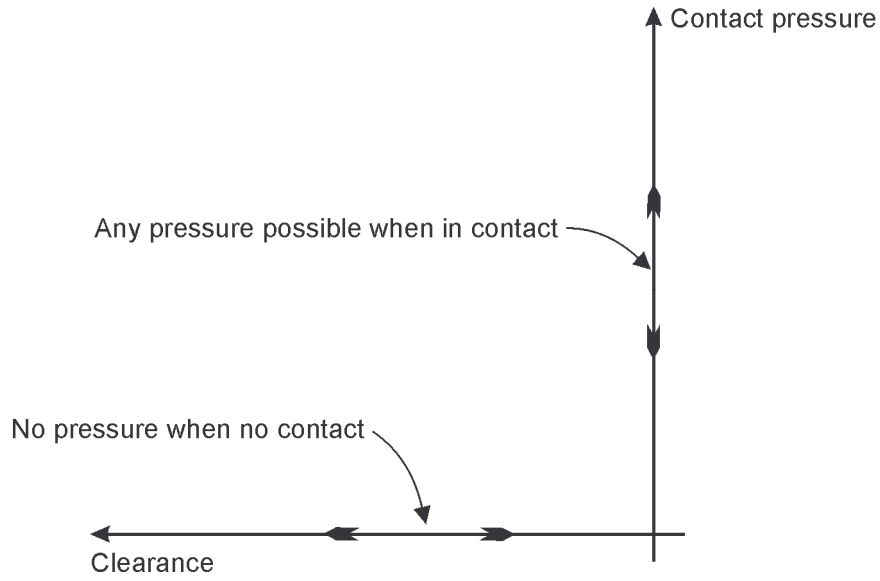

FIGURE 2.3a: A schematic of the built-in hard contact formulation

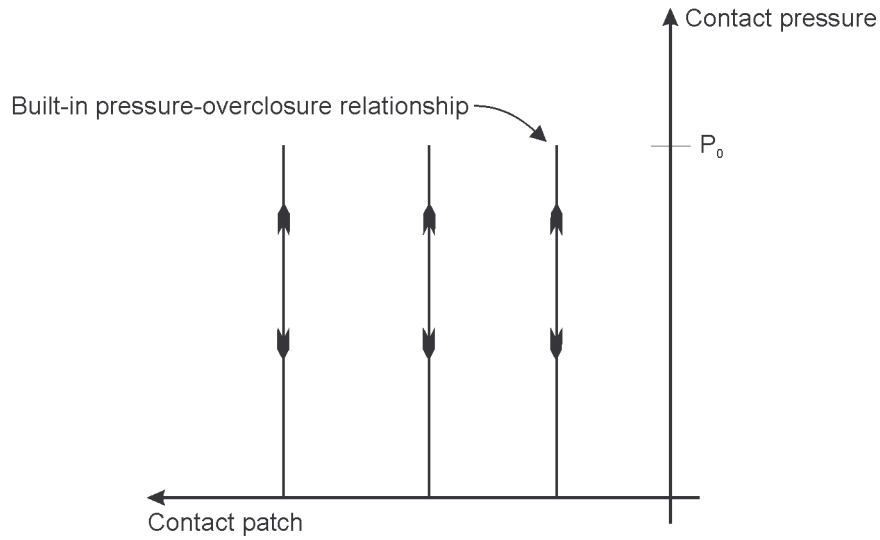

FIGURE 2.3b: A schematic of the discontinuous pressure-overclosure relationship

(b) Softened contact

Unlike the discontinuous pressure-overclosure relationship in hard contact, a softened contact formulation (illustrated in Figure 2.4) follows an exponential pressure

versus overclosure relationship. For this case, the contact pressure can be non-zero even for a small clearance between a slave node and the master surface (any clearance that is smaller than c_0 in Figure 2.4 results in a non-zero contact pressure). At zero clearance, the pressure reaches a value of P_0, and increases exponentially thereafter. A softened contact formulation ensures that if the contact clearance at a node changes by a "small" amount, there is no abrupt change in the corresponding contact pressure.

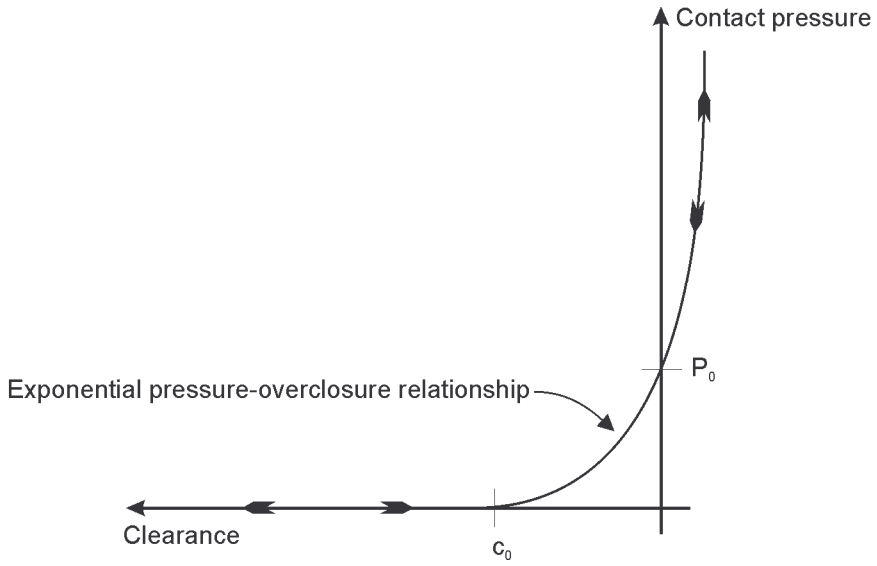

FIGURE 2.4: A schematic of the softened pressure-overclosure relationship

In particular, if a slave node that is in contact at one instant comes off contact at the next instant with a clearance that is smaller than c_0, the contact pressure does not change significantly (of course, this aspect of the behavior is affected by the specific choices of c_0 and P_0). With a hard contact formulation, the pressure would have dropped abruptly to zero in this situation. The softened contact formulation is often recommended as the method to fix convergence problems associated with contact chattering with the built-in hard contact formulation.

As mentioned earlier, the present problem is contact intensive. In addition, the contact involved in this problem is discontinuous in time since the contact patches can change significantly in the course of the simulation. In other words, there is a potential for significant occurrences of the situation where segments of the surfaces that are in contact at one instant may not necessarily remain in contact at another. Abaqus provides some numerical control mechanisms to help in such situations. These mechanisms are invoked by utilizing the "*CONTROLS, AUTOMATIC TOLERANCES" [1] option. This control algorithm over-rides the strict rules that define conventional contact, by allowing for some margin of errors with regards to the open-close behavior.

2.2.3.2 Surface behavior in the tangential direction

The behavior of the contact interaction in the tangential direction is assumed to be governed by Coulomb friction. Equation 2.6 shows the basic governing equation on which Coulomb friction is based on.

$$F_f \leq \mu P \qquad (2.6)$$

In the equation above, F_f refers to the Coulomb frictional force that acts in a direction tangential to the surfaces in contact (opposite to the force tending to cause motion), μ refers to the coefficient of friction, which is an empirical property of the contacting materials, and P refers to the contact pressure exerted between the surfaces in contact (acts in a direction normal to the surfaces in contact). When there is no relative motion between the contacting surfaces (surfaces at rest), the Coulomb frictional force may take any value varying from 0 to F_f that is sufficient enough to balance the net external force tending to cause motion. This situation is generally referred to as static friction and the

corresponding coefficient of friction can be denoted by μ_s - called the coefficient of static friction. The maximum value for the coulomb frictional force corresponds to a threshold value beyond which the surfaces start sliding against each other. At the threshold value, the inequality in Equation 2.6 can be replaced by the equality. Once the surfaces start sliding against each other, the corresponding frictional force would be smaller than its static counterpart and the surfaces experience what is generally referred to as kinetic friction. The coefficient of friction in this situation is represented by μ_k - the coefficient of kinetic friction.

For the current problem, the coefficients of friction were measured through experiments [21]. The experimental set-up consist of two blocks, namely: (i) a fixed block, and (ii) a moving block, positioned on top of the fixed base - each having elgiloy strips attached to them (i.e., on the bottom of the moving block, and on the top of the fixed block) in the longitudinal and transverse directions, respectively. The movable block is then pushed by a force gauge - attached to the assembly - that tends to slide the elgiloy strips against each other. The force gauge then records the loads including the peak load required to initiate sliding, and helps in calculating the corresponding coefficients of friction involved in the process. The values were found to be 0.2 for the surface-to-surface contact of the alloy strip with the arbor and the cup, and 0.13 for self contact of the strip with itself. These values were specified in the Abaqus simulations. The tangential behavior follows a “stick-slip” pattern [20], which adds to the complexity of the simulations. Penalty method is used for handling friction [1]. As per this method, the solver allows for ‘some’ deviations from the strict contact enforcement rules for tangential behavior. Accordingly, it permits a certain degree of relative motion of the

contacting surfaces when they are supposed to “stick”- the magnitude of which is determined by the value of ‘elastic slip’ specified in the model. A higher magnitude of the elastic slip can lead to a rapid convergence of the solution to a problem, but can spoil the solution accuracy. On the other hand, a smaller magnitude can slow-down the convergence rate. The current model uses the default value of elastic slip, specified by Abaqus, which provides a conservative balance between the efficiency and the accuracy of the solution. Abaqus calculates this value as a small fraction of the characteristic length of the contact surface, and is called the “slip tolerance”. The default value of slip tolerance is 0.005.

Note: The terminology, ‘perfect lubrication’, used in this dissertation corresponds to a coefficient of friction (for self contact among the spring coils) of $\mu = 0$, whereas, ‘no lubrication’ corresponds to a coefficient of friction of $\mu = 0.13$.

2.2.4 Viscous stabilization to prevent local instabilities

Non-linear static problems can be unstable. Such instabilities may be of a geometric nature- such as buckling, or of material nature- such as material softening. If the instability manifests itself in a global load-displacement response with a negative slope, the problem can be treated as a buckling or as a collapse problem. Henceforth, it can be handled through modifications to the standard Newton’s method for solving nonlinear equations. However, if the instability is localized, there will be a local transfer of strain energy from one part of the model to the neighboring parts, and the global solution methods (modified Newton’s method) may not work [1]. This class of problems has to be either solved dynamically or statically with the aid of artificial damping. Viscous stabilization is a numerical technique available in Abaqus/Standard which is

used for stabilizing unstable quasi-static problems through the automatic addition of volume-proportional damping to the model. The goal of this stabilization technique is to dissipate the energy due to the local instabilities, without affecting the overall accuracy of the model. This is achieved by supplying viscous forces to the model to counter the instability effects. However, in order not to affect the physics of the actual problem significantly, the magnitude of these viscous forces should remain as low as possible. Equations 2.7 and 2.8 show how the inclusion of the viscous forces affects the global equilibrium equations.

$$F_v = cM^* v, \tag{2.7}$$

$$P - I - F_v = 0. \tag{2.8}$$

In the equations above, F_v refers to the nodal viscous forces, P refers to the external applied nodal loads, I refers to the internal nodal forces, M^* is an artificial mass matrix calculated with unit density, c is the damping factor, $v = \Delta u / \Delta t$ is the vector of nodal velocities, Δu refers to the incremental displacement, and Δt is the increment in time.

The torsional spring problem considered in this research also encounters instabilities of the local kind, primarily during the spring forming process. Section 2.3 provides a detailed explanation of this phenomenon and the method utilized to mitigate the effects of such instabilities through the use of viscous stabilization.

Once viscous stabilization is used in a step, it needs to be re-specified in the subsequent steps as well, for a multi-step analysis. Otherwise, if the instabilities have not subsided at the end of the previous step, then the sudden termination or modification of the viscous forces at the beginning of the subsequent steps may potentially lead to

convergence difficulties. Due to this reason, the subsequent steps of this problem (to be discussed in later chapters) also use the same damping factor as the one used for the initial step (spring forming).

The effect of the artificial damping on the solution is assessed by monitoring the different energy components in the model. For accurate results, the ratio of the static dissipation energy (output variable- ALLSD in Abaqus) to the strain energy (output variable- ALLSE in Abaqus) in the model should remain as low as possible. The selection of the appropriate damping factor for this model was carried out by systematically reducing the damping factor to the lowest permissible level that leads to the combination of the two desirable characteristics: convergence and a low energy dissipation ratio. Accordingly, the value of damping factor was selected to be $c = 5e-04$. The results shown in this chapter, as well as in the following chapters, correspond to this value of the damping factor.

2.2.5 Other controls used in the model

In order to obtain the solutions to the strongly nonlinear problem effectively, the model also uses additional control mechanisms other than those mentioned in the earlier sections. This section provides a brief overview of the choice of these controls relative to this problem:

(a) Unsymmetric equation solver

Abaqus/Standard generally uses the Newton's method to solve nonlinear problems. The method results in a system of linear simultaneous algebraic equations, whose coefficient matrix is referred to as the stiffness matrix. For a large class of problems, typically involving only conservative forces, this matrix is symmetric.

However, in some problems - for example, those involving Coulomb friction (a non-conservative force) - the stiffness matrix is not symmetric. In Abaqus, the selection of the symmetric or the unsymmetric matrix storage and solution scheme is carried out based on the model and the step definition used. The model discussed here uses the unsymmetric storage method in order to improve the convergence associated with the discontinuous frictional contact. This approach can be switched on by using "Unsymm=Yes" in the step definition. By default, Abaqus/Standard uses the symmetric matrix storage scheme, represented by "Unsymm=No" [1].

(b) Severe discontinuity iterations

Abaqus/Standard follows the implicit technique of 'iterating' to reach a solution to a non-linear problem. The iterations may be classified as: (i) equilibrium iterations - in which the solution varies smoothly, or (ii) severe discontinuity iterations (SDIs) - in which abrupt changes in the constraint conditions occur from one iteration to the next. Examples of severe discontinuity iterations include changes in the contact status in the normal direction (e.g., open-to-close, or vice versa in going from one iteration to the next), or changes in the contact status in the tangential direction (e.g., stick-to-slip, or vice versa in going from one iteration to the next). By default, Abaqus/Standard [1] continues to iterate until the severe discontinuities are sufficiently small (or no severe discontinuities occur) and the equilibrium tolerances are satisfied. This scheme is invoked by using "Convert SDI = Yes" in the step definition. Alternatively, a different approach can be chosen in which Abaqus/Standard will continue to iterate until (strictly) no severe discontinuities occur. This approach can be invoked by using "Convert SDI = No" in the step definition. The model developed here uses the default approach. As per this

approach, a force discontinuity is generated whenever open-to-close, or stick-to-slip transitions in contact take place. This force discontinuity leads to force residuals that are checked against the time average force [1]. The iteration process would stop when the severe discontinuity exceeds a certain limit value, which is set by the solver based on the model and the step definitions used. The non-default approach of forcing the iteration process to continue until no severe discontinuities occur can lead to convergence problems, particularly in situations involving many contact points or where the contact conditions are only weakly determined (as in the case of the current problem). This can result in an excessive number of iterations, and the problem may not attain convergence.

(c) Automatic settings for time-incrementation parameters for severely discontinuous problems

These settings are invoked through the use of the "Analysis=Discontinuous"-parameter associated with the *CONTROLS option. They are generally used to improve the efficiency of the nonlinear solution procedure for severely discontinuous behavior - such as frictional sliding. By invoking this capability, the solver allows for relatively large number of iterations before beginning any checks on the convergence rate [1].

(d) Line search techniques during nonlinear solution procedures

Line search techniques are used to improve the robustness of the solution procedures for non-linear problems. Abaqus/Standard generally uses the Newton's method to solve non-linear problems. The method involves defining the Jacobian of the system, and checking for quadratic convergence for the obtained solution estimate [1]. However, for problems involving severe nonlinearities (like discontinuous behavior and Coulomb friction), this process can result in a large number of nonlinear iterations and/or severe cut backs during the iterative procedure; and thereby lead to an enormous

computational cost. The line-search algorithm is a solution control that helps to prevent divergence of equilibrium iterations resulting from the above mentioned nonlinearities. It automatically detects such situations and applies a scale factor (called 'line-search scale factor') to the computed solution correction [1]. This can help in achieving a faster convergence rate, and reducing the computational cost. Abaqus uses an iterative process to determine the value of the line-search scale factor that can minimize the component of the residual vector in the direction of the correction vector. The current model uses 4 line-search iterations. The remaining parameters which are required to be specified in the line-search algorithm are set as the default values provided by Abaqus. These defaults are chosen in order to achieve a 'modest' accuracy for the line search scale factor, while minimizing the additional cost of line-search iterations.

2.3 Procedures and Results

The process of forming the spring involves two stages; namely, the winding phase, and the arbor release phase. During the winding phase, the arbor (initially concentric with the cup) is rotated so as to pull the flat wire into a spiral form inside of the cup. A tied constraint is used to model the initial length (≈ 3.5 mm) of the strip which is annealed and then fixed to the arbor. Any translational motion of the arbor is prevented during this phase. At the end of this process, once most of the strip gets pulled inside the cup, about 2 mm of the rear end of the strip is welded onto the cup. Figure 2.5 illustrates contour plots for the von-Mises stress (σ_e), and equivalent plastic strain at the end of the winding process, for the case of a perfectly plastic material and "no lubrication". The results for the equivalent plastic strain suggest that the spring coils have been subjected to

plastic deformation during the first stage of the forming process, leading to the formation of 'kinks' or hot-spots (as shown in the PEEQ profile of Figure 2.5).

The first three coils of the strip, that are closest to the arbor, can be observed to have undergone yield to a larger extent (evident from the presence of kinks in these coils, in which the maximum von-Mises stress is equal to the yield stress value of 1.66 GPa). The majority of the remaining coils deformed only with negligible plastic deformation - on the outer-most ends of the strip section - which is of the order of less than 5 - 10% of the maximum plastic strain in the inner coils.

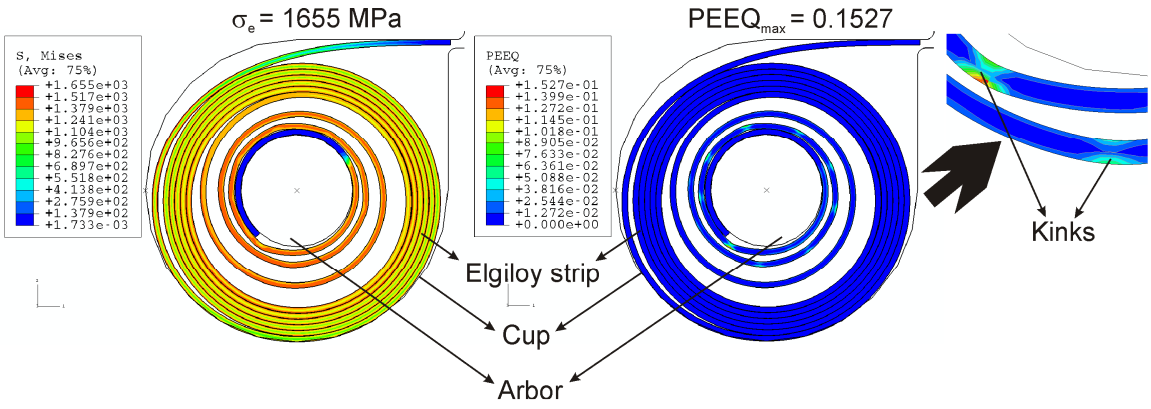

FIGURE 2.5: Contour plots of the von-Mises stress and equivalent plastic strain at the end of the initial winding phase

These outer coils are clustered together, and appear to have moved radially outwards from the inner coils which experience relatively larger plastic deformations.

An important feature of the deformed shape of the elgiloy strip at the end of this stage of the forming process is the formation of a number of kinks in the plastically deformed inner coils. The occurrence of such 'kinks' (or hot-spots) was investigated in some detail. The results suggest that these kinks may be thought of as partial 'plastic hinges', comprising of an elastic core at the center of the strip surrounded by an outer

plastic region (illustrated in the inset of Figure 2.5). These kinks were formed as a result of the large plastic deformations of the coils during the initial winding process. It also appeared that the first one or two kinks that were formed may have contributed to the formation of subsequent kinks through contact interactions. The following paragraph provides a detailed explanation of the phenomenon of kink formation during the initial winding process. It also sheds light into the utility of viscous stabilization to control the local instabilities arising during the winding process.

Kink formation during the spring forming process:

At the beginning of the initial winding stage of the spring forming process, about 97% of the overall length of the strip remains relatively unconstrained outside the cup. During the process of winding the spring, as the arbor rotates and the annealed portion of the strip comes into contact (for the first time) with the immediate outer coil, a large plastic deformation of the latter occurs at the region of contact- as a consequence of the annealed region pushing onto the outer coil. This region of large plastic deformation is the first kink. This results in a large vertical displacement of the tail end of the strip. Figure 2.6-a. shows the contour of the equivalent plastic strain in the spring coils upon the formation of the first kink (for the cases of perfect plasticity and perfect lubrication). It also illustrates the large vertical displacement of the tail end of the strip which is a consequence of the kink formation. Figure 2.6-b. shows a plot of the variation of the vertical displacement of the tip of the unconstrained end of the strip as a function of a fraction of the step time. The graph indicates a sharp change in the vertical displacement of the tip which corresponds to the formation of the first kink. This phenomenon is a case of a local instability which leads to a local transfer of strain energy to the neighboring

parts of the strip. Such local instabilities occur throughout the analysis of the winding process.

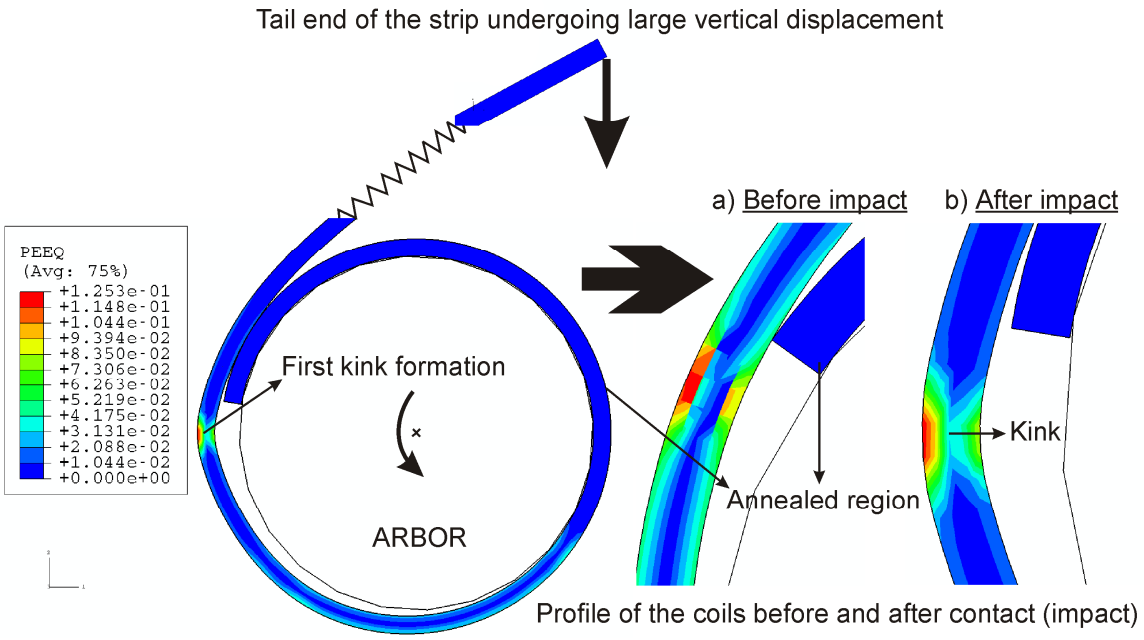

FIGURE 2.6-a: A schematic illustration of the formation of the first kink

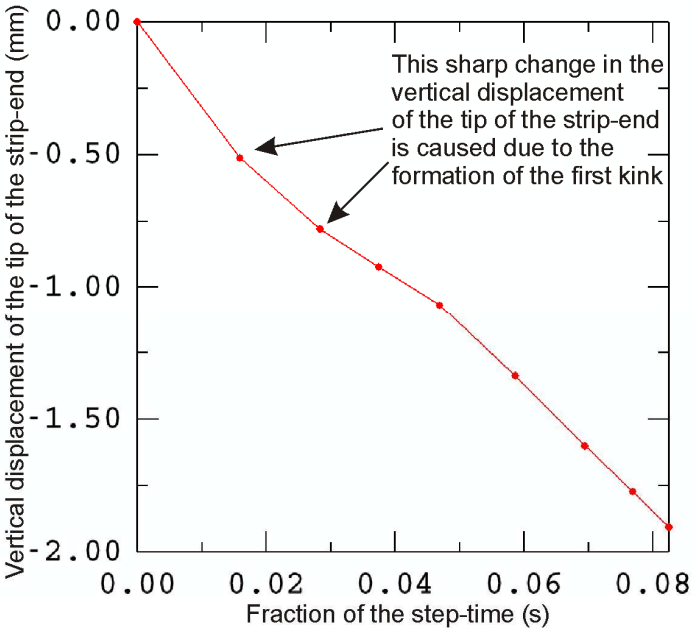

FIGURE 2.6-b: Plot of the vertical displacement of the tip of the strip end against time during the first kink formation

Subsequently, as the arbor further rotates (during the winding stage), more kinks are formed at regular intervals. But, contrary to the first kink, not all of them are formed as a result of contact. Some of the kinks are formed as a result of the large bending deformation of the coils as they wrap around the arbor during the winding stage.

A question that naturally arises is: Why do these kinks occur in the first three coils at apparently regular intervals, instead of possibly occurring everywhere in these coils? The results suggest that this behavior may be attributed to two primary reasons, namely: (i) the absence of continuous contact among the inner coils during the winding stage, and (ii) a discontinuous outward and inward 'mechanical-hinge' type of motion (in-plane) of the coils about these hot-spots, during the winding stage. This phenomenon is illustrated by the arrows shown in Figure 2.7. It was also observed that, once three or four coils were formed inside the cup, the remaining coils of the strip simply 'rolled' inside without undergoing any major plastic deformation.

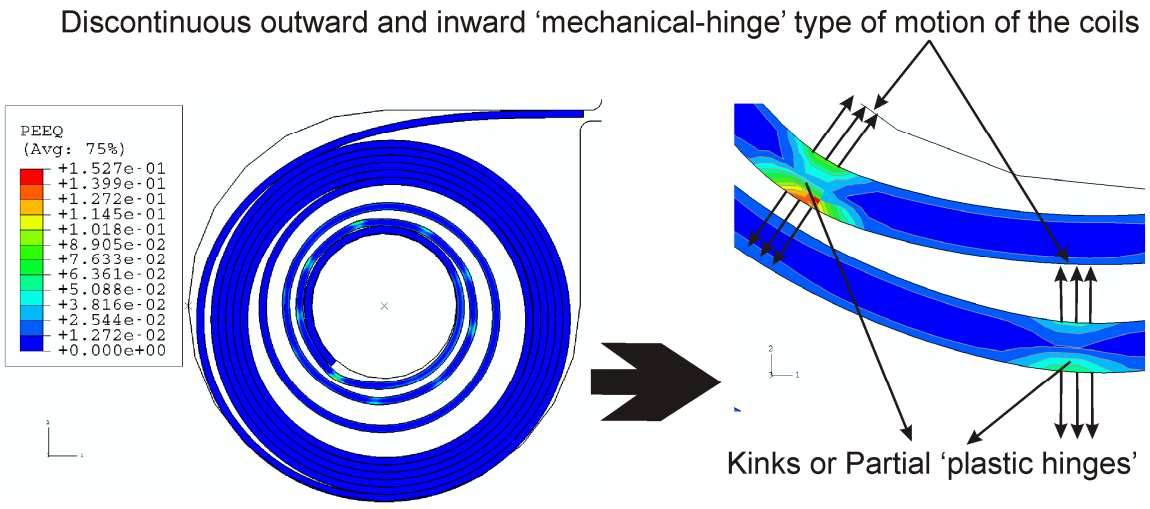

FIGURE 2.7: PEEQ profile showing occurrence of partial 'plastic hinges'

This explains the absence of kinks in the remaining length of the strip. The maximum equivalent plastic strain in the remaining length of the strip was found to be less than 5 – 10% of the value in the inner coils.

The influences of friction and material plasticity on the state of the coils were also investigated. Analyses were carried out both with- and without- lubrication. As mentioned earlier, the values for the coefficients of friction used in these simulations were measured experimentally by Lawton *et al.* [21]. The results suggest an increase of about 10 % in the plastic strain levels in the kinks as a result of friction. Figure 2.8 shows a comparison of the distribution of the equivalent plastic strain in the spring coils at the end of the initial winding stage, for the different coefficients of friction for self contact (with and without lubrication), and a perfectly plastic material.

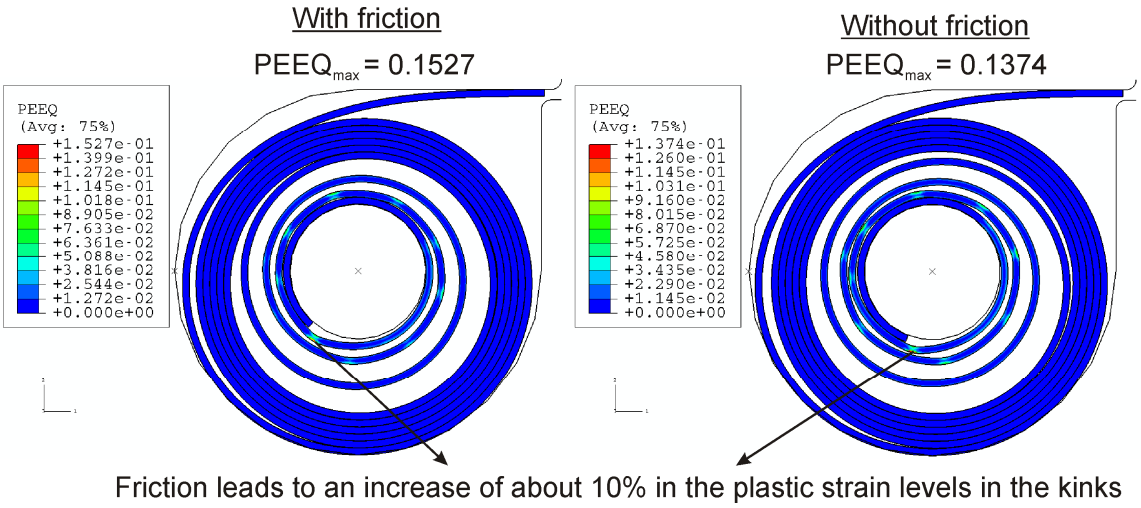

FIGURE 2.8: Comparison of the PEEQ profiles of the spring for the different coefficients of friction (for self contact)

Material hardening (as modeled by an increase in the yield stress with plastic straining in the plasticity models), increases the stress levels, and reduces the equivalent plastic strain in the coils (as expected). In addition, and as a consequence of the reduced

plastic deformation, material hardening was found to make the kinks less prominent. Figure 2.9 illustrates the contour plots for the von Mises stress, and the equivalent plastic strain in the spring coils, for the cases of material hardening and no lubrication. These plots can be compared to the contours shown in Figure 2.5- for the case of perfect plasticity. The contours shown here are illustrative of the increased stress levels, and reduced plastic deformation of the strip as a result of hardening. It can also be seen that the kinks that are formed are less prominent when compared to the case of perfect plasticity. The results suggest a reduction of about 75% in the plastic strain levels in the kinks, as a result of hardening. In addition, the plastic strains in the outer coils (on the outer-most ends of the strip section) were found to be about 15 - 25% of the maximum plastic strain in the inner coils.

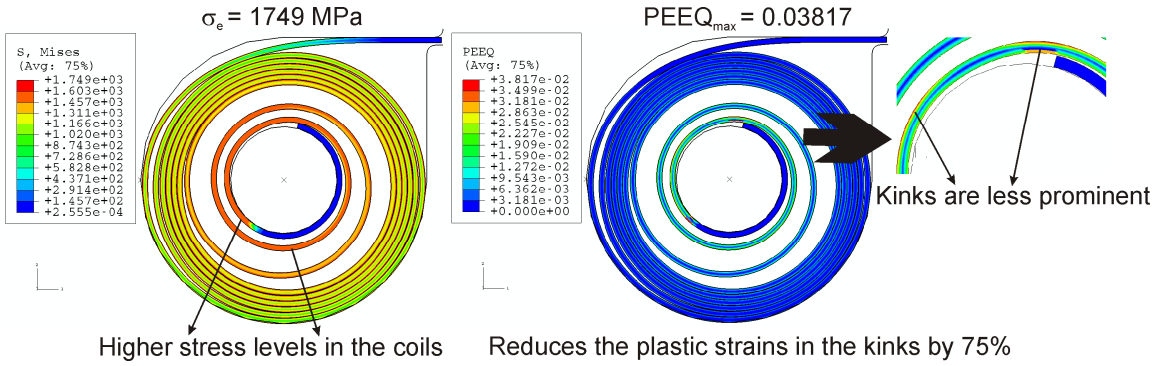

FIGURE 2.9: Contour plots of the von-Mises stress and equivalent plastic strain for the case of hardening plasticity (initial winding stage)

At the end of the winding phase, fixed displacement boundary conditions are applied to the nodes at the end of the strip in order to model the welding of its tail end to the cup. Subsequently, all the degrees of freedom in the arbor are released, as a result of which the arbor freely rotates and translates until it completely releases the torque and

forces built-up during the winding process. This step corresponds to physically releasing the arbor during the forming process, after it has been held fixed and rotated to pull in the coils inside the cup. During this process, on an average, the stresses in the coils drop by about 1 GPa compared to the values at the end of the winding stage, and a majority of the coils cluster together and move radially outwards towards the cup. The arbor undergoes a rotation of about 1¼ revolutions in the clockwise (reverse) direction upon being released. Figure 2.10 shows a comparison of the actual spring profile after it is formed (wound and released), with the corresponding profile from the finite element model. It can be observed that the profile corresponding to the finite element model is a reasonably good representation of the released profile of the spring, both in terms of the position of the arbor at the end of its release, and the clustering of the majority of the coils against the inner surface of the cup.

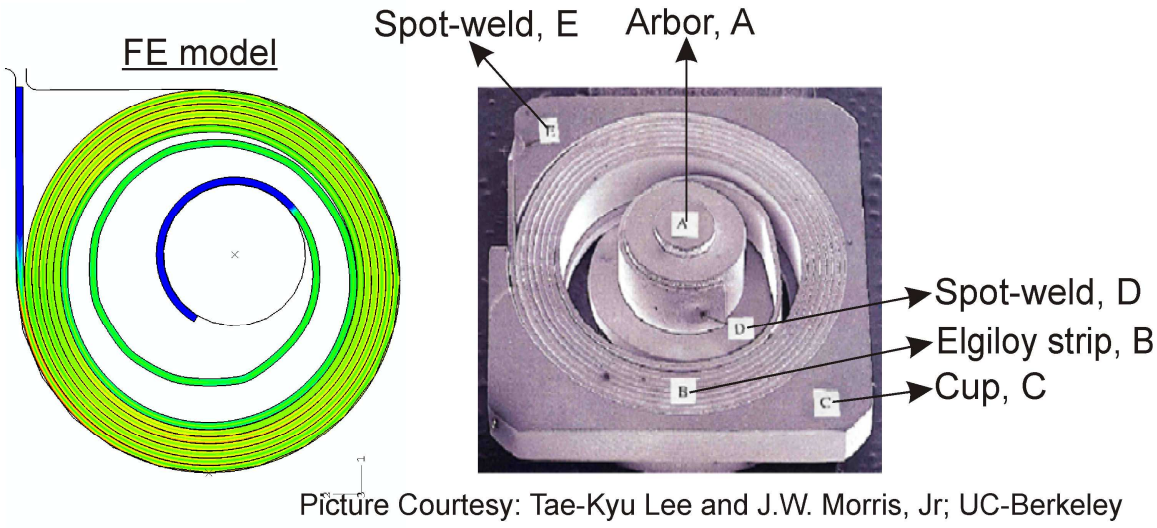

FIGURE 2.10: Comparison of the real formed profile of the spring (right) with the finite element model, at the end of the arbor release

2.4 Conclusions

A finite element model has been developed which attempts to capture the details of the spring forming process, focusing on the state of residual stresses, plastic strains, and contact conditions in the spring coils at the end of the forming process. These quantities characterize the base-state of the spring, which in turn affects its subsequent response. The results suggest that the initial winding process leads to extensive plastic deformation of the first two to three coils of the spring that are close to the arbor, while the remaining coils (outer) deform with a negligible plastic deformation (only on the outer-most ends of the strip section). The ‘kinks’ in the coils closer to the arbor can be considered as partial ‘plastic-hinges’ formed as a result of the large plastic deformation of the spring material during the forming process. The results obtained also suggest that the discontinuous self contact, large deformations, and non-linear material behavior (plasticity) have a major role to play in defining the spring response. The released profile of the spring captured by the FE model showed close resemblance to the actual clock spring profile- in terms of the position of the arbor as well as the alignment of the coils.

CHAPTER 3: INSTANTANEOUS/STATIC MOMENT-ROTATION RESPONSE

3.1 Objectives

The primary objective of this chapter is to discuss the results of the modeling phase which simulates the actual application of the torsional spring, i.e., the 'wind-ups'. In particular, we discuss the instantaneous moment versus rotation response that characterizes the static response of the spring when subjected to an applied torque or rotation. The modeling is accomplished by superposing additional rotations on the formed spring through the arbor reference node, and noting the corresponding reaction moments, that are provided as output quantities by Abaqus. The results obtained from the finite element model are compared with the experimental results and the design specifications. In addition, the torsional springs have also been found to exhibit significant hysteresis when subjected to rotation-controlled loading and un-loading cycles. This chapter also discusses the details of modeling such hysteresis response, and correlating it with the experimentally observed behavior.

3.2 Procedures and Results: Instantaneous moment versus rotation response

The 'wind-up' is modeled as a nonlinear static procedure (similar to the previous phase for the spring forming process) where the arbor is subjected to an additional rotation, thereby subjecting the formed spring coils to additional deformation. Clearly, the "base state" of the spring for the application is the state at the end of the forming process. The nonlinear solution scheme in Abaqus ensures that the effects of the state of

the coils in the base state are accounted for in computing the torsional stiffness of the spring during its application.

During this phase of the modeling effort, the arbor - which was released at the second stage of the forming process - is first translated so that it is concentric with the cup. This is followed by the application of a rotational boundary condition to the center (reference node) of the arbor such that the arbor rotates in the counter-clockwise direction about the normal to the plane of the spring assembly. Figure 3.1 illustrates this phenomenon with a schematic diagram of the spring profiles- before and after centering of the arbor. The arbor is prevented from any further translational motion during the actual application.

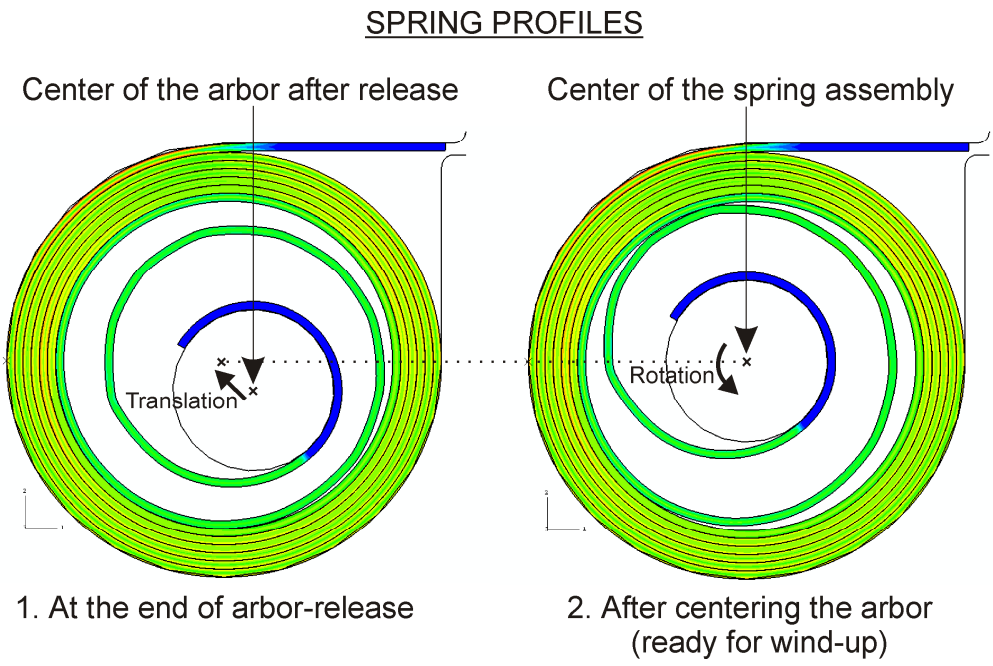

FIGURE 3.1: A schematic representation of arbor-centering and wind-up

The process of loading tightens the coils of the spring, and the spring provides a certain amount of resistive torque which can be measured as the reaction-moment at the

center of the arbor. The process involves extensive discontinuous contact among the spring coils, and leads to additional large material deformations as well. Based on the design specifications and the expected ranges of applications, wind-up levels of 1 revolution and 2.25 revolutions are of primary interest in the project. The results obtained suggest that during the 1 revolution wind-up, the spring coils are not subjected to any additional plastic deformation, whereas, for 2.25 revolutions, a majority of the coils are subjected to extensively large plastic deformations. The results also show that the corresponding moment versus rotation response is strongly non-linear with a non-smooth behavior. These results are discussed in details in the rest of this chapter.

Figures 3.2-a. and -b. illustrate the moment-rotation response and the von-Mises stress contours in the spring coils for the wind-ups (actual application). The plots correspond to the cases of perfect plasticity and “no lubrication”. From the plots it can be observed that, for the case of the 1 revolution wind-up, the maximum von Mises effective stress in the spring coils is around 1.55 GPa, which is lower than the yield stress value of 1.66 GPa. This is suggestive of the absence of any additional plastic deformation in the coils at this level of wind-up. In addition, the maximum stress levels are observed in the first three coils of the strip that are closest to the arbor. The stresses in the remaining coils are about 10 - 15% lower than the stress levels in the inner coils. These remaining coils are clustered together, and are located radially outwards from the inner coils (onto the cup surface). This profile is similar to the spring profile at the end of the initial stage of the forming process (refer to Figure 2.5 shown in Chapter 2). The moment (or resisting torque) at 1 revolution (shown in Figure 3.2-a) is 3.76 N.mm, which is about 10% off from the upper limit of the design specification range of 2.9±0.5 N.mm.

For the case of 2.25 revolutions, on the other hand, the spring coils get extensively tightened and are closely packed against one another compared to the case at the wind-up of 1 revolution.

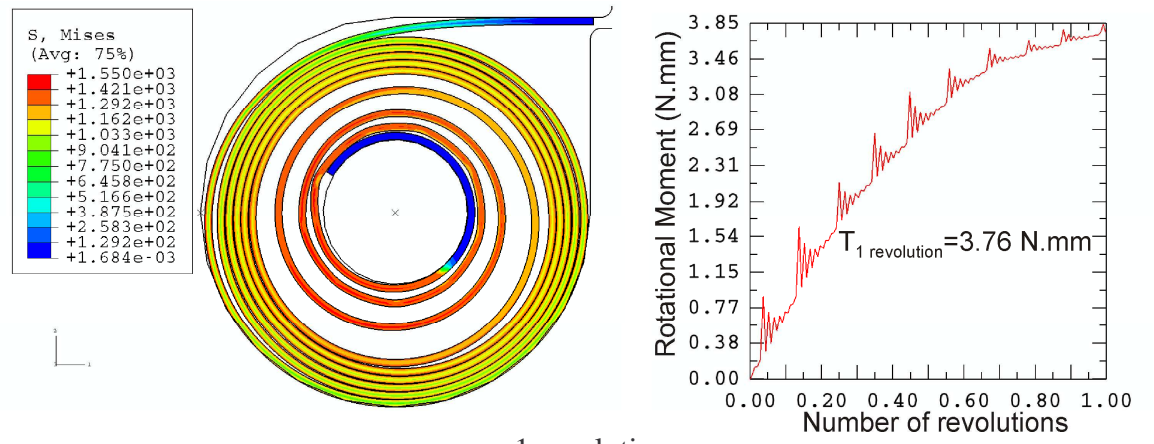

a. 1 revolution

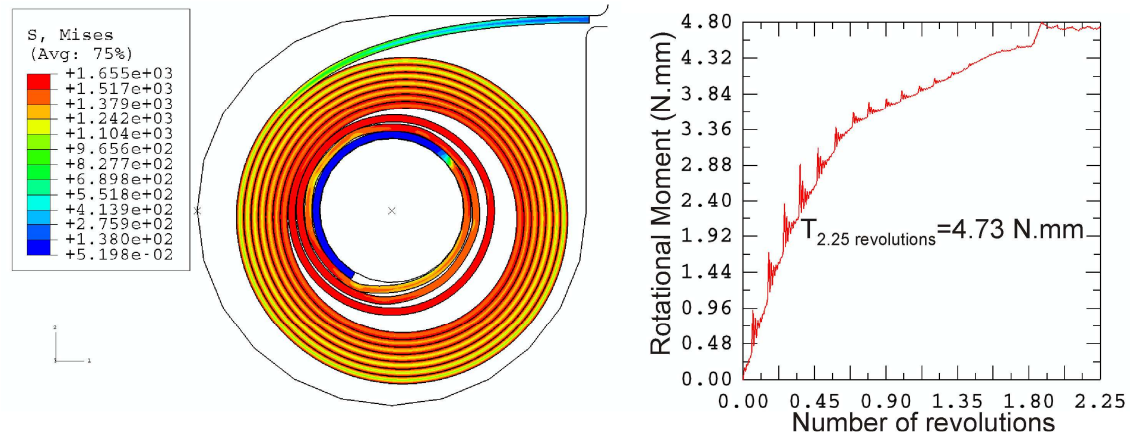

b. 2.25 revolutions

FIGURE 3.2: Moment-rotation plots for wind-ups

The first 3 to 4 coils which are closer to the arbor do not undergo any additional plastic straining during the wind-up in addition to the permanent residual strain that they acquired during the spring forming process. The remaining coils undergo plastic deformations on the outer-most ends of the strip section. More coils undergo plastic yielding at the wind-up of 2.25 revolutions compared to the case at the end of the initial

winding phase. These coils cluster along with the inner coils towards the center of the cup. The moment at 2.25 revolutions is 4.73 N.mm, which is within the design specification range of 4.35±0.55 N.mm.

As evident from the moment versus rotation responses shown in Figures 3.2-a. and -b., the numerical results show non-smooth/oscillatory behavior. The origin of the non-smooth response was further investigated. The results suggest that this phenomenon may be due to the discontinuous local in-plane motion (outward and inward 'mechanical-hinge' type of motion) of the spring coils about the kinks, during the wind-ups. Figure 3.3 (which shows the equivalent plastic strain profile in the coils) illustrates this phenomenon with the outward arrows pointing from the regions in the coils corresponding to the kinks. The kinks - being regions of large plastic deformation - contribute as weak spots (in a structural sense) on the strip. Therefore, during the wind-up - as the coils get radially pulled towards the rotating arbor - each of the coils which have the kinks undergo local movements in the outward and inward directions (discontinuously) about the kinks (which act as weak spots), in the plane of the model. A question that arises is: Why do the inward/outward motions lead to a non-smooth response? The results suggest that this phenomenon can be attributed to the following reasons: The movement of a coil (about a kink) in the outward direction increases the torque arms of the material points on the strip about the center of the arbor, and this contributes to an increase in the overall rotational moment of the spring system. On the other hand, the movement of a coil in the inward direction contributes to a reduction in the rotational moment of the system since it decreases the torque-arms of the material points on the strip. These outward/inward motions occur in a discontinuous manner for each of the coils which have kinks

associated with them. This in turn leads to a cyclic increase and decrease of the overall rotational moment of the spring system, thereby causing the non-smooth moment-rotation response.

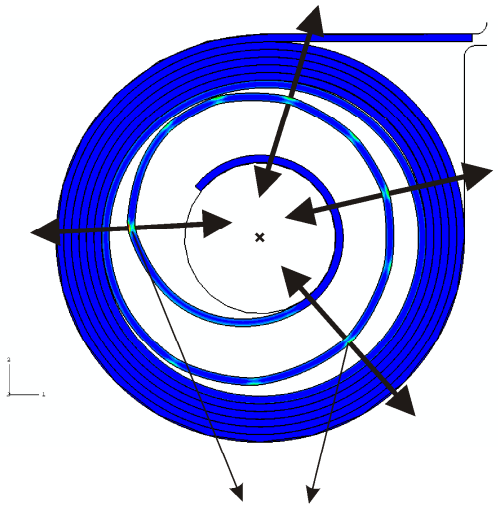

Discontinuous - outward and inward - “mechanical-hinge” type of motion of the coils about the kinks (the figure corresponds to the instantaneous state of the spring just before the wind-up starts)

FIGURE 3.3: PEEQ profile corresponding to the state of the spring during the wind-up

An interesting observation is that the non-smooth moment-rotation response smoothens out in relative terms when the arbor is wound beyond 1 revolution. This phenomenon can be observed in Figure 3.2-b which corresponds to the moment-rotation response for 2.25 revolutions. Investigation into this behavior suggests that beyond a wind-up of 1 revolution the spring coils get extremely tightened leading to very high stress levels (of the order of yield stress) in the majority of the coils. This restricts the local outward and inward in-plane motion of the coils about the kinks. This in-turn leads to the transition to a smoother response beyond 1 revolution.

The values for the resisting torque obtained from the finite element model were found to be reasonably close to the design specifications. Table 3.1 shows a comparison

of the resisting torque for various levels of loading and for different cases of material plasticity and friction. The design specifications are also provided. The torque data provided on the first two rows of the table correspond to the values at the end of the initial winding stage, and the arbor release stage of the spring forming process. It can be observed that the torque at the end of the initial winding stage is reasonably close to (or slightly higher than) the value at the end of 1 revolution. This observation points to the fact that- at the end of the initial winding stage (of the forming process); the spring builds-up significant torque, which is approximately equal to the resisting torque for the actual application. During the arbor release stage, the spring coils completely release the torque which was built-up during the winding stage. This explains the zero torque values in the second row of the table.

TABLE 3.1: Comparison of resisting torque from the finite element model to the design specifications

Levels of wind-up	Torque values obtained from the FE model (N.mm)				Design Specifications (N.mm)
	Perfect Plasticity		Hardening Plasticity		
	Perfect lubrication	No lubrication	Perfect lubrication	No lubrication	
End of winding	3.835	3.861	4.149	4.296	-NA-
Arbor release	0.000	0.000	0.000	0.000	-NA-
1 revolution	3.549	3.759	4.177	4.422	2.9 ± 0.5
2.25 revolutions	4.448	4.730	4.792	5.215	4.35 ± 0.55

We can also observe from the above table that material hardening increases the resisting torque significantly, whereas lubrication reduces it, although to a relatively lower extent. The dependency of resisting torque on the hardening and friction (stick-slip) parameters was further investigated. Figures 3.4-a. and -b. show profiles of the von-

Mises stress and the equivalent plastic strain in the spring coils (with no lubrication) at the end of 1 revolution, for the different cases of material plasticity (i.e., with and without hardening). From the results, hardening was observed to increase the stress levels and reduce the plastic strains in the spring coils (as expected). Since resisting torque is a strong function of the stresses in the coils, the above mentioned increase in the stress-levels leads to a corresponding increase in the torque produced by the spring. For the wind-up of 1 revolution (as shown in Figure 3.4-a), hardening was found to increase the stress levels by about 14%. The corresponding increase in resisting torque is about 18%. For the wind-up of 2.25 revolutions, these values change to 13%, and 10%, respectively. It is interesting to note that the regions of maximum von Mises stress are located at different points on the strip for either cases of material plasticity (as illustrated in Figure 3.4-a). In addition, it can also be observed that relatively more coils are clustered together and located radially outwards from the inner coils, for the case of hardening plasticity. The spring coils do not undergo any additional plastic straining during the wind-ups, in addition to the residual plastic strain that they acquire during the spring forming process. Hardening was observed to reduce the plastic strains in the coils by approximately 75% (Figure 3.4-b shows the PEEQ profile for 1 revolution). This holds true for the case of 2.25 revolutions as well.

The influence of frictional contact on the resisting torque of the spring was investigated in details. For this purpose, the history of contact parameters of certain spring nodes involved in contact was studied. Figures 3.5-a. and -b. show the history of CSLIP (accumulated slip in the local-1 direction tangential to the surface at the point of contact at each instant) and CSHEAR (frictional shear stress which acts in a tangential

direction to the contacting surfaces) [1] for two typical nodes (say, A and B) on the spring coils, which are in contact with the surfaces of the neighboring coils. A positive value for CSLIP indicates 'slipping' of a node in the local-1 direction tangential to the surface at the point of contact.

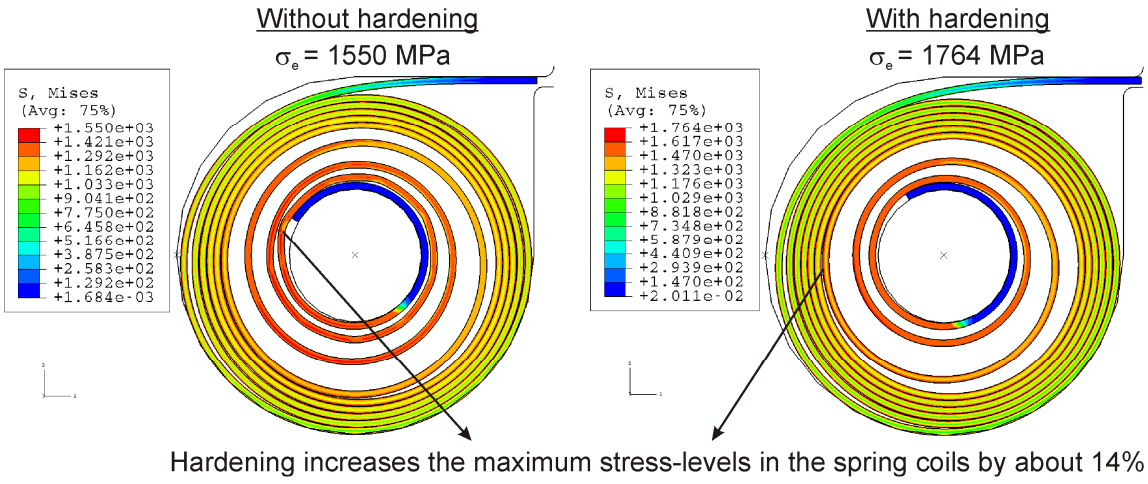

a. von-Mises stress profiles

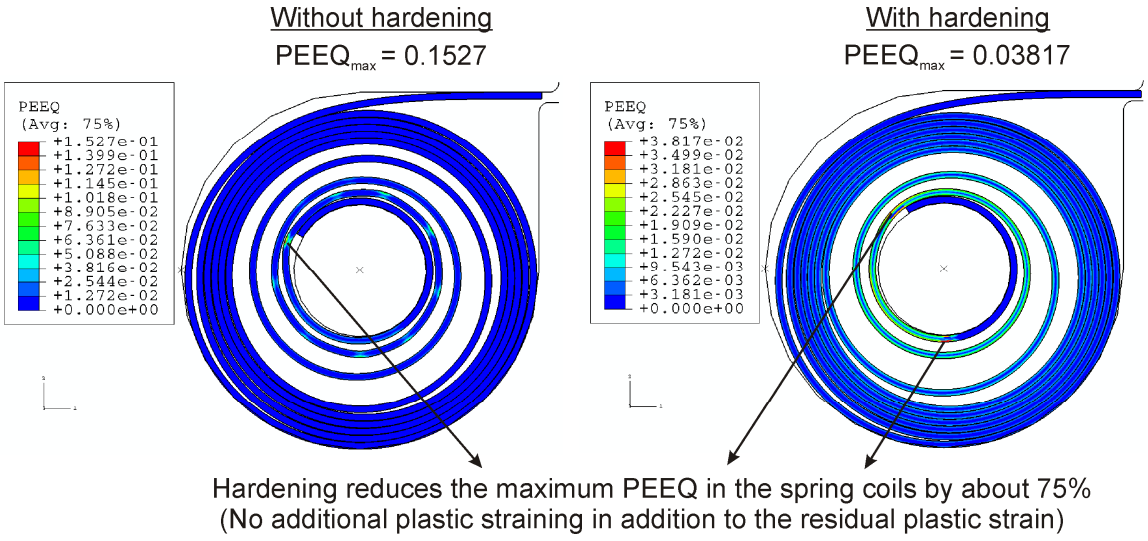

b. PEEQ profiles

FIGURE 3.4: Comparison of spring profiles for the cases of with and without hardening

A zero value for CSLIP corresponds to 'sticking' of the node to the contacting surface. Similarly, a positive CSHEAR refers to frictional shear stress acting on the node in the local-1 direction tangential to the contacting surface. It can be observed from the figures shown below that the nodes experience an extensive nature of the stick-slip behavior during contact.

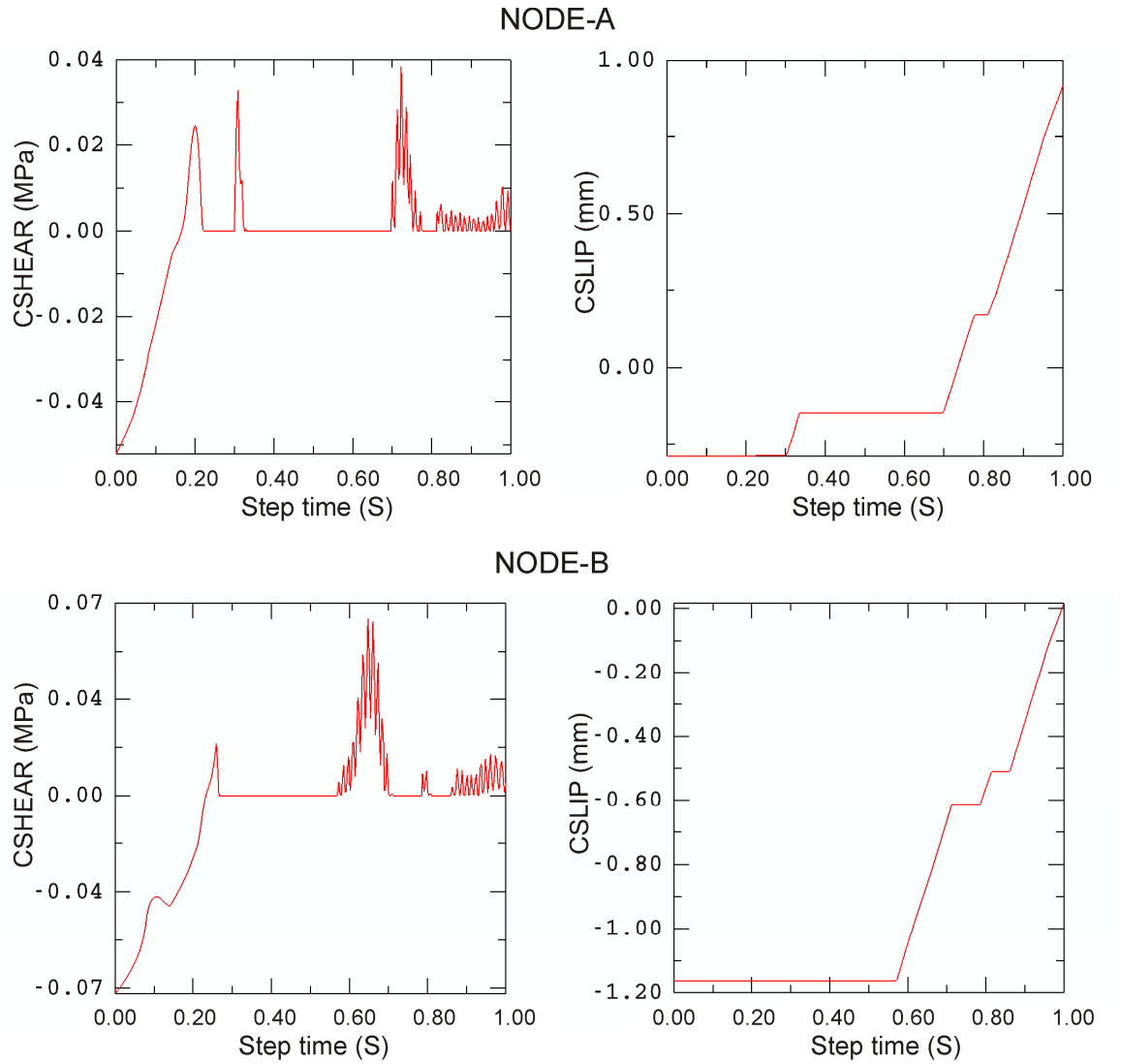

FIGURE 3.5: Comparison of CSHEAR and CSLIP for two nodes involved in contact

Based on the results obtained for material plasticity and frictional contact, it can be inferred that the residual stresses (resulting from the spring forming process), and frictional self-contact (stick-slip behaviors) have a significant influence on the structural response of the spring system.

As mentioned in Chapter 2, the simulations utilized a built-in viscous stabilization scheme in Abaqus to help mitigate the effects of local instabilities in the solution. The viscosity is purely artificial, and should be chosen such that its effects on the physical solution are minimal. To this end, the influence of viscous stabilization on the moment-rotation response was also investigated. Values for the factor of stabilization in the range of $5E-05 \le F \le 3E-04$ were found to generate converging solutions to the discretized problem. Figure 3.6 illustrates the variation of the instantaneous moment with the factor of stabilization, for the wind-ups of 1 revolution and 2.25 revolutions, respectively.

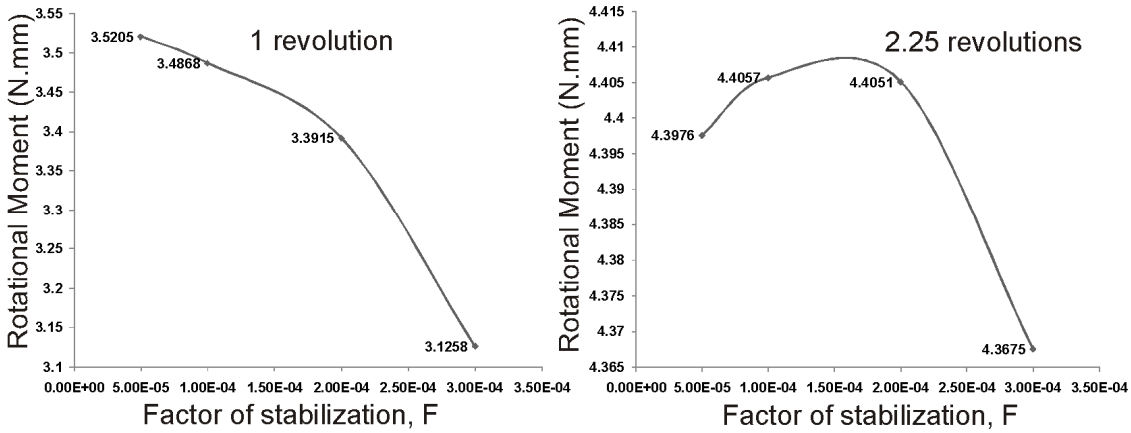

FIGURE 3.6: Comparison of resisting torque for varying factors of stabilization

For both 1 and 2.25 revolutions, the values of the resisting torque were found to increase initially with reducing factor of stabilization- F; with a reduced rate of increase towards the lower range of the value of F. In fact, for 2.25 revolutions the situation is

reversed and the torque appears to be decreasing for the values of F towards the lower limit of the above range. The simulations failed to converge at values of F lower than the range shown in these figures. As mentioned in Chapter 2, the results shown in all the chapters of this dissertation correspond to the lowest factor of stabilization for which the simulations converged: $F = 5E-05$.

3.2.1 Influence of a softer material

The influence of a softer material on the moment-rotation response was also computed in order to get some information on the sensitivity of the numerical results on the material properties. This kind of parametric study is important in any kind of simulations, because the different parameters of the model often cannot be measured exactly. More commonly an analyst works with a range of values, as opposed to a fixed value, for certain parameters. To this end, we obtained results assuming that the initial yield stress of elgiloy is 1.58 GPa, instead of the original value of 1.66 GPa. Table 3.2 shows a comparison of resisting torque for a softer elgiloy material with that of the earlier one, for different cases of material plasticity and loading. It is to be noted that, for the results shown in the table, the ultimate tensile strength is the same for both the cases of the initial yield stress (i.e., approximately 1.86 GPa), and all the results correspond to 'perfect lubrication'. The results obtained suggest that reducing the yield stress by about 5 % reduces the torque by about 5 - 7 % for the case of perfect plasticity, and by less than 1 % for hardening plasticity. This behavior confirms that the resisting torque of the spring has a direct dependency on the stress state of the spring coils. The higher the stress-level in the spring coils, the higher is the torque that the spring is able to provide.

TABLE 3.2: Comparison of torque values of a softer elgiloy material to a harder one

Levels of wind-up	Resisting torque obtained from the FE model (N.mm)				Design Specifications (N.mm)
	Perfect Plasticity		Hardening Plasticity		
	Original material	Softer material	Original material	Softer material	
1 revolution	3.549	3.303	4.177	4.159	2.9 ± 0.5
2.25 revolutions	4.448	4.220	4.792	4.751	4.35 ± 0.55

3.2.2 Mesh convergence studies

Mesh convergence studies were carried out with the goal of optimizing the finite element results. For this purpose, the original mesh was refined with the number of elements along the thickness of the strip increased to 8; i.e., double the number of elements used for the coarser model. The total number of variables used in the new model was about 60,000, with about 28,000 elements. The results for the resisting torque from the refined mesh were found to be only 1 – 2 % different from the results for the coarser mesh. Table 3.3 shows a comparison of the torque values for the fine mesh with that of the coarse mesh, for the different cases of loading. The results suggest that the original model (coarser mesh) provided a very good representation of the physics of the spring, and further mesh refinement did not provide any additional insights.

TABLE 3.3: Comparison of torque values based on the mesh convergence studies

Mesh ratios	Resisting torque (N.mm)	
	1 revolution	2.25 revolutions
Coarse mesh	3.55	4.45
Fine mesh	3.54	4.52

3.3 Procedures and Results: Cyclic moment versus rotation response

The objective of this phase of the modeling effort is to predict the hysteresis associated with the cyclic moment versus rotation response of the torsional spring, and correlate it with the experimentally observed behavior. This is accomplished by subjecting the formed spring to rotation-controlled loading and unloading cycles. The process involves rotating (loading) the spring in the counter-clockwise direction by either 1 revolution or 2.25 revolutions and then rotating it back in the reverse (or clockwise) direction by the same amount. It is observed that the resisting torque, when plotted against the arbor rotation, suggests a remarkable amount of hysteresis. The results are discussed in the following paragraphs.

It was observed that the torque at a given value of rotation was lower during unloading than during loading. This phenomenon is called “hysteresis”, and the torque lost between a wind and unwind within a loading-unloading cycle will be referred to as “hysteresis loss”. Torque was also “lost” at a given rotation during successive winds. The torque-loss involved here will be referred to as the “torque lost in successive winds”. For both the cases, the loss in torque was computed outside of Abaqus - based on the numerical results - as the average of the differences in the torque readings at the various rotational positions of the arbor. The influence of material hardening on the amount of lost torque was also investigated.

Figures 3.7-a. and -b. show the cyclic loading-unloading plots obtained from the finite element simulations for both perfect-plasticity and hardening-plasticity, and for 1 and 2.25 revolutions, respectively (and for the case of no lubrication). For a perfectly-plastic material, the torque lost in successive winds was found to be significant only for

the first two winds, for both 1 revolution and 2.25 revolutions (the loss is more significant for 2.25 revolutions). For the remaining winds, the torque lost in successive winds was found to be approximately zero.

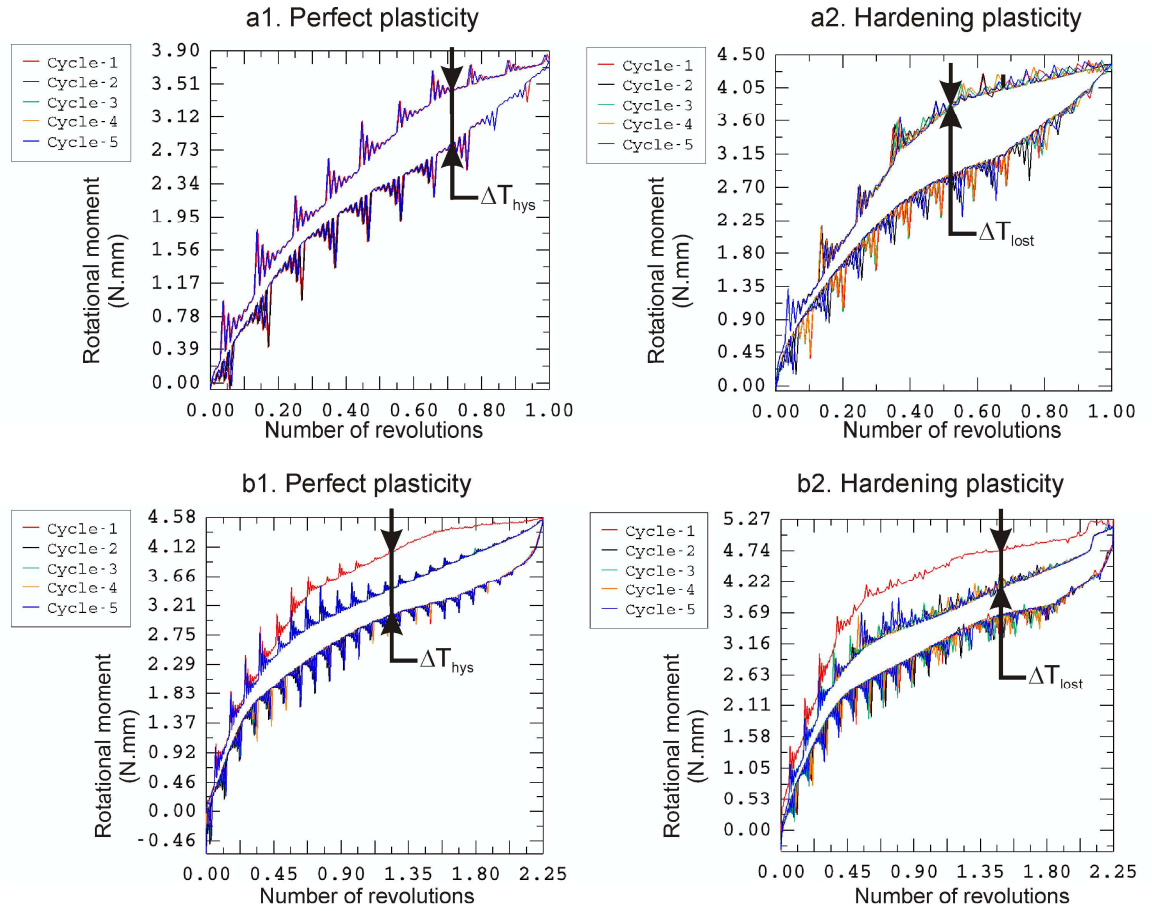

FIGURE 3.7: Cyclic moment-rotation plots: a. 1 revolution b. 2.25 revolutions

Figures 3.8-a. and -b. show the cyclic moment-rotation plots (for both wind-ups and hardening plasticity) - separately - for the first wind and unwind, and for the first two winds and unwinds, respectively. It can be observed that the torque lost between the first two winds is very significant for both perfectly-plastic and hardening-plastic materials. For a hardening-plastic material, on the other hand, additional torque was lost even for the subsequent winds, although the magnitude of torque lost from one winding to the next

was found to decrease with the number of winds. However, for both perfect-plasticity and hardening-plasticity, except for the case of 2.25 revolutions for the first two winds and unwinds, the additional winds were observed to have negligible influence on the hysteresis loss of the spring system. It can be observed from the plots corresponding to the hardening-plastic material (Figures 3.7-a. and -b.) that the loading and unloading curves for each of the successive winds (beyond the first wind and unwind-corresponding to 2.25 revolutions) are shifted vertically downwards from the previous winds by a certain amount.

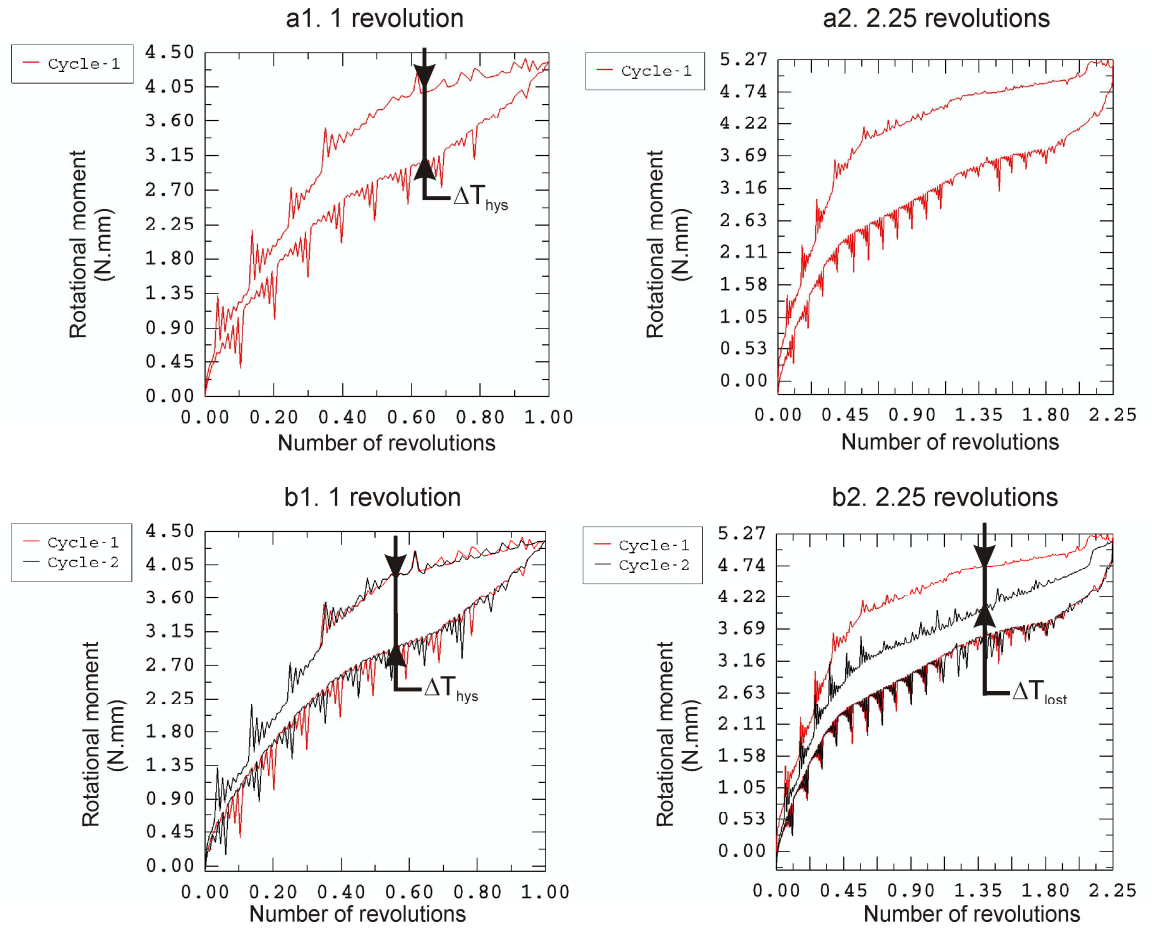

FIGURE 3.8: Cyclic moment-rotation plots: a. First wind-unwind b. Two winds-unwinds

However, the extent of shift is approximately the same for both loading as well as unloading curves, which explains the absence of any additional torque-loss-in-hysteresis during the successive winds.

Figure 3.9 shows a comparison of the cyclic moment versus rotation plot obtained from the finite element model to the corresponding plot obtained from the experiments, for 2.25 revolutions (and for the case of hardening plasticity). It can be observed that the torque values as well as the torque lost values obtained from the finite element simulations are reasonably close to the experimental values. The experimental graph [21] also shows the uncertainties in the torque values.

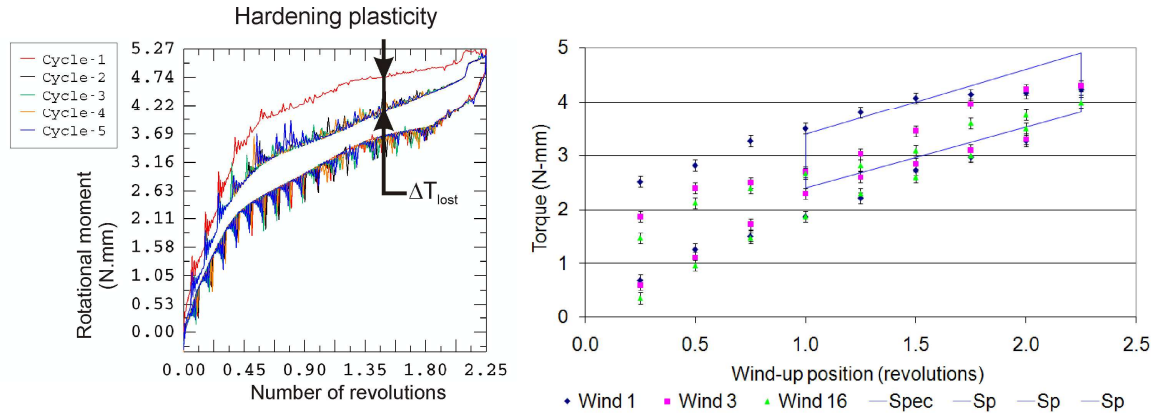

FIGURE 3.9: Comparison of the finite element results with the experimental results [10]

Tables 3.4-a. and -b. show a comparison of the torque lost - both in hysteresis as well as in successive winds over five winds and unwinds - for both perfectly-plastic and hardening-plastic spring materials. As evident from the results shown in the table, the magnitude of the torque lost was found to increase with material hardening- for both kinds of torque losses.

TABLE 3.4: Comparison of the torque-lost readings for different cases of material plasticity and winds

a. Torque lost in successive winds

Average torque lost in successive winds - ΔT_{lost} (mN.mm)				
Combination of winds	Perfect Plasticity		Hardening Plasticity	
	1 rev	2.25 revs	1 rev	2.25 revs
Wind1 - Wind2	8.28	530	28.2	550
Wind2 - Wind3	≈ 0.00	≈ 0.00	15.9	18.4
Wind3 - Wind4	≈ 0.00	≈ 0.00	14.7	15.1
Wind4 - Wind5	≈ 0.00	≈ 0.00	10.4	5.89

b. Torque lost in hysteresis

Average torque lost in hysteresis (within a cycle) - $\Delta T_{hysteresis}$ (mN.mm)				
Combination of Winds	Perfect Plasticity		Hardening Plasticity	
	1 rev	2.25 revs	1 rev	2.25 revs
Wind1 - Unwind1	425	1050	600	1160
Wind2 - Unwind2	425	475	600	615
Wind3 - Unwind3	425	475	600	615
Wind4 - Unwind4	425	475	600	615
Wind5 - Unwind5	425	475	600	615

Friction was observed to have a negligible influence on the cyclic-moment-rotation response of the spring. Hence, the results for lubrication versus no-lubrication are not shown here separately.

3.4 Conclusions

The finite element model that is developed is capable of predicting the static moment versus rotation response of the torsional spring reasonably well. The numerical results for the resisting torque are found to be reasonably close to the experimental results and the design specifications. The results suggest the response to be strongly non-linear with a non-smooth behavior. Non-linear material behavior (i.e., plasticity) appears to be the major contributor influencing the static response. Friction and large deformations appear to make relatively smaller contributions. The yield stress of the spring material is

observed to have a direct influence on the spring response. The results of the mesh convergence studies confirm the quality of the original mesh to be able to capture the spring response with reasonable accuracy. Torsional springs are also observed to exhibit significant hysteresis when subjected to rotation-controlled loading and unloading cycles. The finite element model is capable of capturing this response, and the numerical results compare well with the experimental results.

CHAPTER 4: LONG-TERM STRESS RELAXATION RESPONSE

4.1 Objectives

The primary objective of this modeling phase is to predict the long-term (time-dependant) stress relaxation response of the pre-loaded torsional spring material, and capture the associated torque drop in the spring. This is achieved by allowing the loaded (wound-up) spring to relax over long periods of time, of the order of years or a decade. This form of time-dependant relaxation of the torque in the spring is observed during the actual application of the torsional springs. On the other hand, a slightly different point of view can be adopted in order to better compare the results from the numerical simulations for the time-dependant response of the spring with the experimental data provided by Lawton *et al.* [21]. In the experiments, the spring is subjected to a fixed torque and the resulting arbor rotation is measured as a function of time. In that sense, the experiments measure the rotational creep of the spring at a fixed applied torque as opposed to its torque relaxation at a fixed rotation. Simulations that applied a fixed torque to the arbor reference node and computed its rotation over a period of time were also carried out. The results are compared with the experimental data provided by Lawton *et al.* [21].

As discussed in earlier chapters, the torsional response of the spring is determined by the "base state" of the coils at the end of the forming process. The base state of the coils at the end of spring forming was determined by a detailed model of the spring forming process, and has been discussed in Chapter 2. The results suggested that the coil

material was subjected to a state of residual stress at the end of the forming process. In the absence of additional loading, it is reasonable to expect some of that residual stress to relax over a period of time due to creep in the spring material. Specifically, if the spring is left on the "shelf" for a long period of time before it is actually used, the base state of the coils may be modified significantly (relative to the state at the end of the forming process) as a result of stress relaxation. We refer to this phenomenon as "aging" of the spring. The influence of various levels of aging on the instantaneous as well as the long-term structural responses of the spring is investigated to provide insights into how the shelf-life of the spring affects its subsequent performance. In addition, the influences of design parameters like friction, material plasticity, and creep, are also investigated.

4.2 'Creep' material model

The long-term relaxation response of a torsional spring is due to the effect of creep of the spring material (elgiloy) on the structural response of the spring system as a whole. In order to model this process, it is necessary to have an accurate mathematical description of the basic creep/relaxation behavior of elgiloy.

In general, the overall creep behavior of any typical material involves 3 major stages [9], namely; primary-, secondary-, and tertiary-creep. The spring system studied here is subjected to large time periods of creep/relaxation of the order of years or a decade. Hence, owing to the large time scales, it is reasonable to treat the creep involved here as secondary creep. Figure 4.1 shows a schematic of the strain-time curve for a typical material creep test.

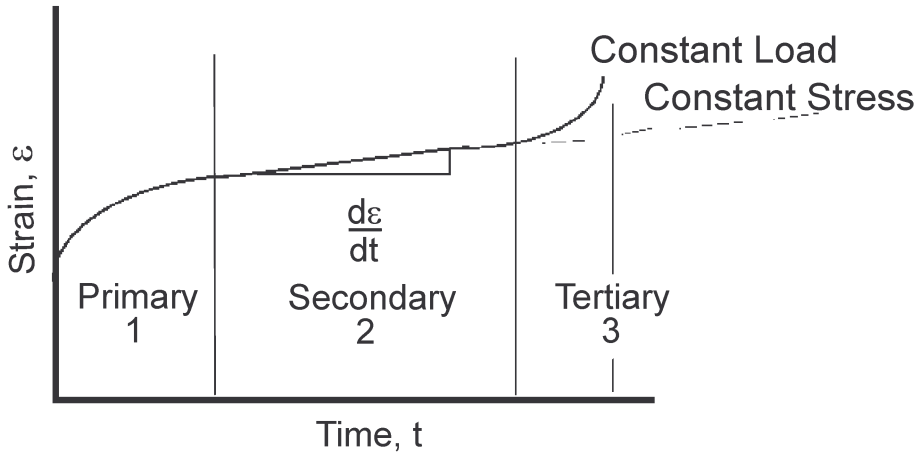

FIGURE 4.1: A schematic of the strain-time curve for a material creep test

Creep properties of the spring material are captured by performing uniaxial tension tests [12] on an elgiloy strip, similar to that used in the spring coils. The test involves holding one end of the strip fixed, and applying a constant tensile load over a period of time at the other end. The elgiloy strip accumulates creep strain, whose magnitude depends on the applied load and the time period over which it is allowed to creep. The data for the rate of creep (at various applied loads) obtained from these tests is then fitted against a steady-state power-law creep model [1], shown in Equation 4.1.

$$\dot{\varepsilon}_{cr} = Aq^n \qquad (4.1)$$

In the above equation, $\dot{\varepsilon}_{cr}$ is the creep strain rate (S^{-1}), q is the von-Mises equivalent stress (MPa), A and n are the power-law creep parameters (which are assumed to be material constants).

The power-law creep model described by Equation 4.1 is available in Abaqus with appropriate generalizations to accommodate a three-dimensional stress state.

Curve fitting of creep strain rates determined at various levels of uniaxial stresses leads to values of A and n of 6E-18 $MPa^{-2.24}S^{-1}$ and 2.24, respectively. Figure 4.2 illustrates a plot of the creep strain rate as a function of the applied stress. The diamonds represent the experimental data points, while the curve represents the best fit to the data points.

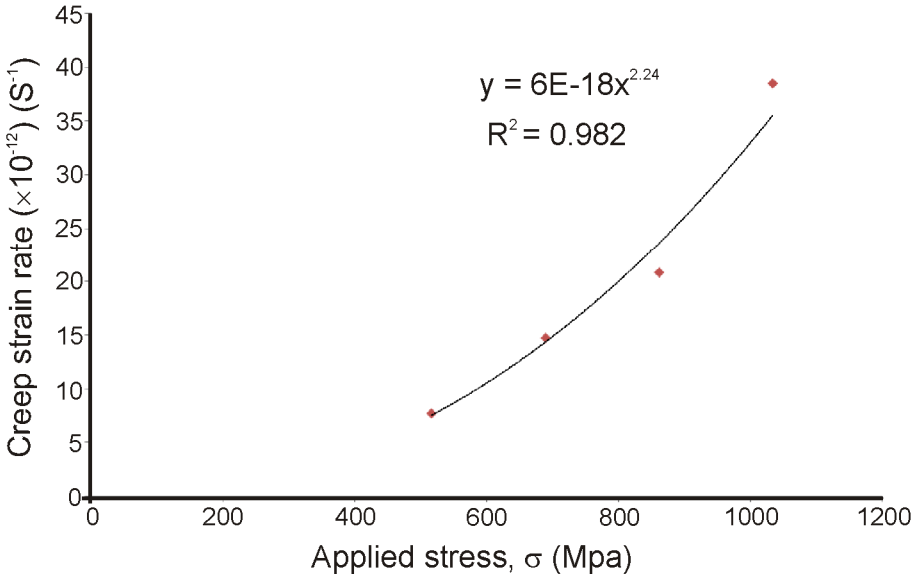

FIGURE 4.2: Plot of the elgiloy creep-strain-rate as a function of the applied stress

The long-term relaxation and creep responses of the spring system are obtained after incorporating the above steady-state material creep behavior in the finite element model described earlier.

4.3 Procedures and Results

The following sub-sections provide the detailed results of the long-term relaxation and creep responses of the torsional spring.

4.3.1 Relaxation simulations

The wound-up (loaded) spring is allowed to relax by fixing all degrees of freedom of the arbor reference node, and hence preventing it from undergoing any translational or rotational motions. The relaxation response of the overall spring system is driven by the stress relaxation in the spring coils, which in-turn leads to a drop in the value of torque at a fixed value of rotation. Recalling that the reaction-moment output at the arbor reference node represents the torque on the spring, any drop in torque is directly available from the output of the finite element simulations. Figures 4.3-a. and -b. show the torque versus time plots for the torsional spring, obtained from the finite element simulations over a period of 1 year of relaxation. The results correspond to the pre-loads of 1 revolution and 2.25 revolutions, respectively; and for the cases of perfect plasticity and "no lubrication". From the plots it can be observed that the relaxation response is non-linear. Moreover, as might be expected, the results indicate that the torque-drop is higher when the spring system is loaded to 2.25 revolutions of the arbor compared to 1 revolution.

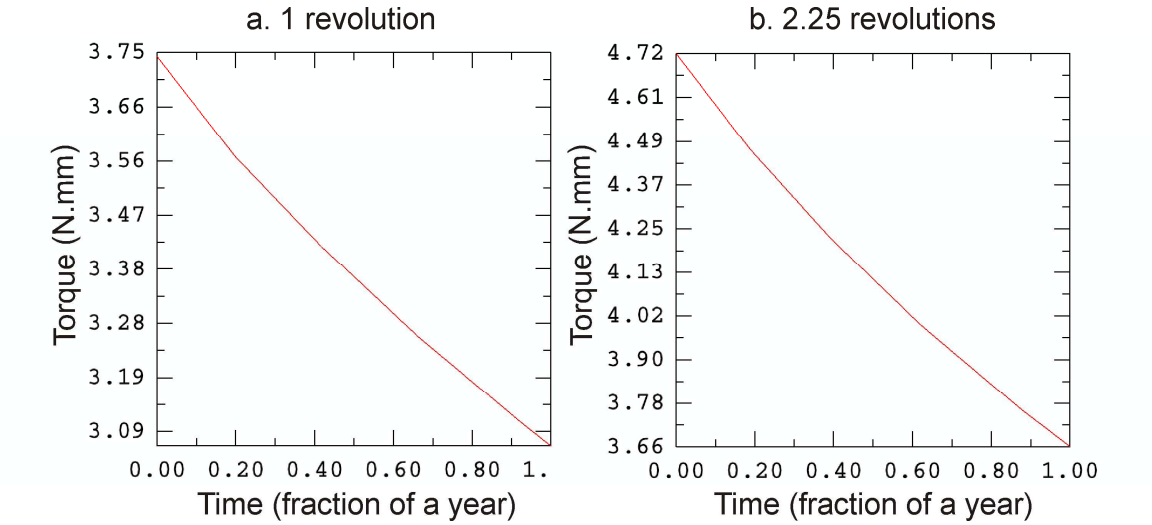

FIGURE 4.3: Torque versus time plots for the torsional spring over a period of 1 year of relaxation corresponding to both the pre-loads

This is due to the relatively higher initial stress-state in the coils of the spring when it is loaded to 2.25 revolutions.

The results obtained indicate an average rate of torque-drop of approximately 1.6 - 2.5 mN.mm/day for a wind-up of 1 revolution, and approximately 2.5 - 3.6 mN.mm/day for the wind-up of 2.25 revolutions of the arbor. Table 4.1 shows a comparison of the values of torque drop for a 'freshly-formed' (zero shelf-life; i.e. the spring is used right after it is formed) spring over varying time periods of relaxation, levels of wind-up, and for different cases of material plasticity and lubrication.

TABLE 4.1: Comparison of the torque-drop values for a freshly formed spring, for different cases of material plasticity, lubrication, and wind-ups

Wind-up positions	Time (days)	Perfect Plasticity		Hardening Plasticity	
		Perfect lubrication	No lubrication	Perfect lubrication	No lubrication
ΔT_{creep} 1 revolution (mN.mm)	1	2.02	2.27	3.04	3.35
	12	24.2	27.1	36.2	40.1
	365 (1 year)	595	658	844	926
ΔT_{creep} 2.25 revolutions (mN.mm)	1	3.34	4.01	4.04	5.06
	12	39.8	47.7	48.0	60.0
	365 (1 year)	923	1057	1079	1303

We also observe that the torque-drop increases significantly when the elgiloy material is modeled with hardening-plasticity (as opposed to perfect plasticity), whereas, lubrication reduces this effect, although to a lower extent. Based on these findings, the residual stresses and frictional self contact were observed to be major contributors that influence the long-term structural response. The magnitude of relaxation of the von-Mises stress in the spring coils during the long-term relaxation phase is about 20% for 1 revolution, and about 25% for 2.25 revolutions, over a period of 1 year of relaxation.

Table 4.2 shows a comparison of the percentages of the maximum von-Mises stress relaxation in the spring coils corresponding to the time periods of 1day, 12 days, and 1 year; for the different levels of pre-load, material plasticity, and lubrication.

TABLE 4.2: Comparison of the percentages of maximum von-Mises stress relaxation for a freshly formed spring

Wind-up positions	Time (days)	Perfect Plasticity		Hardening Plasticity	
		Perfect lubrication	No lubrication	Perfect lubrication	No lubrication
$\%\sigma_{vM}$ 1 revolution	1	0.07	0.06	0.12	0.11
	12	0.86	0.90	1.00	1.08
	365 (1 year)	19.6	20.3	22.5	23.1
$\%\sigma_{vM}$ 2.25 revolutions	1	0.06	0.06	0.11	0.11
	12	0.91	0.91	1.07	1.13
	365 (1 year)	21.1	20.8	23.7	23.5

The influence of viscous stabilization on the long-term relaxation response of the spring is also investigated. It may be noted that the viscous stabilization affects the relaxation response only through its effect on the stress-state of the spring at the end of the forming process. There are no local instabilities occurring during loading and relaxation; hence viscous stabilization has no additional discernable effect during these steps. Figure 4.4 shows the variation of torque-drop for a day of relaxation as a function of the factor of stabilization (for the cases of perfect plasticity and “perfect lubrication”). The plot suggests that the torque-drop increases upon reducing the factor of stabilization. This behavior is in close similarity with the variation of resisting torque as a function of the factor of stabilization, which was discussed in Chapter 2. From Figure 4.4, it can also be seen that, in the optimal case -- as the value for the factor of stabilization approaches zero -- the corresponding value for the torque-drop approaches about 2 mN.mm, for a day

of relaxation. Note that the values provided in Figure 4.4 correspond to the 'absolute' torque-drop of the torsional spring over a day of relaxation, and do not correspond to the average torque-drop per day when the simulation spans a longer period of time (the latter case was discussed in the earlier sections).

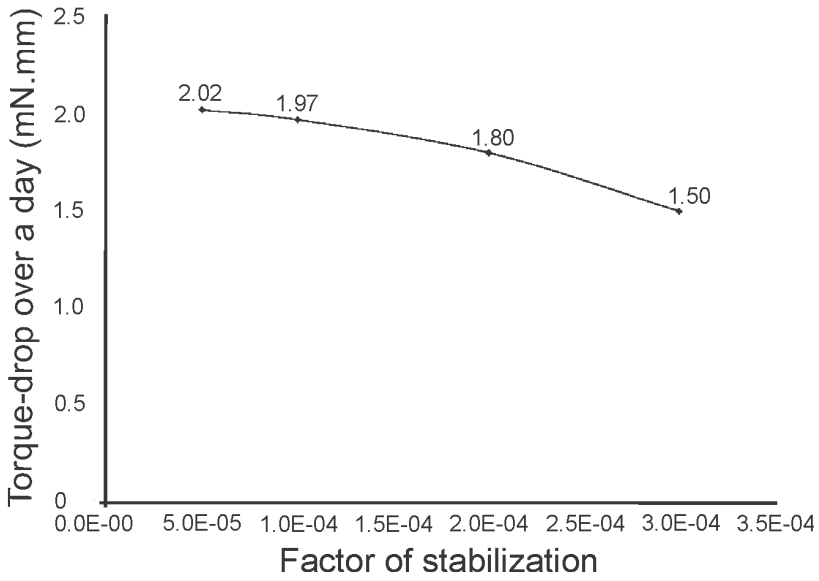

FIGURE 4.4: Plot of the torque-drop in a day as a function of the factor of stabilization

4.3.2 Influence of 'aging' on the response of the spring

The influence of aging (finite shelf-life of the spring) on the instantaneous torque-rotation as well as the long-term torque relaxation responses is investigated. The process of aging involves allowing the formed (coils wound and arbor released, as described in Chapter 2) spring to relax over a specified period of time, which is typically of the order of several years before it is subjected to the actual application (i.e., additional wind-ups). The aging time considered in this research extends from 1 year to 10 years.

Recall that at the end of the forming phase, all the degrees of freedom of the arbor reference node are released. This state is maintained during the aging process, such that

the arbor is free to rotate and translate during aging. The material-creep model which is used to drive the aging response of the spring is the same as the one discussed earlier, which is also used to drive the long-term relaxation response.

The results obtained indicate a significant amount of stress relaxation in the spring coils due to aging. Figure 4.5 shows a comparison of the von-Mises stress contours in the spring coils (for the cases of perfect plasticity and "perfect lubrication") at the end of a 10 year aging process to that of a freshly-formed spring. The results suggest a stress relaxation of about 67% in the spring coils due to 10 years of aging.

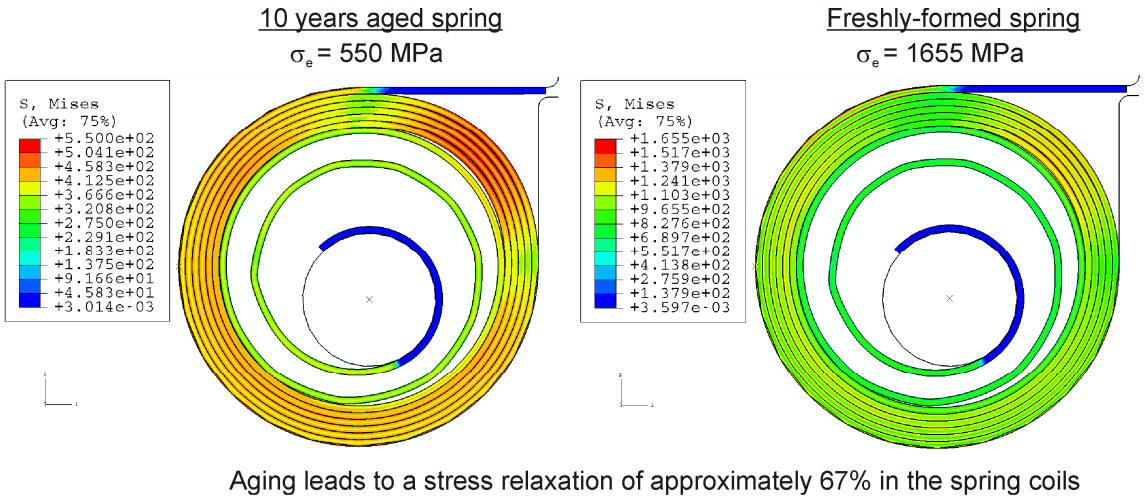

FIGURE 4.5: Comparison of the von-Mises stress profile of the torsional spring- aged for 10 years (left) to that of a freshly-formed spring

The results also predict a clockwise rotational creep of the arbor of approximately 80 milli-radians. Figure 4.6 shows a contour plot for the equivalent creep strain- CEEQ in the spring coils, at the end of the 10 years of aging. The result corresponds to the case of perfect plasticity and "perfect lubrication". A maximum equivalent creep strain of approximately 8E-03 was predicted by the finite element model due to 10 years of aging.

The results also suggest that the maximum creep strain occurs on the outer-most coil of the spring.

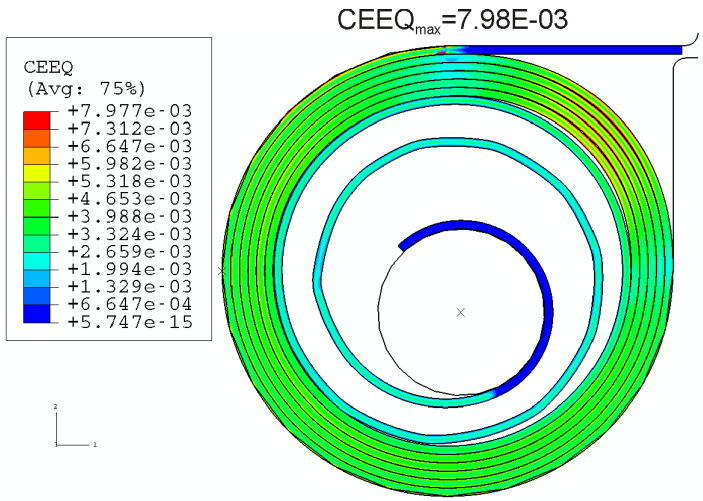

FIGURE 4.6: Contour plot of the equivalent creep strain in the spring coils after the 10 years of aging

The aged spring is then subjected to wind-ups (i.e., the spring is loaded) in order to capture its instantaneous torque-rotation response. The results indicate a significant reduction in the resisting torque (for a given rotation) for the aged spring, when compared to a freshly-formed spring. Figure 4.7 shows the moment-rotation response of a spring aged for 10 years, along with the corresponding von-Mises stress contours, for the cases of perfect plasticity and perfect lubrication and for different levels of loading. Figure 4.8-a. shows a comparison of the moment versus rotation response of a spring aged for 10 years to that of a freshly-formed spring for a pre-load of 1 revolution (for the cases of perfect plasticity and perfect lubrication). From the plots it can be seen that the moment-rotation response is extremely non-smooth for an aged spring, the magnitude of the local oscillations in the response being higher than the case for a freshly-formed spring (which is discussed in Chapter-3).

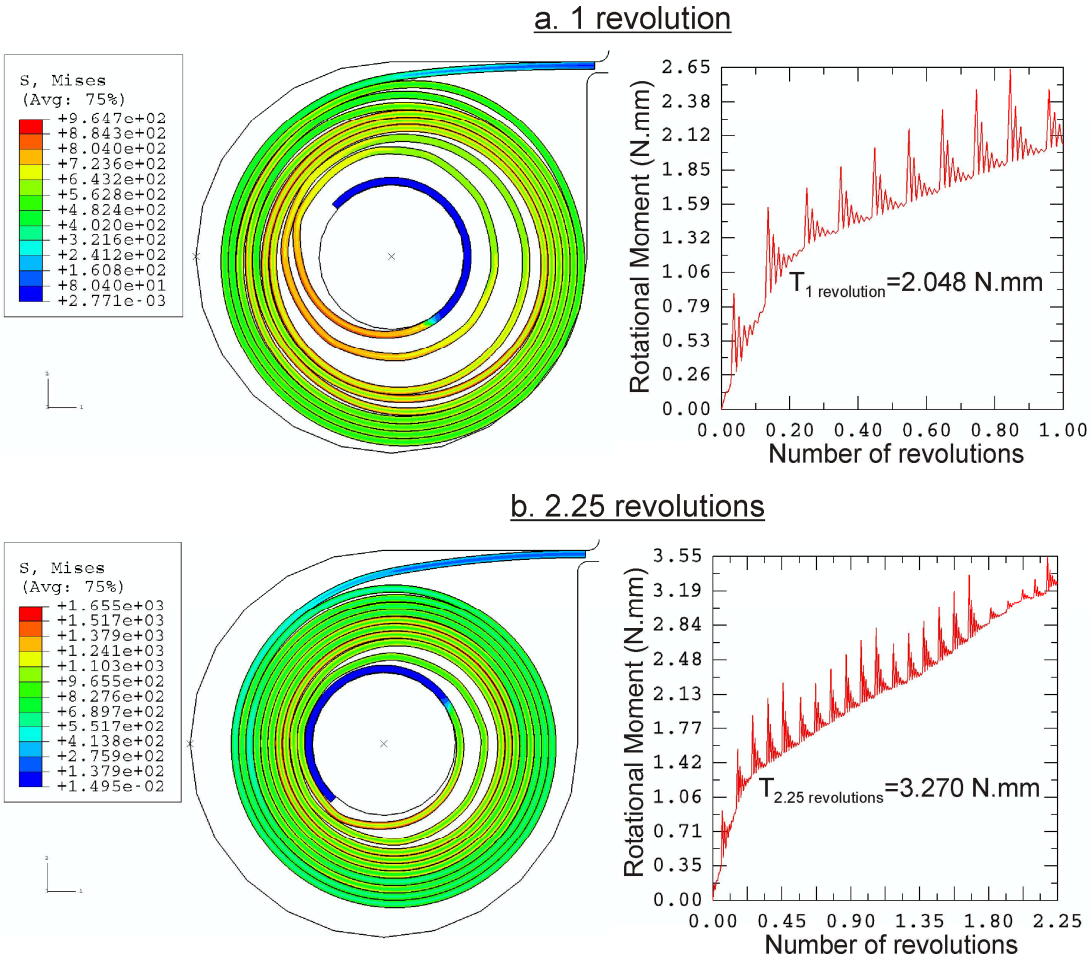

FIGURE 4.7-a&b: Moment-rotation responses for a 10 years aged spring under wind-ups of 1 revolution and 2.25 revolutions

Investigation into this behavior suggests that the lowering of the residual stresses in the spring coils- as a result of aging, results in a correspondingly lower level of total stress during the subsequent wind-ups. Such a relatively lower overall stress level in the coils, compared to the yield stress of the material, ends up having the side-effect of retaining the kinks that were introduced in the inner coils during the forming phase of the spring. This in-turn increases the in-plane 'mechanical-hinge' type of motion of the coils during the wind-ups (discussed in Chapter 3), thereby leading to a relatively higher non-smooth response. Figure 4.8-a. shows a comparison of the von-Mises stress contour of a

spring aged for 10 years to that of a freshly-formed spring for a pre-load of 1 revolution. The maximum von Mises stress in the coils reduces by about 36% during the wind-up of 1 revolution as a result of the aging process. This general behavior appears to occur for the case of 2.25 revolutions of the arbor as well, since a majority of the coils still remain at low stress levels with only a few locations in 2 or 3 coils undergoing yield. Hence, a higher level of non-smooth response is found to prevail even for the case of 2.25 revolutions- for a spring aged for 10 years, when compared to a freshly-formed spring.

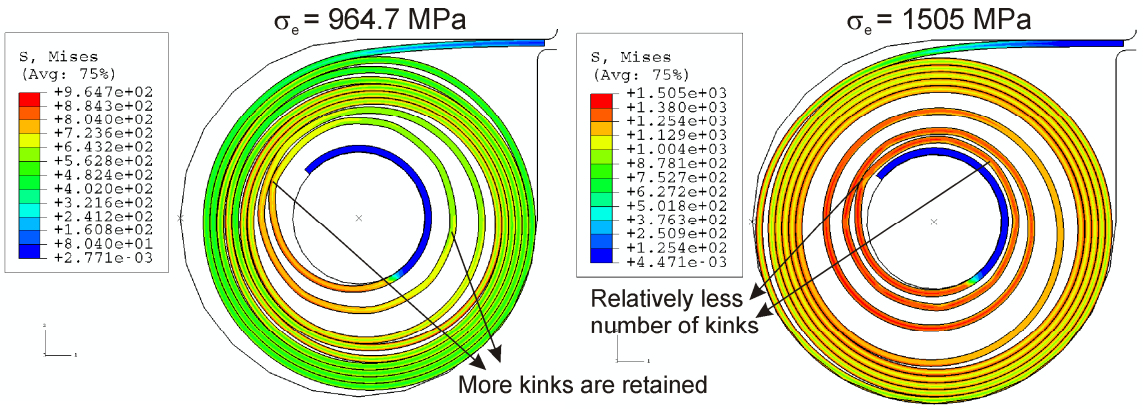

Aging reduces the stress levels in the spring coils during the subsequent wind-ups

a. Profiles of the von-Mises stress

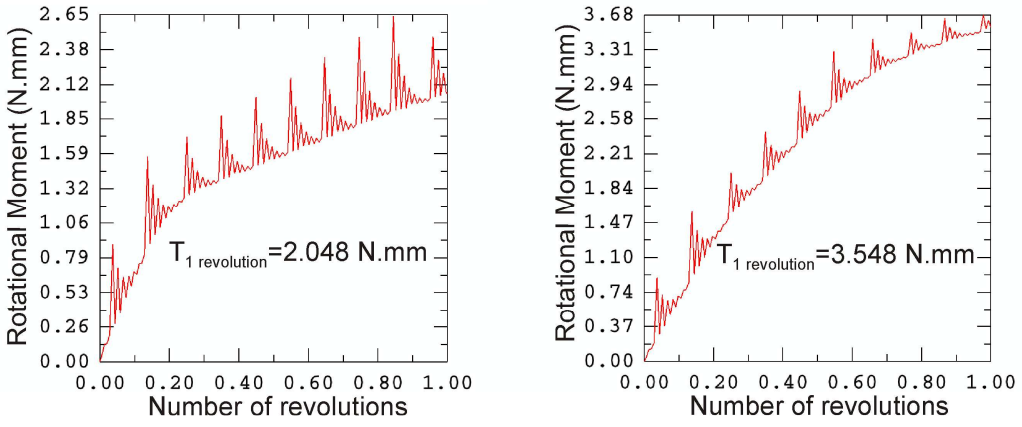

b. Moment versus rotation responses

FIGURE 4.8: Comparison of the results of a torsional spring- aged for 10 years (left), to that of a freshly-formed spring at a pre-load of 1 revolution

For a freshly-formed spring, on the other hand, the non-smooth response was found to subside after 1 revolution (discussed in Chapter 3) owing to the relatively higher stress levels in the coils as a result of extensive tightening of the coils- beyond a wind-up of 1 revolution. However, for a spring aged for 10 years, the lowering of the overall stress levels in the coils as a result of the aging process leads to the retention of the kinks in the inner coils even at the subsequent wind-up of 2.25 revolutions. The presence of these kinks sustains the non-smooth behavior of the torque-rotation response beyond a wind-up of 1 revolution.

Table 4.3 shows a comparison of the resisting torque at 1 revolution and 2.25 revolutions, respectively, for a spring subjected to 10 years of aging to that of a freshly-formed spring. For both the cases, perfect plasticity and perfect lubrication are assumed. The design specifications are also provided in the table for reference. It can be observed that as a result of 10 years of aging, the resisting torque drops approximately 42% for 1 revolution, and approximately 27% for 2.25 revolutions.

TABLE 4.3: Comparison of the torque values of an aged spring to a freshly-formed one

ADDITIONAL WIND-UPS à	1 revolution	2.25 revolutions
SPRING TYPE	Resisting torque (N.mm)	
Freshly formed spring	3.55	4.45
Aged spring (for 10 Years)	2.05	3.27
Design specifications	2.9 ± 0.5	4.35 ± 0.55

In the next phase of the study on aged springs, the wound-up aged spring is allowed to relax over a period of time of the order of several years in order to capture its long-term relaxation response and compare it to that of the freshly-formed spring as well

as the experimental measurements of Lawton *et al.* [21]. Table 4.4 shows a comparison of the torque-drop over a period of 1 year, for a spring aged for 10 years to that of a freshly formed spring, under the assumptions of perfect plasticity and perfect lubrication. The experimental data obtained by Lawton *et al.* [21] are also provided. For the case of a freshly-formed spring, the finite element model predicts a torque-drop that is 30 and 46 times higher compared to the experimental predictions, for the cases of 1 revolution and 2.25 revolutions of the arbor, respectively. However, for a spring aged for 10 years, these multiples dropped to 10 and 26 times, respectively, for the same levels of wind-up.

TABLE 4.4: Comparison of the torque-drop values (over 1 year) for a 10 years aged spring to a freshly-formed one for the cases of perfect plasticity and perfect lubrication

ADDITIONAL WIND-UPS à	1 revolution	2.25 revolutions
SPRING TYPE	Torque-drop values (mN.mm)	
Freshly formed	595	923
Aged (10 Years)	193	528
Experimental results	≈ 20	≈ 20

The discrepancy in the magnitude of the torque relaxation between the finite element and the experimental results was further investigated. Given that the instantaneous results from the finite element simulations are reasonably close to the design specifications, the above discrepancies in the time-dependant torque-drop results is somewhat unexpected. While the reasons for the discrepancy are not entirely transparent, we present some plausible arguments in the rest of this subsection. To understand this matter further, we present in Chapter-5 a first-principles analytical approach that relies on the instantaneous finite element results to obtain an order-of-

magnitude estimate for the torque drop. The results of that study also appear to be in-line with the finite element estimates.

At this point we suspect that the primary reason for the discrepancies between the numerical and the experimental results may be inaccuracies in the determination of the material creep parameters that drive the time-dependant component of the finite element simulations. More recent experiments conducted by Lawton *et al.* [21] suggest that the earlier estimates for the creep parameters may have been obtained before the spring material reached a state of steady creep. We expect that the steady-state rates of creep may be significantly smaller compared to the previously measured values that were used to drive the numerical simulations. Since the material creep parameters determined from such steady-state creep test data drives the long-term response of the spring, lower values of the measured steady-state creep rate in the uniaxial tests may translate to significant reductions in the torque-drop results predicted by the finite element simulations.

An interesting and rather unintuitive observation that can be made from the experimental results for torque-drop is that the measured values of torque-drop over a period of 1 year is the same for the cases of 1 revolution and 2.25 revolutions of preload. On the contrary, the finite element results indicate that the torque-drop depends strongly on the level of preload. Thus, it can be observed from Table 4.4 that the torque-drop over a time period of 1 year for a spring that has been aged for 10 years is 193 mN.mm for one revolution preload and 528 mN.mm for 2.25 revolutions preload. The finite element results appear more intuitive physically based on the fact that a higher average stress state in the coils associated with 2.25 revolutions can be expected to lead to higher rates of relaxation compared to the relatively lower stress states due to a 1 revolution preload. We

expect that the higher rate of stress relaxation in the coils would translate to a higher rate of torque-drop.

The influence of the time-period of aging on the relaxation response of the spring is investigated and the results summarized in Figure 4.9, which represents the variation of the torque-drop over 1 year of relaxation as a function of the period of aging. As suggested by the figure, the behavior follows an exponential decay. This indicates that beyond a period of 10 years, the aging time does not have significant influence on the torque-drop response.

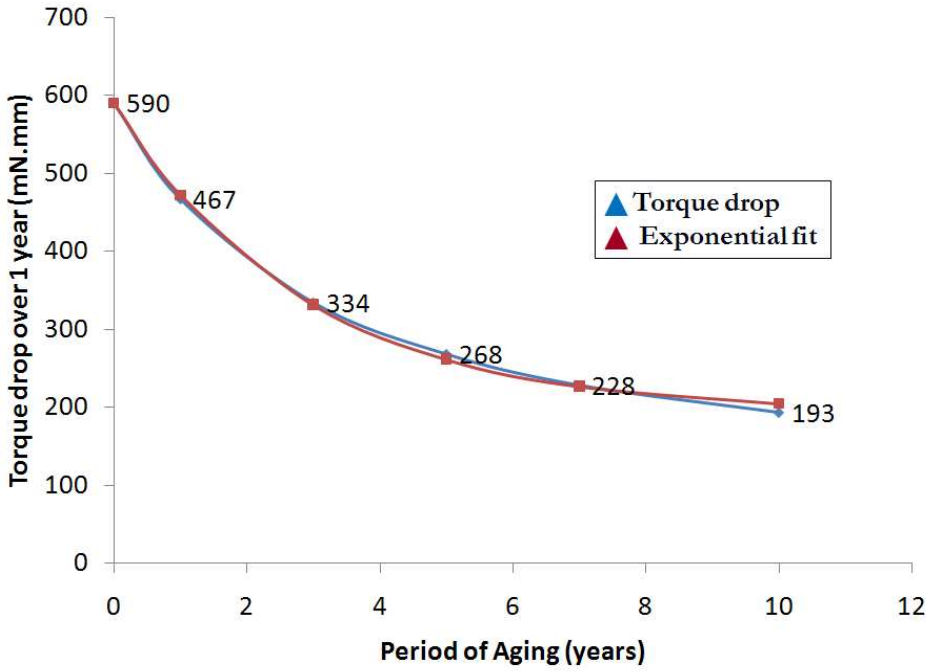

FIGURE 4.9: Plot of the variation of torque-drop (over 1 year of relaxation) as a function of the aging time

4.3.3 Simulations of rotational creep of the spring

The setup of the finite element model for determining the relaxation response of the torsional spring system is analogous to the set up experienced by the spring during the

actual application. It involves restraining the motion of the arbor in all its degrees of freedom after the spring is loaded, and allowing the stresses in the coils to relax over long periods of time- thereby leading to a drop in the resisting torque. The experiments [21], on the other hand, measure the long-term rotational creep of the arbor by subjecting the spring to a constant torque and restraining the arbor from any translational motion. The measured values of the rotational creep at various levels of wind-up are then converted to estimates for lost torque using a rigidity modulus. Thus, the finite element model captures the long-term stress relaxation in the spring coils and the associated torque-drop at constant rotation, whereas the experiments measure the long-term rotational creep of the arbor at a constant applied torque. It is very difficult, if not impossible to directly capture the relaxation response of the spring using the currently available experimental techniques. In order to replicate the experimental procedure for determining the long-term response of the spring system more closely, a set of finite element simulations were carried out to compute the rotational creep of the spring system under a constant applied torque.

The formed spring is subjected to a constant applied torque that is numerically equal to the torque obtained from previous models at 1 revolution of the arbor. The arbor is restricted from any translational motion during this process. The applied torque leads to rotation of the arbor that in turn tightens the coils of the spring. The amount of rotation over a certain period of time is a measure of the rotational creep of the spring system.

The rotational creep computed based on the finite element simulations are compared to those obtained from experiments in Table 4.5. The applied torque on the spring is 3.55 N.mm, which approximately corresponds to the value of the resisting

torque at 1 revolution. The finite element model predicts an average rate of rotational creep of approximately 12.5 mrads/day.

From the table it can be observed that the rotational creep predicted by the finite element simulations is much higher than the experimental results. For example, the finite element results for the rotational creep over a period of 1 year is approximately 35 times higher than the corresponding experimental results. The results showing significantly larger predictions for creep from the finite element simulations are consistent with the earlier observations for the loss in torque in the spring due to stress relaxation in the coils. The rotational creep results further suggest that the discrepancies between the numerical and the experimental results are not due to the differences in the methodology of measurements, but rather due to other reasons such as possible inaccuracies in the determination of the material creep parameters from the uniaxial tension tests.

TABLE 4.5: Comparison of the rotational creep values obtained from the finite element model to the experimental results

Results	Rotational creep at 3.55 N.mm of torque (mrads) (corresponding to a wind-up of 1 revolution)		
	1 day	12 days	1 year
FE model	75	215	4558
Experiments	16	30	132

The influence of higher torque loads on the rotational creep response is also investigated. For this purpose, the formed spring is subjected to a higher magnitude of torque of 4.7 N.mm, which is approximately equal to the resisting torque at a wind-up of 2.25 revolutions. The spring system is then allowed to creep. The results indicate a much

smaller value for the rotational creep than obtained with a torque load of 3.55 N.mm. The average rotational creep rate in this case is approximately 1.23 mrads/day.

Table 4.6 shows a comparison of the rotational creep over a 1 year period obtained from the finite element model for different values of the applied torque. The corresponding experimental results are also provided. The rotational creep for an applied torque of 4.7 N.mm is only about $1/10^{th}$ of the rotational creep for an applied torque of 3.55 N.mm. This observation suggests that while the magnitude of the torque-drop increases at a higher applied rotation, the magnitude of the rotational creep reduces with an increase in the applied torque.

TABLE 4.6: Comparison of the rotational creep values obtained from the finite element model to the experimental results - for varying torque loads

Rotational creep over a period of one year (mrads)		
Torque loads	3.55 N.mm ($\approx T_{1\ rev}$)	4.7 N.mm ($\approx T_{2.25\ revs}$)
FE model	4558	450
Experiments	132	132

The reason behind the lowering of the rotational creep at higher torque loads is investigated. The results suggest that at extremely high loads, the spring coils get extensively tightened, leading to 'geometric locking' of the coils. This restricts the rotational displacement of the arbor during creep, which in-turn reduces the rotational creep. Figure 4.10 illustrates the 'locking' phenomenon. The similarities in the experimentally measured values for the torque-drop at 1 revolution and 2.25 revolutions of the arbor (also shown in Table 4.4) may also be attributed to this 'locking' phenomenon.

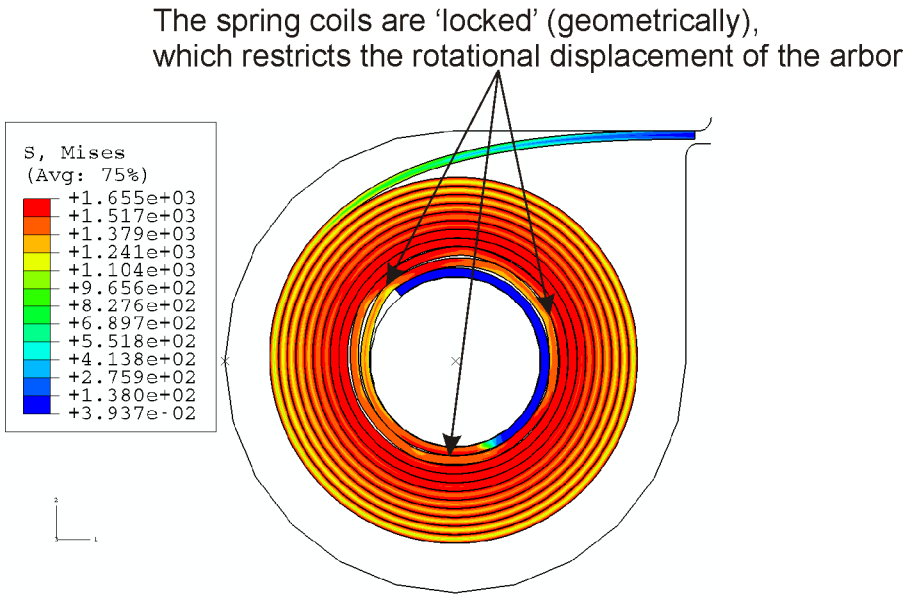

FIGURE 4.10: Representation of 'geometric-locking' of the spring coils at a wind-up of 2.25 revolutions

4.3.4 Mesh convergence studies

Mesh convergence studies are carried out with the goal of optimizing the finite element results obtained for the long-term relaxation response of the spring including the effects of aging. The refined mesh which was used earlier for mesh convergence studies of the moment-rotation response is used for the present study of the long-term relaxation response as well. The number of elements used along the thickness of the strip is 8; i.e., twice the number of elements used for the coarser model. The total number of variables used for the refined mesh is about 60,000, with about 28,000 elements.

Mesh convergence studies are first conducted on the moment-rotation response of an aged spring (similar studies on the freshly-formed spring were discussed earlier in Chapter 3). Table 4.7 shows a comparison of the resisting torque for the two different meshes for a spring aged for 10 years, under different loading conditions. The results indicate that the resisting torque for an aged spring change only by 1 - 2% as a result of

the mesh refinement. This suggests that the original mesh is sufficiently refined to accurately capture the behavior of an aged spring.

TABLE 4.7: Comparison of resisting torque for an aged spring (10 years) based on the mesh convergence studies

Levels of wind-up	Resisting torque (N.mm)	
	1 revolution	2.25 revolutions
Coarse mesh	2.05	3.27
Fine mesh	2.07	3.34

Influence of mesh refinement on the long-term relaxation response of the spring is also investigated. With a refined mesh, the values of torque-drop change only by 1% and 5%, respectively, for the cases of 1 revolution and 2.25 revolutions of preload. Table 4.8 shows a comparison of the torque-drop values for a freshly-formed spring to that of a spring aged for 10 years, for the two different meshes.

TABLE 4.8: Comparison of the torque-drop values for a freshly-formed spring to that of a 10 years aged spring based on the mesh convergence studies

Levels of wind-up	Torque-drop values (mN.mm)			
	Freshly formed spring		Aged spring (10 years)	
	1 rev	2.25 revs	1 rev	2.25 revs
Coarse mesh	595	923	193	528
Fine mesh	581	965	195	555

The results obtained from the mesh convergence studies suggest that the original mesh is able to accurately capture the long-term relaxation response of the torsional spring.

Note: The above results for mesh convergence studies correspond to the case of "perfect lubrication" and "perfect plasticity".

4.4 Results for the instantaneous and long-term responses of the torsional spring based on the recent values of the creep and yield parameters of the elgiloy material

The results of the most recent uniaxial tension tests conducted by Lawton *et al.* [21] suggest that there is an uncertainty in the values of the material creep parameters obtained from the experiments. Since these creep parameters are used to drive the long-term relaxation response of the spring system, any change in their values can lead to a significant change in the torque-drop response predicted by the finite element model. The new reported values are: - $A = 2E\text{-}20\ MPa^{-2.8}S^{-1}$ and $n = 2.8$. Similarly, the recent data available for the yield properties of the elgiloy material [10] suggest that the material may be softer than it was originally thought to be. Accordingly, the new value for the yield stress of the elgiloy material was reported to be $\sigma_y = 1580$ MPa, in comparison to 1655 MPa considered earlier. The following sub-sections discuss the results obtained from the finite element simulations which incorporate the new values for the creep and yield parameters of the elgiloy material.

4.4.1 Influence of the new material properties on the instantaneous response of the spring

Finite element simulations were carried out incorporating the new values for the yield stress and the creep parameters of the elgiloy material. During the wind-up stage of the spring - for the new simulations, contrary to the earlier cases - the arbor is subjected to a sequential wind and un-wind cycle before it is actually wound-up to capture the resisting torque. The purpose of this additional operation is to remove any major torque-loss that would creep-in due to the cyclic moment versus rotation response of the spring. From the recent data obtained on the spring system [10], it is understood that the actual

application follows the same approach. Tables 4.9-a. and -b. show the results for the resisting torque for a freshly-formed spring and for a spring aged for 10 years, respectively. The results correspond to the pre-loads of 1 revolution and 2.25 revolutions, and for the different cases of material plasticity and lubrication. The design specifications are also provided.

TABLE 4.9: Comparison of the resisting torque values for the different cases of material plasticity, loading, and lubrication, based on the new yield and creep parameters

a. Resisting torque values for a freshly-formed spring

Levels of wind-up	Torque values obtained from the FE model (N.mm)				Design Specifications (N.mm)
	Perfect Plasticity		Hardening Plasticity		
	Perfect lubrication	No lubrication	Perfect lubrication	No lubrication	
1 revolution	3.282	3.524	4.156	4.412	2.9 ± 0.5
2.25 revolutions	4.216	4.528	4.743	5.142	4.35 ± 0.55

b. Resisting torque values for a spring aged for 10 years

Levels of wind-up	Torque values obtained from the FE model (N.mm)				Design Specifications (N.mm)
	Perfect Plasticity		Hardening Plasticity		
	Perfect lubrication	No lubrication	Perfect lubrication	No lubrication	
1 revolution	2.831	3.024	3.367	3.581	2.9 ± 0.5
2.25 revolutions	3.972	4.370	4.477	4.926	4.35 ± 0.55

The results obtained from the sequential wind and unwind cycle indicate that the torque-loss between the first wind and unwind vary between approximately 0.02 mN.mm to about 26 mN.mm based on the type of lubrication, material plasticity, and pre-load. The results also suggest that for the case of perfect plasticity, the resisting torque reduces by approximately 4 - 8% as a result of the new value for the yield stress. For the case of

hardening plasticity, the percentage reduction is less than 2%. On an average, it can be seen that the new resisting torque values are in a relatively better comparison with the design specifications compared to the values obtained earlier (shown in Table 3.1 in Chapter 3).

For a spring which is aged for 10 years, on the other hand, the resisting torque values are found to increase by approximately 30% for a pre-load of 1 revolution, and by about 20% for 2.25 revolutions, as a result of the reduced yield stress. This increase in the torque values can be attributed to the fact that the amount of stress relaxation during the process of aging reduces as a result of the reduction in the maximum residual stress at the end of the forming stage.

For all the results shown above, material hardening increases the resisting torque significantly, whereas lubrication reduces it, although to a lower extent. This behavior is in close comparison with the response seen with the earlier value for the yield stress.

4.4.2 Influence of the new material properties on the long-term response of the spring

The influence of the new creep and yield parameters on the long-term relaxation response of the spring system is also investigated. Tables 4.10-a. and -b. show the long-term torque-drop values of a freshly-formed spring and a spring aged for 10 years, respectively. The results correspond to varying time periods of relaxation, levels of wind-up, and for different cases of material plasticity and lubrication. For a freshly-formed spring, the new results indicate an average rate of torque-drop of approximately 0.28 - 0.63 mN.mm/day for the wind-up of 1 revolution, and approximately 0.55 - 1.00 mN.mm/day for the wind-up of 2.25 revolutions of the arbor. For an aged spring (subjected to 10 years of aging), these values drop to approximately 0.18 - 0.35

mN.mm/day for the wind-up of 1 revolution, and approximately 0.48 - 0.90 mN.mm/day for the wind-up of 2.25 revolutions. The new results obtained for the torque-drop are in a relatively close agreement with the experimental results, in comparison to the results discussed earlier in the chapter (shown in Table 4.1).

TABLE 4.10: Comparison of the torque-drop values for the different cases of material plasticity, loading, and lubrication, based on the new yield and creep parameters

a. Torque-drop values for a freshly-formed spring

Wind-up positions	Time (days)	Perfect Plasticity		Hardening Plasticity	
		Perfect lubrication	No lubrication	Perfect lubrication	No lubrication
ΔT_{creep} 1 revolution (mN.mm)	1	0.30	0.35	0.60	0.68
	12	3.55	4.18	7.21	8.17
	365 (1 year)	103	121	203	230
ΔT_{creep} 2.25 revolutions (mN.mm)	1	0.59	0.75	0.83	1.11
	12	7.15	9.05	9.97	13.3
	365 (1 year)	202	255	277	366

b. Torque-drop values for a spring aged for 10 years

Wind-up positions	Time (days)	Perfect Plasticity		Hardening Plasticity	
		Perfect lubrication	No lubrication	Perfect lubrication	No lubrication
ΔT_{creep} 1 revolution (mN.mm)	1	0.19	0.22	0.32	0.36
	12	2.29	2.69	3.84	4.41
	365 (1 year)	67.2	78.8	111	128
ΔT_{creep} 2.25 revolutions (mN.mm)	1	0.51	0.68	0.72	0.99
	12	6.09	8.20	8.67	11.8
	365 (1 year)	174	232	242	327

The magnitude of relaxation of the von-Mises stress in the spring coils over a period of 1 year of relaxation is about 5% for a pre-load of 1 revolution, and about 6% for 2.25 revolutions. The results also suggest a stress relaxation of about 31% in the spring

coils due to 10 years of aging in comparison to 67% which was predicted by the earlier creep parameters. Figure 4.11 shows a comparison of the profiles of the equivalent creep strain- CEEQ obtained from the finite element simulations for the new creep properties to the simulations for the old creep properties. The results suggest that the maximum equivalent creep strain in the spring coils reduces by about 58% due to the new creep properties.

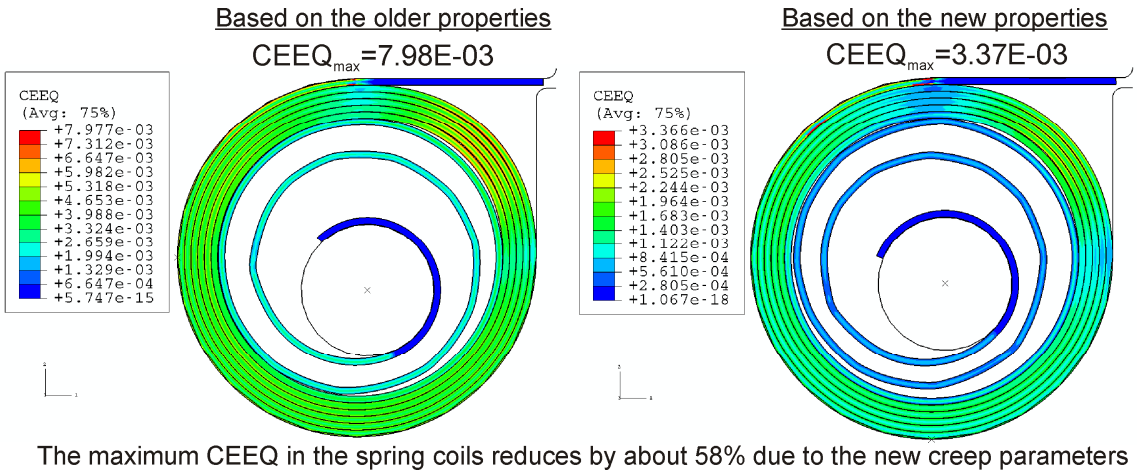

FIGURE 4.11: Comparison of the equivalent creep strain distribution in the spring coils due to the change in the creep parameters

Table 4.11 shows a comparison of the torque-drop results obtained from the finite element model to the experimental data obtained by Lawton *et al.* [21] - for the different pre-loads of the spring. The finite element results are provided for both- a freshly-formed spring as well as a spring aged for 10 years; and the results follow the assumption of "no lubrication". The results indicate that for the case of a freshly-formed spring, the finite element model predicts a torque-drop that is 6 - 18 times higher compared to the experimental predictions, depending on the nature of material plasticity and pre-load.

However, for a spring aged for 10 years, this range dropped to 4 - 16 times, depending on the same factors (material plasticity and pre-load).

TABLE 4.11: Comparison of the torque-drop values over 1 year of relaxation, obtained from the finite element model to the experimental results

Additional wind-ups à	ΔT_{creep} for 1 revolution (mN.mm)		ΔT_{creep} for 2.25 revolutions (mN.mm)	
Material Plasticity à	Perfect Plasticity	Hardening Plasticity	Perfect Plasticity	Hardening Plasticity
Freshly-formed spring	121	230	255	366
Aged spring (10 years)	78.8	128	232	327
Experimental results	≈ 20		≈ 20	

From the table above, it can be seen that the discrepancy in the magnitude of torque relaxation between the finite element results and the experimental results still persist, although to a relatively lower scale when compared to the earlier results. This discrepancy needs to be further investigated.

4.4.3 Influence of the new material and creep properties on the rotational creep of the spring

Finite element simulations were carried out in order to understand the influence of the new properties (yield and creep) of the elgiloy material on the rotational creep of the spring. Tables 4.12-a. and -b. show the results obtained for the rotational creep of the spring from the finite element model at torque-loads corresponding to the pre-loads of 1 revolution and 2.25 revolutions, respectively. The results obtained for a freshly-formed spring and a spring aged for 10 years are separately provided. The results follow the assumptions of hardening plasticity and “no lubrication”. The data from the experiments carried out by Lawton *et al.* [21] are also provided for the purpose of comparison. Table

4.12-b. shows a comparison of the rotational creep obtained at a torque-load corresponding to the wind-up of 1 revolution to the data at 2.25 revolutions.

For the purpose of obtaining rotational creep - as mentioned in the earlier sections - the formed spring is first subjected to a certain amount of constant torque which is numerically equal to the torque obtained from the previous models at 1 revolution or 2.25 revolutions of pre-load (torque is captured at the second wind after the first wind and unwind cycle is completed). The arbor is restricted from any translational motion during this process. The amount of rotation of the arbor over a certain period of time is then measured.

TABLE 4.12: Comparison of the rotational-creep values between the FE model and the experiments

a. Rotational creep at a pre-load of 1 revolution

Comparison of results	Rotational creep at $T_{1\ revolution}$ (mrads)		
	1 day	12 days	1 year
FE model- Freshly-formed spring	48	86	1418
FE model- 10 years aged spring	48	73	822
Experiments	16	30	132

b. Rotational creep at a pre-load of 2.25 revolutions (approx.) and comparison with the case of 1 revolution

Rotational creep over a period of one year (mrads)		
Torque loads à	$\approx T_{1\ revolution}$	$\approx T_{2.25\ revolutions}$
FE model- Freshly-formed spring	1418	720
FE model- 10 years aged spring	822	525
Experiments	132	132

It was observed from the simulations that on subjecting the arbor to the torque obtained at 1 revolution from the earlier models, the arbor rotated by approximately 1 revolution. On the other hand, on subjecting the arbor to the amount of torque obtained at 2.25 revolutions (from the earlier models), the arbor rotated only by approximately 2 revolutions. The results suggest this behavior to be due to the geometric locking of the coils at higher levels of wind-up.

From the table it can be observed that the rotational creep predicted by the finite element simulations is much higher than the experimental results. However, the results are in relatively closer comparison to the experimental data compared to the earlier results. For example, the finite element results for the rotational creep over a period of 1 year is approximately 11 times higher than the corresponding experimental results for the case of a freshly-formed spring, and about 6 times higher than the same for a spring aged for 10 years. For the earlier results which were based on the older material parameters, the above multiple was observed to be approximately 35 times. For a pre-load of 1 revolution, the results suggest an average rotational creep of approximately 3.88 mrads/day for a freshly-formed spring, and about 2.25 mrads/day for a spring aged for 10 years.

The rotational creep obtained for the pre-load of 2.25 revolutions (rather, 2 revolutions) is consistent with the earlier observations in that it is much smaller than the rotational creep obtained at 1 revolution. This behavior can again be attributed to the phenomenon of ‘geometric-locking’ of the spring coils at higher torque loads which restricts any rotational movement of the arbor (discussed in detail in the earlier sections of this chapter). The rotational creep results obtained at 2.25 revolutions of pre-load is

about 4 - 5 times higher than the experimental results, respectively, for a freshly-formed spring and for a spring aged for 10 years. The average rotational creep predicted by the finite element model for a pre-load of 2.25 revolutions is about 1.97 mrads/day for a freshly-formed spring and about 1.44 mrads/day for a spring aged for 10 years.

Once again, the results for relatively larger predictions for creep from the finite element simulations are consistent with the observations for the loss in torque in the spring due to stress relaxation in the coils. This discrepancy in the comparison of the finite element results with the experimental predictions requires a much detailed investigation. The earlier finding that the uncertainty in the determination of the material creep parameters has a major role to play in the discrepancy of the results has been proven right. However, the additional and relatively smaller discrepancy that still remains has to be further investigated. Chapter 6 provides details on the development of a second generation model which captures the geometry of the cup exactly, and attempts to eliminate even smaller nuances in the original model when it is compared to the actual clock spring profile.

4.5 Comparison of the influences of material yield to material creep on the relaxation response of the torsional spring

In design and analysis problems, it is important to understand the relative contributions of the different material and/or design parameters on the response of a system in order to bench-mark the role played by each. The relevance of this study lies on the fact that the material parameters which drive the response of an overall mechanical system can vary based on the quality of materials-processing and the accuracy of the experimental procedure which is used to capture them. Based on these facts, a detailed investigation is carried out to compare the influence of material yield to that of material

creep on the long-term response of the torsional spring. For these purposes, two sets of finite element simulations were considered: (i) simulations with the same material yield properties and different creep properties, and (ii) simulations with the same creep properties and different yield properties. The yield stress of the material considered for case-(i) is σ_y = 1655 MPa and the corresponding creep properties are, respectively, A = 6E-18 $MPa^{-2.24}S^{-1}$ and n = 2.24, and A = 2E-20 $MPa^{-2.8}S^{-1}$ and n = 2.8. Similarly, for case-(ii) the creep properties considered are A = 6E-18 $MPa^{-2.24}S^{-1}$ and n = 2.24, whereas, the corresponding yield stresses are σ_y = 1655 MPa and σ_y = 1580 MPa, respectively. Tables 4.13-a. and -b. show a comparison of the torque-drop values obtained for the above mentioned cases- corresponding to the pre-loads of 1 revolution and 2.25 revolutions, respectively.

The results shown in the tables below correspond to the case of "no lubrication", and assume linear hardening for the plastic behavior. The corresponding ultimate tensile strength is $\sigma_{UTS} \approx$1860 MPa, with the associated plastic strain of $\varepsilon^{pl} \approx$0.014. The results indicate that the creep properties have a significantly larger influence on the torque-drop response of the spring when compared to the material yield parameters. As shown in Table 4.13-a, over a period of 1 year of relaxation, the changed creep parameters lead to a reduction in the torque-drop by approximately 75% for a pre-load of 1 revolution. For a pre-load of 2.25 revolutions, this value drops to 71%. On the other hand, on reducing the yield stress, the torque-drop values reduce by approximately 0.43% and 1.24%, respectively, for 1 revolution and 2.25 revolutions of pre-loads.

The average torque-drop for case-(i) is 0.63 mN.mm/day and 1.03 mN.mm/day, respectively, for the pre-loads of 1 revolution and 2.25 revolutions.

TABLE 4.13: Comparison of the torque-drop values for varying material parameters

a. Comparison of torque drop values for varying creep parameters

Pre-loads	Time (days)	Hardening Plasticity	
		$A = 2E\text{-}20\ MPa^{-2.8}S^{-1}$ $n = 2.8$	$A = 6E\text{-}18\ MPa^{-2.24}S^{-1}$ $n = 2.24$
ΔT_{creep} 1 revolution (mN.mm)	1	0.67	3.35
	12	8.2	40.1
	365 (1 year)	230.95	926
ΔT_{creep} 2.25 revolutions (mN.mm)	1	1.14	5.06
	12	13.69	60.0
	365 (1 year)	376.08	1303

b. Comparison of torque-drop values for varying yield parameters

Pre-loads	Time (days)	Hardening Plasticity	
		$\sigma_y = 1580$ MPa	$\sigma_y = 1655$ MPa
ΔT_{creep} 1 revolution (mN.mm)	1	3.35	3.35
	12	39.86	40.1
	365 (1 year)	922.01	926
ΔT_{creep} 2.25 revolutions (mN.mm)	1	4.97	5.06
	12	58.78	60.0
	365 (1 year)	1286.80	1303

For case-(ii), these values change to 2.53 mN.mm/day and 3.53 mN.mm/day, respectively. The relatively larger dependence of the torque-drop response on the creep parameters can be attributed to the fact that the creep parameters have a direct and a combined multiplicative as well as exponential influence on the long-term relaxation response of the spring through the power law expression for material creep (discussed in Equation 3 earlier). On the other hand, the yield stress only has an indirect influence since it forms the base of the expression for the creep strain rate of which the creep

parameter- n is an exponent. Hence, the relative influence on the relaxation response of the spring reduces.

4.6 Conclusions

A finite element model is developed to capture the long-term relaxation response of the spring. Non-linear material behavior (i.e., plasticity and creep) was found to be the major contributor influencing the long-term relaxation response. Friction and large deformations appear to make relatively smaller contributions. The results from the finite element model when compared with the experimental results suggested that the creep parameters which are obtained from the uniaxial tension tests may not be the "steady-state" values. Based on the new creep and yield parameters of the elgiloy material, the values for the resisting torque predicted by the finite element model are in a relatively closer comparison to the design specifications. The model predicts an average torque-drop rate of approximately 0.28 - 1.00 mN.mm/day for a freshly-formed spring, and approximately 0.18 - 0.9 mN.mm/day for a spring aged for 10 years, depending on the magnitude of loading, and the specific choices of material plasticity and friction. For simulations involving 1 year of relaxation, the finite element model predicts an average drop in the von-Mises stress of approximately 5 - 6% only, compared to 20 - 25% predicted by the earlier model (which used the older creep data). Aging is found to significantly reduce the resisting torque as well as the torque-drop at a given spring rotation. The results suggest a relaxation of the residual stresses by approximately 31% as a result of aging for a period of 10 years. The results also suggest that the torque-drop decays exponentially as a function of the time period of aging, with 10 years being the saturation point beyond which further aging does not affect the torque drop. The finite

element model is modified to capture the rotational creep of the spring under constant applied torque. The results indicate an average rate of rotational creep of approximately 3.88 mrads/day (2.25 mrads/day, for a spring aged for 10 years) for a pre-load of 1 revolution, and about 1.97 mrads/day (1.44 mrads/day, for a spring aged for 10 years) for a pre-load which is approximately equal to 2.25 revolutions. The geometric 'locking' of the spring coils is found to reduce the rotational creep at higher loads. The creep parameters are found to have a significantly larger influence on the long-term relaxation response of the spring system, when compared to the yield parameters. Even after using the most recent and relatively more accurate creep and yield parameters of the elgiloy material, the experimental results for the relaxation and creep responses are found to be much lower than the corresponding finite element results. The reason(s) behind this discrepancy need to be investigated in details. This necessitates the need for a second generation model for the torsional spring that is discussed in details in Chapter 6.

CHAPTER 5: ANALYTICAL MODELING

5.1 Objectives

The objective of this modeling phase is to develop simple analytical models, based on the principles of Statics and Mechanics of Solids, to provide a rough verification for the order-of magnitudes and the trends of the finite element results for the time-dependent response of the torsional spring. The work presented here focuses on the development of an effective creep law for the spring as a whole which can approximately describe the creep or relaxation response of the torsional spring - as functions of the material and other design parameters. This creep law can potentially be used in a systems-level model to describe the behavior of such a spring using only a limited number of degrees of freedom, instead of the more detailed (and computationally expensive) component-level model developed in the earlier sections. In addition, some connections are provided between the peak moments that describe the instantaneous responses of the spring at 1 and 2.25 revolutions and the text book solutions for pure bending using the linear beam-bending theory and an elastic-perfectly-plastic material.

5.2 Procedures and Results

For any mechanical engineering problem - irrespective of the methodology that is used for the solution process (namely, finite element method, experiments, etc.) - it is important to attempt to validate the results, using analytical techniques wherever it is possible to do so. Depending on the complexity of the problem, and the desired accuracy

of the solution, the analytical model can either be of a detailed nature that produces accurate (or close to accurate) results, or, it can be an approximate model with several simplifying assumptions that can be used to produce rough estimates to the actual solution. It is particularly important to provide an inexpensive check over the more detailed and expensive numerical computations. The analytical modeling effort described here is based on some of the basic principles of Statics and Mechanics of Solids. To develop this model, we assume that the finite element simulation results for the instantaneous responses of the torsional spring are reasonably accurate. The finite element results for the instantaneous responses of the spring are then utilized, along with the creep material properties of elgiloy, to describe the moment relaxation of the spring as a function of time. The following sections of this chapter provide further details on the analytical techniques used, and the corresponding predictions.

5.2.1 Development of a Torsional Creep Law

An analytical model that can approximately describe the long-term relaxation response of the torsional spring about a pre-loaded state is developed using simple techniques based on the principles of Statics and Mechanics of Solids. The future goal of this effort is to develop a "Torsional Creep Law" which can predict the long-term moment-rotation response of a typical torsional spring, accounting for design parameters such as geometry, frictional coefficients, and material properties.

NOTE: The finite element results for the instantaneous and long-term responses of the torsional spring, which are used for comparing with the analytical results, correspond to an elastic perfectly-plastic elgiloy material with yield strength of $\sigma_y \approx 1.6$ GPa, and creep parameters of $A = 6E\text{-}18\ MPa^{-2.24}S^{-1}$ and $n = 2.24$.

To illustrate the basic approach, a typical cross-section of a freshly-formed torsional spring that is wound-up to 1 revolution is considered. Figure 5.1 shows a schematic of the section of the torsional spring. The triad 1-2-3 represents a local Cartesian coordinate system associated with the spring cross-section, with axis-1 being normal to the plane of the cross-section.

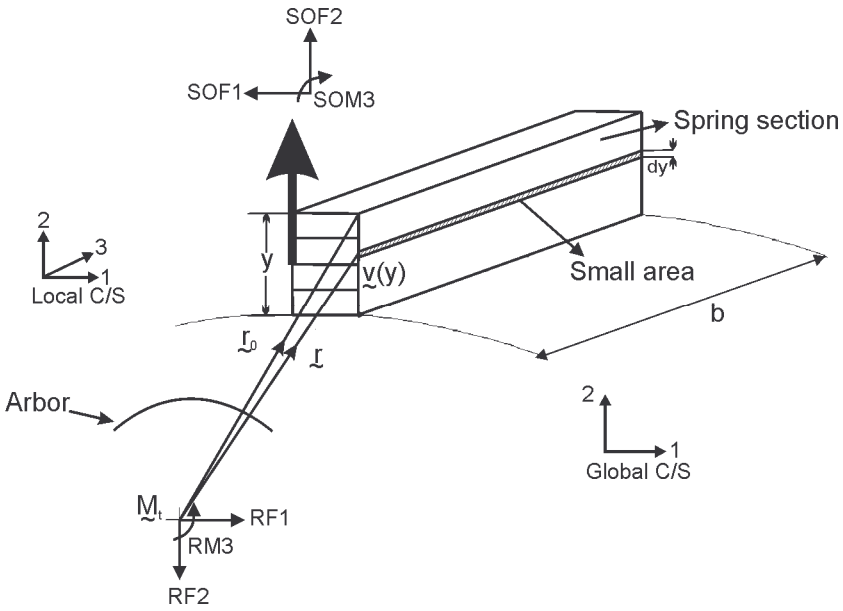

FIGURE 5.1: A schematic of a section of the torsional spring (for analytical model)

We employ the equations of planar static equilibrium, which result in the following relations (Equations 5.1 and 5.2) among the components of the reaction forces and moments at the arbor center, and the sectional forces and moments at the cross-section of the elgiloy strip shown above (in the absence of any external forces and moments acting on the spring system).

$$\sum \underset{\sim}{\mathbf{F}} = \underset{\sim}{\mathbf{0}} \text{ and } \sum \underset{\sim}{\mathbf{M}} = \underset{\sim}{\mathbf{0}}, \tag{5.1}$$

$$\mathrm{RF1} = \mathrm{SOF1},\ \mathrm{RF2} = \mathrm{SOF2},\ \mathrm{RM3} = \mathrm{SOM3}. \tag{5.2}$$

In the equations above, RF1 and RF2 are the components of the reaction force at the arbor center, RM3 is the reaction moment at the arbor center, SOF1, SOF2, and SOM3 are the sectional forces and moment at the spring section considered.

The instantaneous reaction moment at the arbor reference node for the spring system can be computed utilizing the finite element solutions for the stresses in the elgiloy strip by considering an infinitesimally thin area- element cross-section (shown in Figure 5.1). The infinitesimal area element is assumed to have a thickness of- dy and a width of- b. The effective sectional force and moment on the entire spring section can be computed by integrating (through the thickness of the section) the net force and moment contribution from this infinitesimal area element. The normal and tangential components of the net force acting on the infinitesimal area element, in the local coordinate system 1-2-3, can be derived from the instantaneous stress components (appropriately transformed to the local system) at these locations provided by the finite element simulations. The required operations are shown in Equation 5.3. The instantaneous moment contribution of the section at the arbor center is then calculated as the integral of the cross-product of the moment-arm (with respect to the arbor center) of the centroid of the infinitesimal area element with the net effective force acting on the element (shown in Equations 5.4, 5.5, and 5.6).

$$d\underset{\sim}{F} = \sigma_n(y,0).b.dy.\underset{\sim}{e}_1 + \sigma_s(y,0).b.dy.\underset{\sim}{e}_2, \qquad (5.3)$$

$$\underset{\sim}{M}_0 = \int_y (\underset{\sim}{r} \times d\underset{\sim}{F}).\underset{\sim}{e}_3, \qquad (5.4)$$

$$\underset{\sim}{r} = \underset{\sim}{r}_0 + \underset{\sim}{v}(y), \qquad (5.5)$$

$$\underset{\sim}{v}(y) = -y.\underset{\sim}{e}_2. \qquad (5.6)$$

In the equations above, $\underset{\sim}{r}$ is the moment-arm of the infinitesimal area element about the arbor center, $\underset{\sim}{r}_0$ is a fixed vector locating a point on the upper boundary of the spring section relative to the arbor center, y is a variable representing position along the thickness direction of the section, $\underset{\sim}{v}(y)$ is a vector representing the variation of position along the thickness of the section, in the direction of the unit tangential vector- $-\underset{\sim}{e}_2$, $d\underset{\sim}{F}$ is the net force acting on the infinitesimal area element, $\sigma_n(y,0)$ is the instantaneous stress component normal to the cross section, $\sigma_s(y,0)$ is the instantaneous stress component tangential to the cross section, and $\underset{\sim}{M}_0$ is a vector representing the net instantaneous moment contribution of the spring section about the arbor center.

Numerical integration techniques such as the Gauss-Lobatto method [6] and Simpson's rule [6, 19] are used for evaluating the integral in Equation 5.4. The purpose of using two different integration schemes is to understand the location of the sampling points in each integration scheme, for a better comparison with the finite element results. For this purpose, the normal and shear stresses computed at the cross-section by the instantaneous finite element solution, extrapolated at the nodes of the section and transformed to the local system are used in conjunction with their corresponding moment-arms about the arbor center. Table 5.1 shows a comparison of the torque results obtained from either integration techniques with the corresponding finite element results - for a wind-up of 1 revolution. As evident from the table, the results obtained from the analytical techniques are found to be in reasonably good agreement with the finite element results. The Simpson's rule resulted in an error of approximately 1.3%, whereas the Gauss-Lobatto resulted in an error of about 3.6%, in comparison to the results from the finite element simulations. The results also suggested that the local normal

component of the sectional force contributes approximately 99.85% of the net instantaneous moment of the spring system, whereas the contribution from the tangential component is negligible (only the remaining 0.15%).

TABLE 5.1: Comparison of the torque results obtained from the analytical techniques to the finite element results

Torque results for a freshly-formed spring at 1 rev. (N.mm)	
Finite element results	3.759
Simpson's rule	3.710
Gauss-Lobatto method	3.624

Once the instantaneous moment is computed, the next phase in the analytical work is to determine the reaction moment at the arbor center as a function of time due to stress relaxation in the spring coils. An approach that is essentially identical to the one used above is followed, except that the instantaneous stresses in Equation 5.3 are replaced by the corresponding relaxed stress components. The latter - which are functions of position along the section thickness and time - are derived from the power-law expression for the creep strain rate which is shown in Equation 4.1 of Chapter 4. In the following steps, we analytically compute the relaxation response at each point along the beam section assuming that the point is subjected to a uniaxial stress state. We start with the creep law shown in Equation 5.7, which essentially represents a special case (uniaxial tension) of the more general creep law presented in Equation 4.1 of Chapter 4. For a linear elastic-plastic constitutive response with creep, the uniaxial stress can be related to the elastic strain (i.e., total strain minus the plastic and creep strains) as shown in Equation 5.8. We assume that during material creep, both the total strain and the plastic strain, and hence their difference remains constant. This is indicated in Equation 5.9.

$$\frac{d\varepsilon_{cr}}{dt} = A\sigma(y,t)^n, \tag{5.7}$$

$$\sigma(y,t) = E(\varepsilon_0 - \varepsilon_{pl} - \varepsilon_{cr}), \tag{5.8}$$

$$\varepsilon_k = \varepsilon_0 - \varepsilon_{pl}. \tag{5.9}$$

In the above equations, $\sigma(y,t)$ is the uniaxial stress which is a function of position along the section thickness- y and time- t, A and n are the power-law creep parameters which are assumed to be material constants, E is the Young's modulus of elasticity of the elgiloy material, ε_0 is the total strain in the elgiloy material, ε_{pl} is the plastic strain, and ε_k is the difference of the total and plastic strains which is assumed to be a constant during material creep.

Substituting Equation 5.9 in Equation 5.7, and on integrating the resulting expression, we arrive at an expression for the creep strain in the material. This operation is shown in the equation below.

$$\int_{\varepsilon} \frac{d\varepsilon_{cr}}{(\varepsilon_k - \varepsilon_{cr})^n} = AE^n \int dt + C \tag{5.10}$$

In the above equation, C is an arbitrary integration constant.

Once the expression for the creep strain is derived, the expression for the long-term stress can be obtained from Equation 5.8. The arbitrary integration constant- C can be eliminated by using the initial condition that the creep strain- ε_{cr} is zero at time- $t = 0$.

Integration of the above equation involves two cases based on the different possibilities for the value of n: (i) $n = 1$ and (ii) $n \neq 1$. Upon integration, case (i) provides the following results for the von-Mises stress and creep strain of the spring material.

$$\varepsilon_{cr} = (\varepsilon_0 - \varepsilon_{pl}).(1 - e^{-AEt}), \tag{5.11}$$

$$\sigma(y,t) = E(\varepsilon_0 - \varepsilon_{pl})e^{-AEt}. \tag{5.12}$$

Similarly, upon integration, case (ii) provides the following results:-

$$\varepsilon_{cr} = (\varepsilon_0 - \varepsilon_{pl}) - [(n-1)AE^n t + (\varepsilon_0 - \varepsilon_{pl})^{1-n}]^{1/(1-n)}, \tag{5.13}$$

$$\sigma(y,t) = E[(\varepsilon_0 - \varepsilon_{pl})^{1-n} + (n-1)AE^n t]^{1/(1-n)}. \tag{5.14}$$

Equations 5.12 and 5.14 can be further simplified by recognizing the expressions for the instantaneous stress within these equations, leading to the following equations:

$$\sigma(y,t) = \sigma(y,0)e^{-AEt}, \tag{5.15}$$

$$\sigma(y,t) = \sigma(y,0)[1 + \frac{(n-1)AE^n t}{\sigma(y,0)^{1-n}}]^{1/(1-n)}. \tag{5.16}$$

where; $\sigma(y,0) = E(\varepsilon_0 - \varepsilon_{pl})$ at t=0 (instantaneous stress)

The current problem involves a secondary steady-state creep response, and the creep parameter $n \neq 1$. Hence, the expressions for the normal and tangential components of the long-term stress would follow Equation 5.16, and may be written as:

$$\sigma_n(y,t) = \sigma_n(y,0)[1 + \frac{(n-1)AE^n t}{\sigma_n(y,0)^{1-n}}]^{1/(1-n)}, \tag{5.17}$$

$$\sigma_s(y,t) = \sigma_s(y,0)[1 + \frac{(n-1)AE^n t}{\sigma_s(y,0)^{1-n}}]^{1/(1-n)}. \tag{5.18}$$

In the above equations, $\sigma_n(y,t)$ is the relaxed stress component normal to the cross section, and $\sigma_s(y,t)$ is the relaxed stress component tangential to the cross-section.

Using the above equations which are nonlinear in time, and following the strategy used for the instantaneous case, the expression for the reaction moment at the arbor center as a function of time may be written as shown in Equation 5.19. The corresponding torque drop can then be calculated as the difference between the instantaneous moment and the long-term moment. Equation 5.20 shows the expression for the long-term torque-drop of the spring system.

$$\underset{\sim}{\mathbf{M}}_t = \int_y (\underset{\sim}{\mathbf{r}}_0 + \underset{\sim}{\mathbf{v}}(y)) \times (\sigma_n(y,0).\left[1+\frac{(n-1).A.E.t}{\sigma_n(y,0)^{(1-n)}}\right]^{\frac{1}{1-n}}.\underset{\sim}{\mathbf{e}}_1 + \sigma_s(y,0).\left[1+\frac{(n-1).A.E.t}{\sigma_s(y,0)^{(1-n)}}\right]^{\frac{1}{1-n}}.\underset{\sim}{\mathbf{e}}_2).b.dy, \tag{5.19}$$

$$\Delta\underset{\sim}{\mathbf{T}}_{cr} = (M_0 - M_t).\underset{\sim}{\mathbf{e}}_3. \tag{5.20}$$

In the above equation (5.20), $\Delta\underset{\sim}{\mathbf{T}}_{cr}$ is a vector representing the torque-drop due to the long-term stress relaxation, acting in the direction- $\underset{\sim}{\mathbf{e}}_3$.

Simpson's rule is used to evaluate the integral shown in Equation 5.19. Table 5.2 shows a comparison of the torque-drop results obtained from the analytical model for a freshly-formed un-lubricated spring subjected to a preload of 1 revolution, to the corresponding finite element results.

TABLE 5.2: Comparison of the torque-drop results obtained from the analytical model to the finite element results (for a freshly-formed un-lubricated spring)

Torque-drop results for a freshly-formed spring (mN.mm)			
Time period	1 day	12 days	1 year
Analytical model	2.82	33.54	777.61
FE model	2.28	27.35	665.74

Figure 5.2 shows a comparison of the torque-drop results obtained from the analytical model for a freshly-formed spring over a period of 1 year of relaxation with the corresponding results of the finite element simulations.

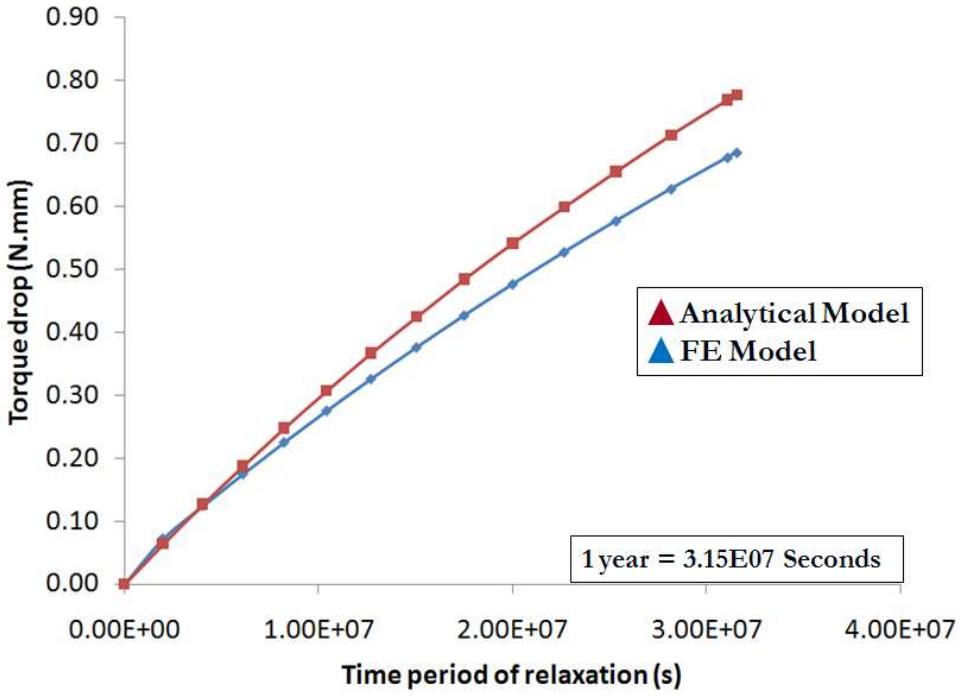

FIGURE 5.2: Comparison of the torque-drop results obtained from the analytical model to the corresponding FE results for a period of 1 year of relaxation

The results shown above correspond to a static pre-load of 1 revolution, and "no lubrication". The long-term torque-drop response is found to be nearly linear for relatively small periods of time (of the order of weeks to months) and nonlinear over longer time-periods. The analytical model estimates a torque-drop of approximately 33.5 mN.mm over a period of 12 days, and approximately 778 mN.mm over a period of 1 year, which are in relatively good agreement (in an order-of-magnitude sense) with the corresponding finite element simulation results. The associated maximum von Mises

stress relaxation is estimated at about 10% at the end of 4 months, and about 24% at the end of 1 year.

As evident from Figure 5.2 and Table 5.1, the results obtained from the analytical model are in reasonably good agreement with the corresponding finite element results. The orders of magnitude of the results agree in all the cases. In that sense, the results from the analytical model appear to validate the earlier results from the finite element simulations.

5.2.2 An approximate method to determine the torque-drop response over short periods of time

The modeling effort discussed here involves development of an approximate method to determine the torque-drop response of the torsional spring over relatively short periods of time (of the order of months) over which the torque-drop seems to remain linear (close to the origin in Figure 5.2). For this purpose, the equations developed in the earlier section are considered. The expression for the moment arm, shown in Equation 5.5, can be rewritten in the component form as shown in Equation 5.21. In addition, as pointed out during the discussion of the results in Section 5.2.2, the tangential component of the sectional force only makes a negligible contribution (less than 0.2%) on the net instantaneous moment of the torsional spring. Hence, upon neglecting the contribution from the shear stress, Equation 5.4 representing the instantaneous moment of the spring can be modified to the one shown in Equation 5.22.

$$\underset{\sim}{\mathbf{r}} = r_1.\underset{\sim}{\mathbf{e}}_1 + r_2.\underset{\sim}{\mathbf{e}}_2, \tag{5.21}$$

$$\underset{\sim}{\mathbf{M}}_0 = b\int_y \left[-(r_2.\sigma_n(y,0)\right].dy.\underset{\sim}{\mathbf{e}}_3. \tag{5.22}$$

To compute the long-term response, Equation 5.22 can be modified by replacing the expression for the instantaneous stress component with the long-term one, obtained from Equation 5.17. The resulting expression may be written as:

$$\underset{\sim}{\mathbf{M}}_t = b\int_y \left[-r_2.\sigma_n(y,0).\left\{1+\frac{(n-1).A.E.t}{\sigma_n(y,0)^{(1-n)}}\right\}^{\frac{1}{1-n}} \right].dy.\underset{\sim}{\mathbf{e}}_3 \tag{5.23}$$

The coefficient of t in Equation 5.23 is a constant in time, and can be denoted by the symbol- k as shown:

$$\underset{\sim}{\mathbf{M}}_t = b\int_y \left[-r_2.\sigma_n(y,0).\{1+k.t\}^{\frac{1}{1-n}} \right].dy.\underset{\sim}{\mathbf{e}}_3 \tag{5.24}$$

$$\text{where } k = \frac{(n-1).A.E}{\left|\sigma_n(y,0)\right|^{(1-n)}}.$$

Note that the purpose of providing an absolute magnitude sign in the denominator of k is to emphasize the fact that only absolute values of the local normal component of instantaneous stress need to be used in the expression, in spite of the nature of the stress being compressive or tensile along any point on the spring section. The use of negative values for the stress component will lead to an undefined expression while computing.

For $k.t << 1$ the binomial expansion [15] of $\{1+k.t\}^{\frac{1}{1-n}}$ can be written as:

$$\{1+k.t\}^{\frac{1}{1-n}} = \left\{1+\frac{1}{(1-n)}.k.t\right\} \tag{5.25}$$

Upon performing the above operation in Equation 5.24, the expression for the long-term moment may be written as:

$$\underset{\sim}{\mathbf{M}}_{\mathbf{t}} = b\int_{y}\left[-r_2.\sigma_n(y,0).\left\{1+\frac{1}{(1-n)}.k.t\right\}\right].dy.\underset{\sim}{\mathbf{e}}_3 \tag{5.26}$$

The torque-drop associated with the long-term response can then be determined by subtracting Equation 5.26 from Equation 5.22. The corresponding expression can be written as:

$$\Delta\underset{\sim}{\mathbf{T}}_{\mathbf{cr}} = b\int_{y}\left[(r_2.\sigma_n(y,0).\frac{k.t}{(1-n)}\right].dy.\underset{\sim}{\mathbf{e}}_3 \tag{5.27}$$

where $k = \dfrac{(n-1).A.E}{\left|\sigma_n(y,0)\right|^{(1-n)}}$ and $n > 1$.

Upon substituting k in Equation 5.27, the final expression for the torque-drop is a linear function in time- t for a given value of n.

$$\Delta\underset{\sim}{\mathbf{T}}_{\mathbf{cr}} = -A.E.t.b\int_{y}\left[(r_2.\left|\sigma_n(y,0)\right|^{n}\right].dy.\underset{\sim}{\mathbf{e}}_3 \tag{5.28}$$

However, the above expression holds only when $k.t << 1$, or alternatively when $t << \dfrac{\left|\sigma_n(y,0)\right|^{(1-n)}}{(n-1).A.E}$.

The expression for the torque-drop in Equation 5.28 suggests that over relatively short time scales, the torque-drop response of the spring should be linear in t. However, a question that arises is: How small are the time scales for which the above linearity is valid?

Gauss-Lobatto method [6] is used to carry out the integration in Equation 5.28. Following the strategy used in Section 5.2.1, the instantaneous normal stress, $\sigma_n(y,0)$, extrapolated at the nodes of the section by the finite element discretization method is

used, in conjunction with the known values of A, E, and n. Figure 5.3 shows a comparison of the torque drop results obtained from the approximate analytical method to the corresponding finite element results for a period of 1 year of relaxation.

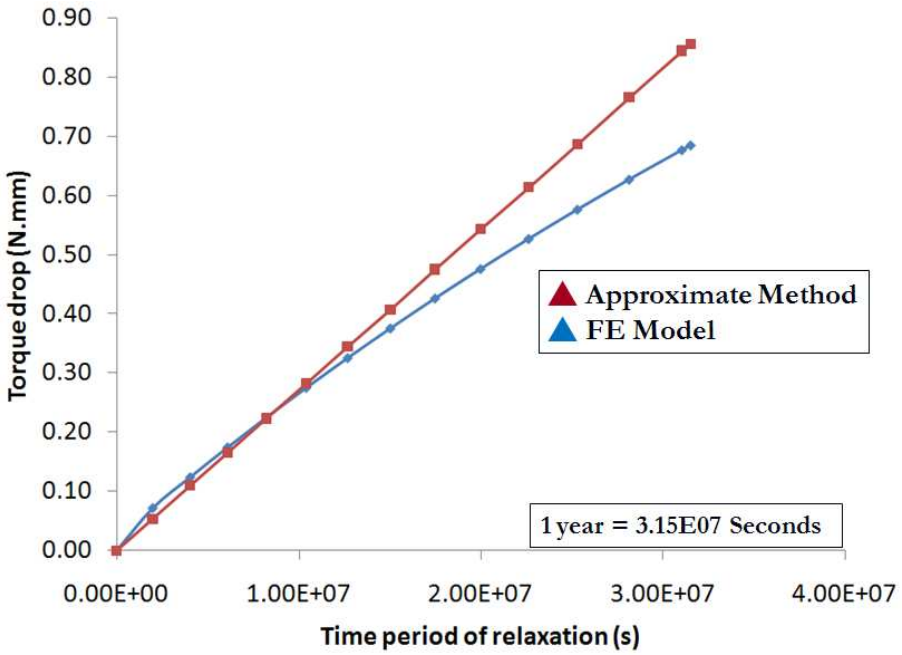

FIGURE 5.3: Comparison of the torque-drop results obtained from the approximate method to the corresponding FE results for a period of 1 year of relaxation

The results shown in the plot correspond to a freshly-formed un-lubricated spring subjected to a pre-load of 1 revolution. It can be seen that for relatively smaller time periods of relaxation, of the order of three to four months (≈1.0E07 seconds), the torque-drop response is nearly linear, which is evident from the closeness of the two curves. Beyond that period of time, the curves begin to diverge from one another, indicating the non-linearity of the response. The above results further confirm that the time-dependant response of the torsional spring is nearly linear for relatively smaller time periods of relaxation of the order of weeks to months and non-linear for longer time periods.

Note: It is to be noted that the expression shown in Equation 5.28 is an approximate estimate for the torque-drop response of the torsional spring over small periods of time of the order of few months. Beyond that period of time, the equation does not hold good.

5.2.3 Connections between the static torques at 1 and 2.25 revolutions with the solution for elastic-plastic beam bending based on the linear beam bending theories

In this section we attempt to make some connections between the static values of the spring torque at 1 and 2.25 revolutions, respectively, and textbook solutions [23] for pure bending of a rectangular cross-section beam made out of an elastic perfectly-plastic material within the context of a linearized theory (i.e. under the assumptions of "small strains").

These connections and rough estimates are developed in order to get a better feel for the results obtained from the finite element model as well as the design specifications for static loading of the springs. Two extreme cases are investigated; they are cases for which during bending, (i) only the outer surfaces of the section reached the yield stress, and (ii) the entire section has yielded. The following paragraphs provide further details for each of these cases.

(i) A beam subjected to pure bending with incipient sectional yield:

For this purpose, a rectangular beam with an in-plane thickness- $2c$ and a width- b is considered, as shown in Figure 5.4. The beam is subjected to pure bending with a bending moment- M_0. We assume that the bending moment is such that only the outer fibers have reached the yield stress.

The expression for the moment is given by [23]:

$$M_0 = \frac{2}{3}\sigma_y b c^2 \qquad (5.29)$$

In the above equation, σ_y is the yield stress for the perfectly plastic material.

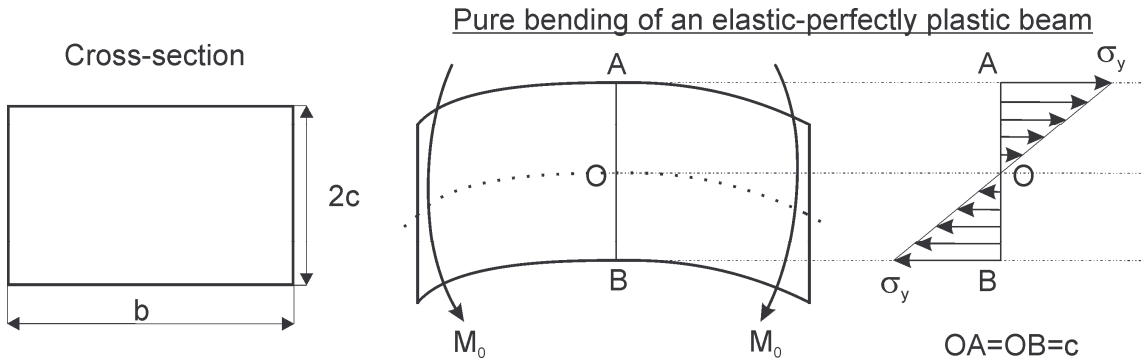

FIGURE 5.4: Schematic of a rectangular beam subjected to pure bending with yield only on the outer fibers

Substituting the values of σ_y, b, and c, we get the bending moment as: $M_0 = \underline{\underline{2.759\ \text{N.mm}}}$.

The design specification for the wind-up of 1 revolution is 2.9±0.5 N.mm. It can be seen that the rough estimate for the instantaneous section moment obtained above is close to the design specification for 1 revolution. It is possible that the above agreement may be more than a coincidence, and it is plausible that the design specification for the 1 revolution case approximately corresponds to the situation of incipient plastic yielding at the spring sections. Assuming this to be the case, in the following paragraphs we compute estimates for the torque lost due to creep as a function of time after a preload of 1 revolution.

Extending the developments presented earlier and assuming that all points along the section relax following the expression for uniaxial relaxation derived earlier (Equation 5.16), the long-term moment may be expressed as:

$$M_t = \frac{2}{3}\sigma_y \cdot \left[1 + \frac{(n-1).A.E.t}{\sigma_y^{(1-n)}}\right]^{\frac{1}{1-n}} .bc^2 \qquad (5.30)$$

In the above equation, as before, A, n are the creep parameters of the material, E is the Young's modulus of elasticity, and t is the time period of relaxation.

Substituting the values for the above mentioned parameters, and subtracting the resulting moment from the instantaneous value computed in Equation 5.29, we find that the long-term drop in the torque over a time-period of 1 year is $\Delta T_{cr} = \underline{\underline{0.699\ N.mm}}$. From the finite element model, the long-term torque drop at a wind-up of 1 revolution was obtained as $\Delta T^{FE}_{cr} = \underline{\underline{0.595\ N.mm}}$ (for the case of "perfect lubrication"). The difference between these two estimates is only about 18%. Thus, under the assumptions outlined above, the analytical estimate for the torque-drop is in relatively good agreement with the finite element simulation results.

(ii) A beam subjected to pure bending with the entire section experiencing yield:

For this case, the above mentioned beam is subjected to a bending moment such that the entire section undergoes yield (Figure 5.5).

The expression for the corresponding moment is given by [23]:

$$M_0 = \sigma_y bc^2 \qquad (5.31)$$

Substituting the values of σ_y, b, and c, we get a value for the bending moment of: $M_0 = \underline{\underline{4.138\ N.mm}}$.

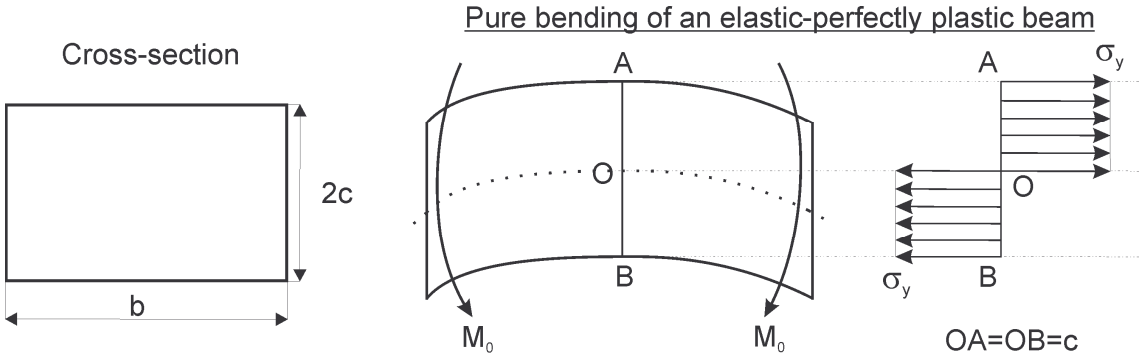

FIGURE 5.5: Schematic of a rectangular beam subjected to pure bending with the entire section undergoing yield

The design specification for the wind-up of 2.25 revolutions is 4.35±0.55 N.mm. The bending moment computed above is close to the design specification. We assume again that the above mentioned proximity of the two quantities is not purely coincidental and that the design specification for 2.25 revolutions corresponds to the situation where the beam cross-section has fully yielded.

As for the earlier case, the long-term relaxation response may be written as:

$$M_t = \sigma_y . \left[1 + \frac{(n-1).A.E.t}{\sigma_y^{(1-n)}} \right]^{\frac{1}{1-n}} .bc^2 \qquad (5.32)$$

Substituting the values of the parameters A, n, σ_y, and E in Equation 5.32 for a period of 1 year of relaxation, and subtracting the result from the instantaneous moment, we get a rough estimate for the long-term torque-drop as $\Delta T_{cr} = \underline{\underline{1.048\ N.mm}}$. From the finite element model, the long-term torque-drop corresponding to the wind-up of 2.25 revolutions was computed to be $\Delta T^{FE}_{cr} = \underline{\underline{0.923\ N.mm}}$ (for "perfect lubrication"). The difference between the analytical and the finite element simulation results is only about 14%. Thus, under the earlier mentioned assumptions, the result suggests that the long-

term torque-drop for the wind-up of 2.25 revolutions obtained from the finite element model is in relatively good agreement with the analytically computed values provided above.

The above comparisons suggest that the results for the long-term response of the torsional spring obtained from the finite element model are reasonable in an order-of-magnitude sense.

5.3 Conclusions

Simple analytical models, that can approximately describe the structural response of a torsional spring, are developed based on the principles of Statics and Mechanics of Solids. The modeling effort primarily involves verification of the static solution, and development of analytical estimates for the time-dependant behavior of the torsional spring. These preliminary results can be used in the future for the development of a torsional creep law which can predict the instantaneous as well as long-term responses of a typical torsional spring accounting for the various design parameters. The results obtained are in good agreement with the finite element results in an order-of-magnitude sense. The torque values obtained for the instantaneous response are found to be only 1 - 4 % off from the corresponding results obtained from the finite element model. The results also suggest that the tangential component of the sectional force (in the local coordinate system 1-2-3) has a negligible contribution on the net instantaneous moment of the spring system. The long-term response captured by the analytical model indicates a nearly linear behavior for relatively smaller periods of time of the order of weeks to months, and a non-linear response for larger time-periods. The torque-drop predicted is approximately 778 mN.mm over a period of 1 year of relaxation, compared to a

prediction of 666 mN.mm from the finite element simulation results for the case of “no lubrication” and a 1 revolution preload. The maximum stress relaxation predicted is about 10% at the end of 4 months, and about 24% at the end of 1 year, which are in good agreements with the finite element results. Overall, the results obtained from the analytical model suggest that the order-of-magnitudes and the trends of the finite element results are reasonable. Some rough calculations based on linear pure bending theories of a beam with a rectangular cross-section made out of an elastic perfectly-plastic material suggests that the design specifications for static torque at 1 and 2.25 revolutions may correspond to the extreme cases of incipient and full sectional yielding.

CHAPTER 6: SECOND GENERATION FINITE ELEMENT MODEL

6.1 Background and Objectives

The previous chapters of this dissertation dealt with the development of a first generation finite element model to capture the instantaneous moment-rotation as well as the long-term relaxation (and creep) responses of the torsional spring. The static response predicted by the model is in relatively close comparison to the design specifications and the results of the experiments. However, the long-term relaxation response and the associated torque-drop captured by the finite element model showed some discrepancies when compared to the experimental results. The numerical results for the torque-drop were found to be much higher than the experimental results obtained by Lawton *et al.* [21]. The results of a detailed investigation carried out by the experimental group suggested that the creep parameters obtained from the uniaxial tension tests may not be corresponding to steady-state creep of the elgiloy material. Experiments were hence repeated in order to capture the steady-state creep properties more accurately. Finite element simulations were then carried out incorporating the new set of creep properties. The results obtained from these simulations for the long-term response of the spring were in relatively closer comparison to the experimental results, when compared to the numerical results with the earlier creep properties. However, the results for the long-term torque-drop were still higher than the corresponding experimental results, although the margin of difference was lowered by approximately 70 – 80% when compared to the

older results. This discrepancy needed further investigation. The purpose of developing a second generation model is to understand and fix any plausible nuances that differentiate the current finite element model from the actual profile of the spring.

6.2 Development of the second generation model

A detailed investigation was carried out to compare the current model with the actual profile of the torsional spring. Figure 6.1 shows a comparison of the finite element model to the actual clock spring profile with an illustration of the differences between the two.

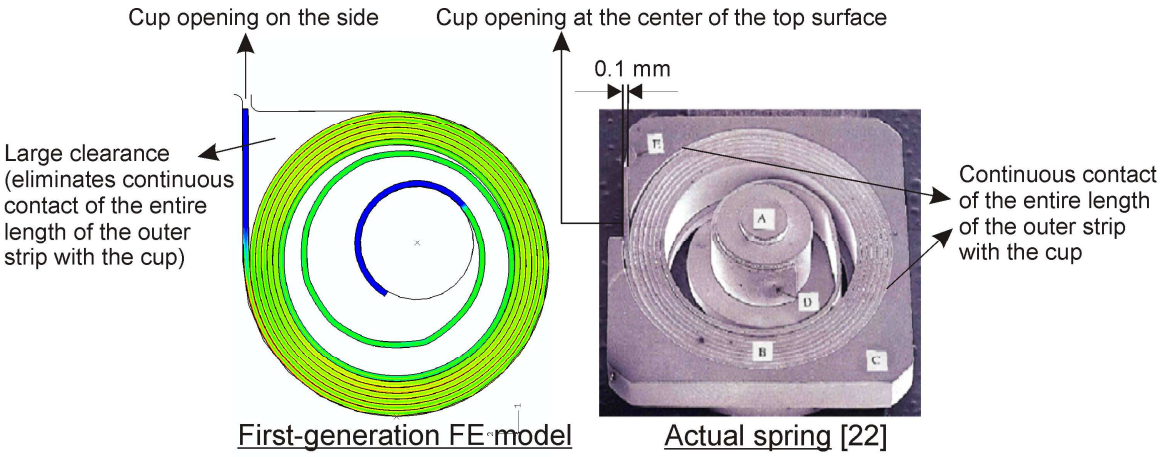

FIGURE 6.1: Comparison of the first-generation finite element model to the actual profile of the torsional spring

The results of the investigation confirmed that conceptually the first generation model is close to the actual profile of the clock spring since the major design parameters like the diameter of the cup, the radius of the arbor, the length of the strip, etc., were the same as in the actual spring. However, there were some discrepancies in the position and the shape of the opening on the cup surface through which the strip enters into the cup during the winding phase of the forming process. In the actual model, the strip enters into

the cup through an opening at the center of the top surface of the cup. On the contrary, in the first generation finite element model, the opening is positioned on the side (corner) of the cup. It was also found that the above discrepancy led to the formation of a large clearance between the wound-up coils and the inner surface of the cup- close to the region of cup-opening (see Figure 6.1). The presence of such a large clearance prevents a portion of the total length of the outer coil of the strip from having a continuous contact with the surface of the cup.

The second generation model is developed to remove the above mentioned discrepancies, and thereby come up with a more accurate, if not an exact numerical replica of the actual torsional spring system. It is important to note that the new generation model uses the same modeling strategy that was used for the first generation model, and the only major difference is in the design of the cup that houses the spring. In addition, it also considers an extended length of the strip of approximately 1.76 mm that is welded onto the outer cup surface [22]. All the remaining design parameters are the same as in the original model. The material and creep models used are the same as the ones used for the first generation model; namely:- yield stress of 1580 MPa, ultimate tensile strength of 1860 MPa with an associated plastic strain of 0.014, and the creep properties of $A = 2E\text{-}20\ MPa^{-2.8}S^{-1}$ and $n = 2.8$. The model uses approximately 42,000 variables for the analysis, with about 18,000 elements (similar to the earlier model).

Similar to the earlier model, the new model also utilizes the built-in viscous stabilization scheme in Abaqus to help mitigate the effects of local instabilities in the solution. The smallest value for which the simulations converged is F=5E-05.

6.3 Procedures and Results

The following sub-sections discuss the results obtained from the new model for the instantaneous moment-rotation as well as the long-term relaxation and creep responses of the torsional spring, along with a comparison to the results of the earlier model. Since the modeling strategy used is the same as the one used for the earlier model, a detailed description of the procedures is not provided and the primary focus is only on the results of the simulations and their comparison to the results of the earlier model.

Note: All the results presented in this chapter correspond to the cases of hardening plasticity and "perfect lubrication".

6.3.1 Spring forming process

The results of the finite element simulations for the winding phase of the forming process suggest that the spring coils undergo significantly larger deformations when compared to the results of the first generation model. Figures 6.2-a. and -b. show a comparison of the von Mises stress and the equivalent plastic strain in the spring coils corresponding to the two generations of the model.

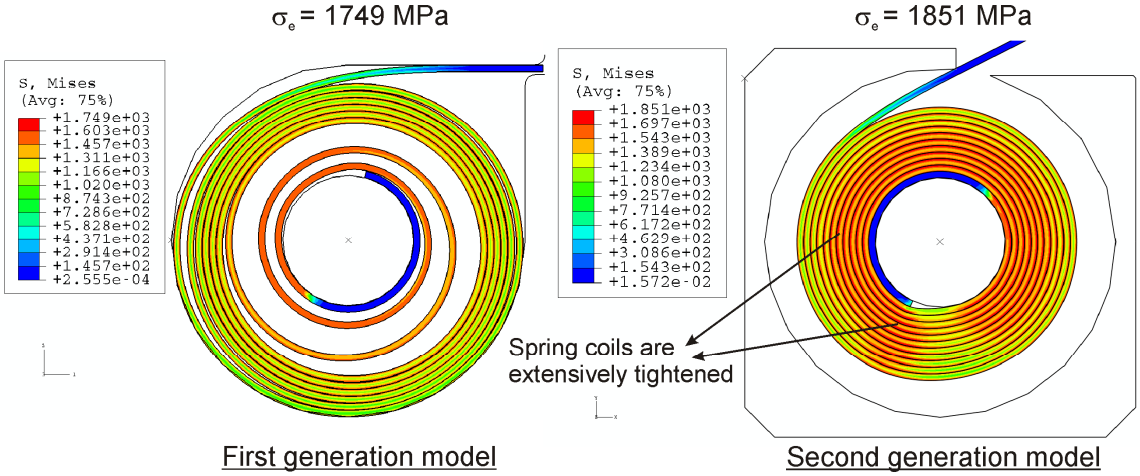

FIGURE 6.2-a: Comparison of the contour plots of the von-Mises stress in the spring coils at the end of the initial winding phase

The results assume hardening plasticity for the material behavior, with "perfect lubrication".

From the above figure, it can be observed that the spring coils are extensively tightened for the case of the second generation model, when compared to the older model. For the new model, all the spring coils are closely packed and positioned, on an average, closer to the arbor. On the other hand, for the first generation model, a majority of the outer coils are clustered together, and appear to have moved radially outwards from the arbor. The new model predicts approximately 6% higher von Mises stress in the spring coils when compared to the first generation model- at the end of the winding phase. The results also suggest that the spring coils undergo about 195% larger plastic deformation during the winding phase when compared to the predictions from the older model. This is evident from the equivalent plastic strain profiles of the two models shown in Figure 6.2-b.

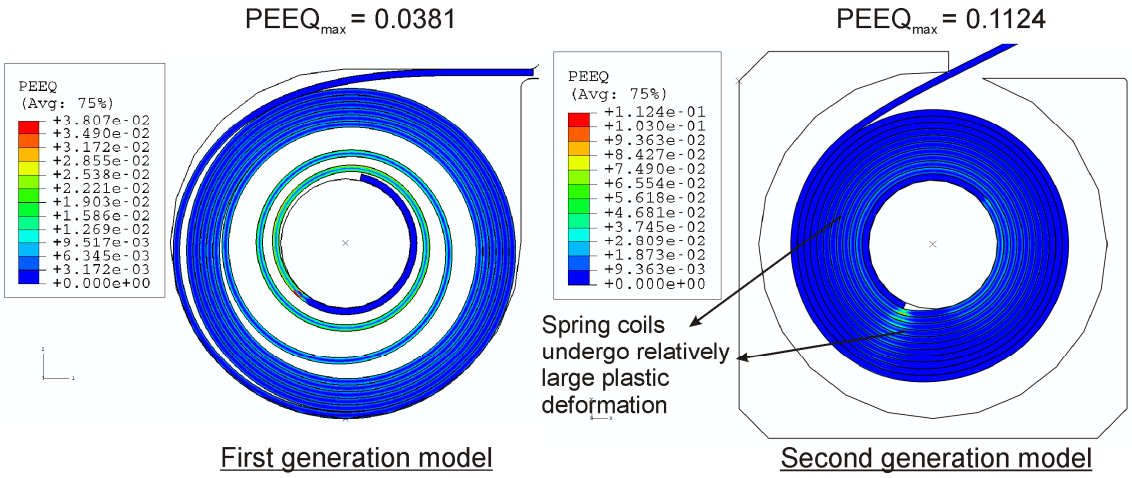

FIGURE 6.2-b: Comparison of the contour plots of the equivalent plastic strain in the spring coils at the end of the initial winding phase

It can be noted from the above figures that a certain length (of approximately 1.76 mm) of the end of the strip remains outside the cup in the new model. This portion of the strip is welded to the outer surface of the cup at the end of the winding phase.

As before, the second phase in the spring forming process involves releasing the arbor. As discussed in Chapter 2, this process involves releasing all the degrees of freedom in the arbor so that it freely rotates and translates until it completely releases the torque and force built-up during the winding phase. Figure 6.3 shows the actual clock spring profile [22] after it is formed (wound and released), along with the corresponding profile from the finite element model.

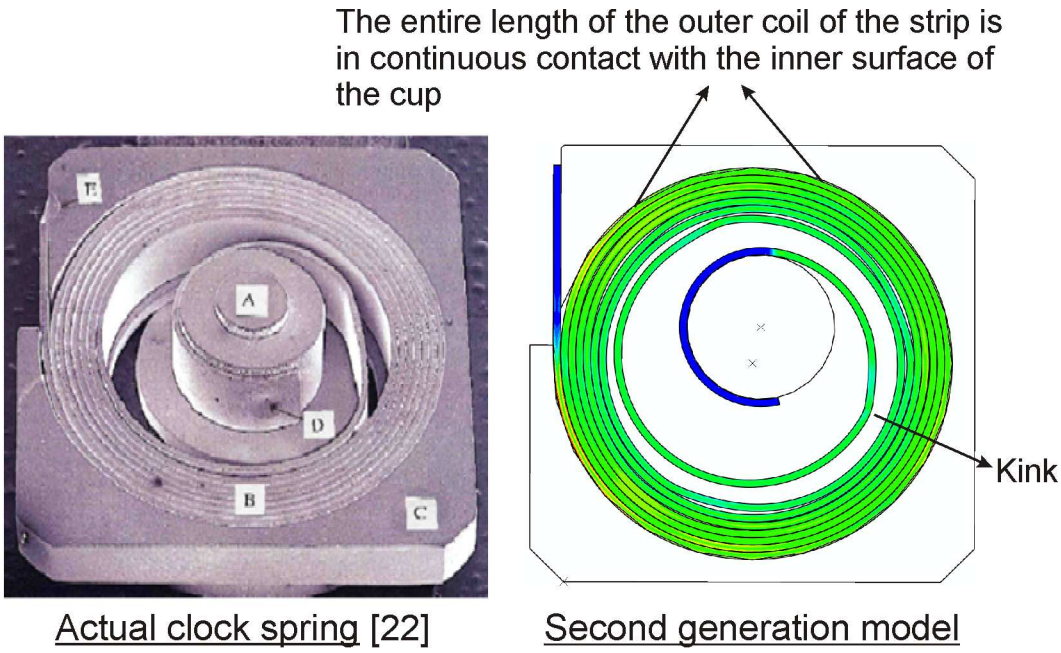

FIGURE 6.3: Comparison of the actual clock spring profile with the 2nd generation finite element model at the end of arbor release

Similar to the predictions of the earlier model, during this process, the stress levels in the coils drop by about 1 GPa. However, contrary to the predictions from the earlier model, the arbor undergoes a rotation of about 3 revolutions in the clockwise (reverse) direction

upon being released. This can be attributed to the extensively high stress-state of the spring coils at the end of the initial winding phase of the forming process. Hence, relatively more revolutions are required by the arbor to release the torque built-up in the spring, in comparison to the case of the first generation model. It can be observed that the second generation model is a relatively better representation of the released profile of the actual spring when compared to the original conceptual model, not only in terms of the position of the arbor at the end of the release, and the clustering of the majority of the coils against the inner surface of the cup, but also in terms of the continuous contact of the outer coil of the strip with the cup surface. The presence of 'kinks' - formed during the forming process - are also evident from the above figure.

6.3.2 Instantaneous moment versus rotation response

The next stage in the modeling effort is to capture the instantaneous moment versus rotation response of the spring during the actual application (i.e., wind-ups). The results obtained are compared to the results of the earlier model. It is important to note that no viscous stabilization was required to model the wind-up application. Figures 6.4-a. and -b. show a comparison of the von Mises stress profiles of the spring between the two generations of the finite element model at wind-ups of 1 revolution and 2.25 revolutions, respectively. The results assume hardening plasticity for material behavior, and "perfect lubrication" for frictional contact. From the results it can be observed that that the second generation model predicts relatively lower levels of stress in the spring coils when compared to the first generation model- for either case of pre-load. For the pre-load of 1 revolution, the second generation model predicts the average stress levels in the spring coils to be approximately 16% lower than the predictions of the earlier model.

For the pre-load of 2.25 revolutions, on the other hand, the difference is approximately 12%. In addition, the earlier model predicted about 2 - 3 spring coils which are closer to the arbor to undergo plastic deformation for the wind-up of 1 revolution, and a majority of the coils to undergo significantly large plastic deformations for the wind-up of 2.25 revolutions.

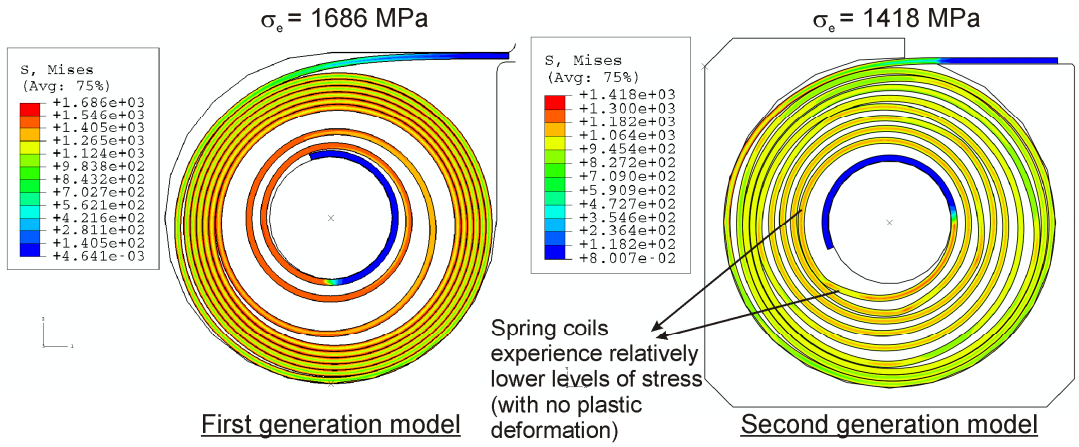

a. 1 revolution

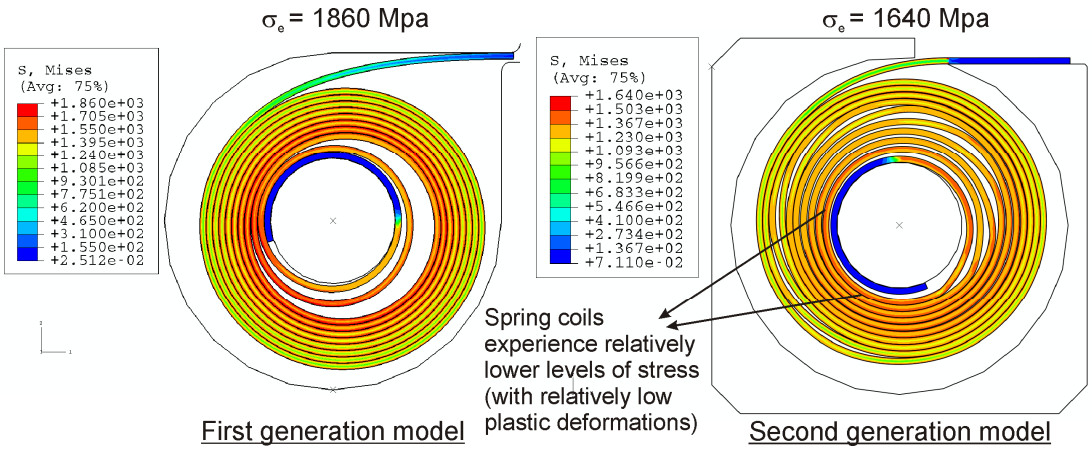

b. 2.25 revolutions

FIGURE 6.4: Comparison of the von Mises stress profiles between the two models

However, on the contrary, the new model predicts the spring coils to undergo only elastic deformation for the wind-up of 1 revolution (evident from the maximum value for the

von Mises stress in the spring coils for the second generation model shown in Figure 6.4-a, which is lower than the yield stress value of 1580 MPa), and relatively lower levels of plastic deformation for the wind-up of 2.25 revolutions- when compared to the first generation model. Even for the wind-up of 2.25 revolutions, only 2 - 3 coils which are closer to the arbor are observed to undergo plastic deformation. Another important observation from the new results is that the spring coils are uniformly spread in the cup for both the wind-ups, compared to the earlier predictions- which suggested that a majority of the coils are clustered together and located radially outwards from the arbor.

The results obtained for the moment-rotation response from the second generation model were observed to resemble the results of the earlier model in terms of the non-linearity of the response and the presence of the non-smooth behavior. However, in contrast to the results for the resisting torque from the earlier model, the results from the new model were found to be in much better agreement with the design specifications, considering the specified tolerance limits. Figures 6.5-a. and -b. show the moment-rotation response plots obtained from the second generation model for the pre-load of 1 revolution and 2.25 revolutions, respectively. The corresponding results obtained from the first generation model are also shown for a comparison. The non-smooth behavior can be attributed to the influence of the kinks in the spring coils. As before (see discussion in Chapter 2 for the first generation model), the results for the new model also indicate that the spring coils undergo an in-plane ‘mechanical-hinge’ type of motion about the kinks during the wind-ups which leads to the non-smooth moment-rotation response. Figure 6.6 shows the equivalent plastic strain (PEEQ) distribution in the torsional spring during the wind-ups, and illustrates the presence of these kinks in the coils. It can be observed from

Figure 6.5-b that when the arbor is wound beyond 1 revolution, the non-smooth moment-rotation response smoothens out in relative terms. This behavior is consistent with the predictions of the first generation model. From the profiles for the equivalent plastic strain, it can also be noted that the spring coils do not undergo any additional plastic straining during the wind-up in addition to the permanent residual strain that they acquired during the spring forming process**.** This is in agreement with the predictions of the first generation model.

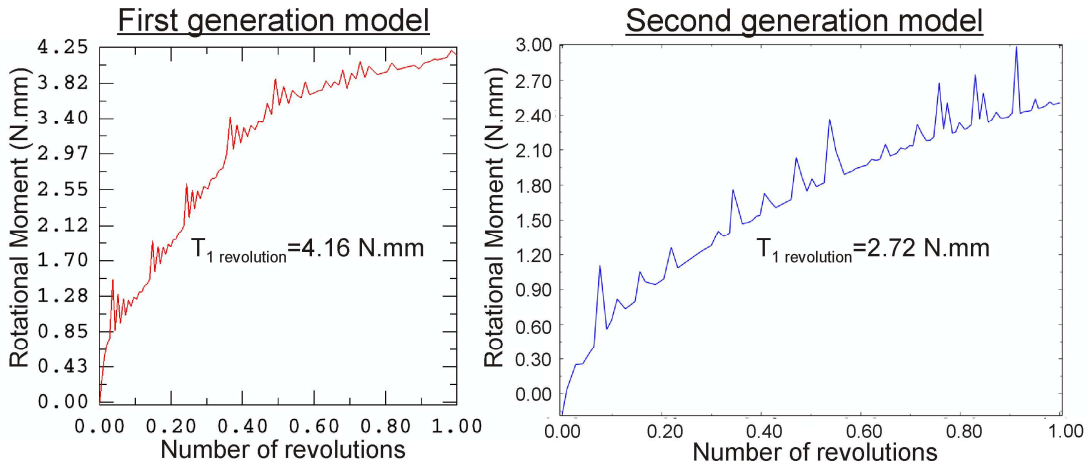

a. 1 revolution

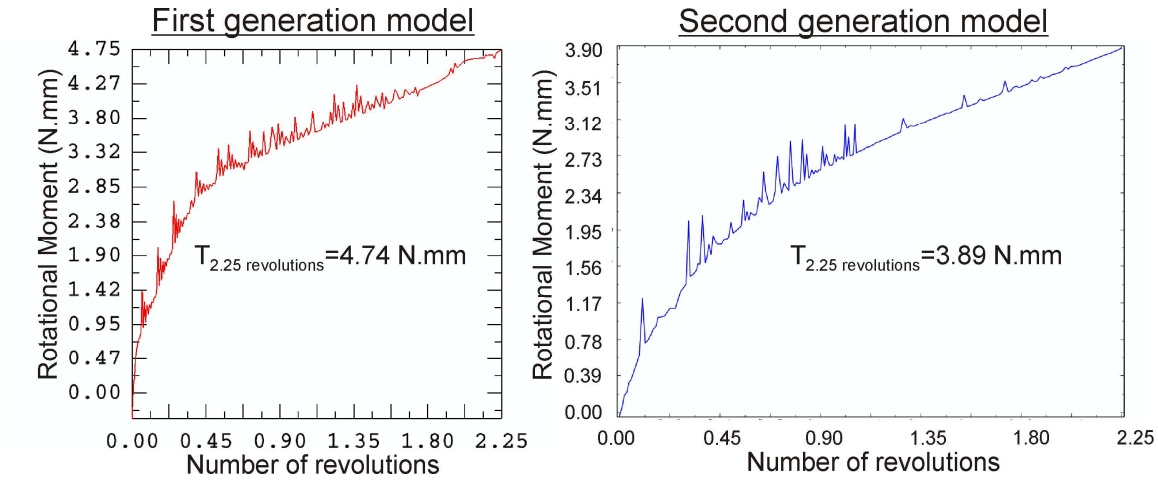

b. 2.25 revolutions

FIGURE 6.5: Comparison of the moment-rotation plots between the two models

Following the modeling strategy used for the first generation model, during the wind-up application the arbor is subjected to a sequential wind and un-wind cycle before it is actually wound-up to capture the resisting torque. As mentioned in the description for the earlier model, the purpose of this additional operation is to remove any major torque-loss that would creep-in due to the cyclic moment versus rotation response of the torsional spring. The actual application follows the same approach. For a pre-load of 1 revolution, the torque loss was predicted to be approximately 0.8 mN.mm, whereas, for 2.25 revolutions the value was found to be approximately 20 mN.mm.

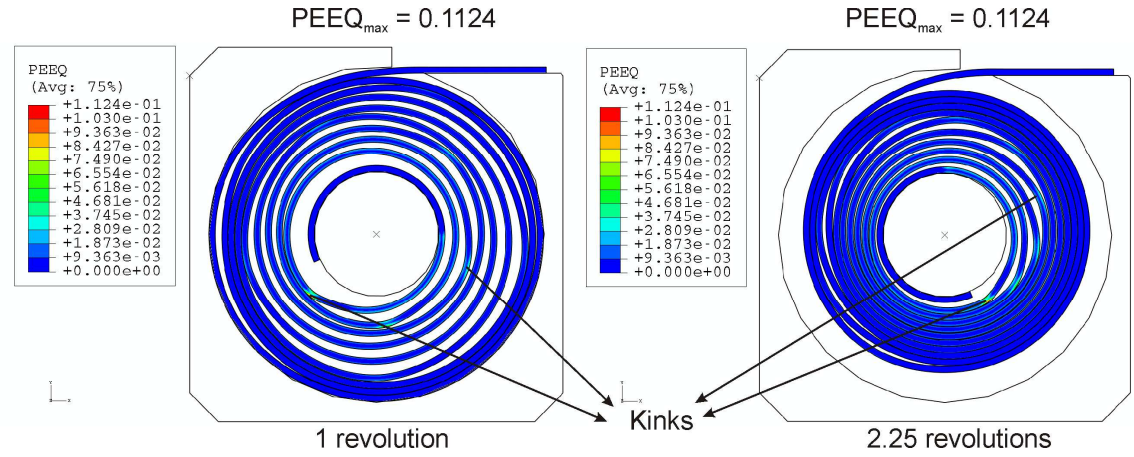

FIGURE 6.6: PEEQ distribution in the spring coils at the end of the wind-ups

Table 6.1 shows a comparison of resisting torque for the torsional spring subjected to pre-loads of 1 revolution and 2.25 revolutions. The design specifications are also provided. The numerical results correspond to the case of hardening plasticity and "perfect lubrication".

As evident from the table, the results obtained for the resisting torque are in good agreement with the design specifications for either cases of wind-up. The new results for the resisting torque are about 35% and 18% lower than the corresponding values obtained

from the first generation model- for a wind-up of 1 revolution and 2.25 revolutions, respectively.

TABLE 6.1: Comparison of resisting torque obtained from the second generation finite element model to the design specifications

Pre-loads	Resisting torque (N.mm)	Design specifications (N.mm)
1 revolution	2.716	2.9 ± 0.5
2.25 revolutions	3.887	4.35 ± 0.55

Overall the results obtained from the second generation model suggest that the model is capable of capturing the moment-rotation response of the torsional spring with a significantly better accuracy compared to the earlier model.

6.3.3 Long-term stress-relaxation response

Once the instantaneous moment-response of the spring was captured, the next stage in the modeling effort was to better understand the long-term stress relaxation response, and the associated torque-drop response, of the spring. It is important to recall that the primary reason behind developing a second generation model was to better understand the discrepancies in the long-term torque-drop response obtained from the first generation model to that of the experimental results.

The material-creep model that was used to drive the long-term relaxation response of the first generation finite element model is used for the new generation model as well. In particular, the creep parameters used are $A = 2E\text{-}20\ MPa^{-2.8}S^{-1}$ and $n = 2.8$. Table 6.2 shows the results for the torque drop obtained from the second-generation finite element model for a 'freshly-formed' (zero shelf-life; i.e. the spring is used right after it is formed) spring over varying time periods of relaxation and levels of wind-up. The results

indicate an average rate of torque-drop of approximately 0.16 mN.mm/day for a pre-load of 1 revolution, and approximately 0.44 mN.mm/day for the pre-load of 2.25 revolutions. It can be observed that the predictions from the second generation model for the torque-drop over a period of 1 year of relaxation is approximately 71% lower for the pre-load of 1 revolution and about 42% lower for the pre-load of 2.25 revolutions - in comparison to the corresponding predictions from the earlier model.

TABLE 6.2: Torque-drop results from the second generation FE model for the different levels of pre-load, and time periods of relaxation

Wind-up positions	Time (days)	Torque-drop results ΔT_{creep} (mN.mm)
1 revolution	1	0.17
	12	2.03
	365 (1 year)	59.6
2.25 revolutions	1	0.46
	12	5.58
	365 (1 year)	160

The magnitude of relaxation of the von Mises stress in the spring coils over a period of 1 year is about 4% for the pre-load of 1 revolution, and about 5% for 2.25 revolutions (i.e., approximately 1% lower for each of the wind-ups, when compared to the magnitude of stress relaxation from the earlier model).

6.3.3.1 Long-term torque-drop results for another set of material-creep properties

There were uncertainties in the material-creep data obtained from the uniaxial tension tests [21]. The latest results obtained by Lawton *et al.* [21] suggest that the

uncertainty in the determination of creep parameters should lie between the following available data-sets for material-creep, namely:-

(i) $A = 2E\text{-}20\ MPa^{-2.8}S^{-1}$ and $n = 2.8$

(ii) $A = 7E\text{-}20\ MPa^{-2.8}S^{-1}$ and $n = 2.8$

Hence, finite element simulations were carried out for the case-(ii) data-set as well, corresponding to the wind-up of 1 revolution. The results for the long-term response for the cases - (i) and - (ii) are tabulated in Table 6.3. It is to be noted that the value for the creep parameter- n is the same for both the cases.

TABLE 6.3: Torque-drop results from the second generation FE model for the different sets of material-creep parameters (for a pre-load of 1 revolution)

Wind-up position	Time (days)	Torque-drop results ΔT_{creep} (mN.mm) Case-(i)	Torque-drop results ΔT_{creep} (mN.mm) Case-(ii)
1 revolution	1	0.17	0.59
	12	2.03	7.07
	365 (1 year)	59.6	193

The torque-drop result for case-(ii) over a period of 1 year of relaxation is observed to be approximately 200% higher than the prediction for case-(i). The average rate of torque-drop for case-(ii) is predicted to be approximately 0.53 mN.mm/day, compared to the rate of 0.16 mN.mm/day predicted for case-(i). It can be assumed that the actual rate of torque-drop for the torsional spring should lie in a range between 0.16 mN.mm/day and 0.53 mN.mm/day for a pre-load of 1 revolution.

6.3.4 Influence of aging on the response of the spring

The influence of aging on the instantaneous torque-rotation as well as the long-term torque-relaxation responses is investigated using the new generation model. The

material-creep model which is used to drive the aging response of the spring is the same as the one which is used to drive the long-term relaxation response. Table 6.4 shows the results for the resisting torque obtained from the new model for a spring aged for 10 years. Here again, the arbor is first subjected to a sequential wind and unwind cycle before it is further wound-up to capture the resisting torque. The results indicate that 10 years of aging reduces the resisting torque by approximately 8% for the wind-up of 1 revolution, and by about 7% for the wind-up of 2.25 revolutions.

TABLE 6.4: Comparison of resisting torque obtained for a 10 years aged spring to the design specifications

Pre-loads	Resisting torque (N.mm)	Design specifications (N.mm)
1 revolution	2.488	2.9 ± 0.5
2.25 revolutions	3.626	4.35 ± 0.55

From the above table it can be observed that the torque values obtained for a spring which is aged for 10 years are in a relatively closer comparison to the design specifications (compared to the results for a freshly-formed spring which are shown in Table 6.1). Figure 6.7 shows a comparison of the equivalent creep strain profiles of the torsional spring for either generations of the model. The results indicate that the maximum value for the equivalent creep strain predicted by the second generation model is 10% higher than the corresponding prediction from the first generation model. The maximum von Mises stress relaxation in the spring coils is observed to be about 33% as a result of the 10 years of aging. This prediction is consistent with the corresponding result from the first generation model. Figure 6.8 shows a comparison of the von Mises stress

distribution in the spring before and after the process of aging (10 years)- based on the predictions from the new model.

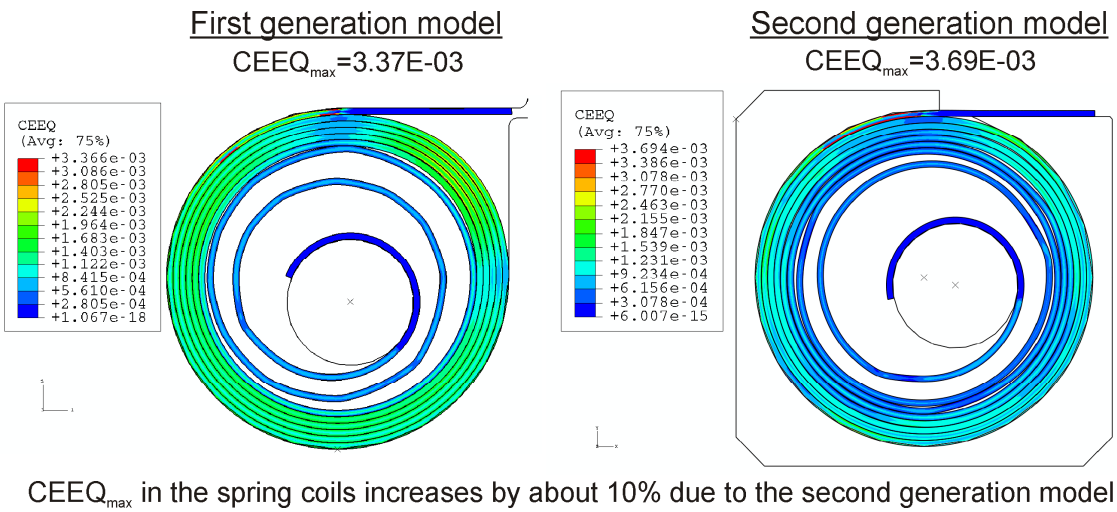

FIGURE 6.7: Comparison of the equivalent creep strain distributions in the two generations of the finite element model

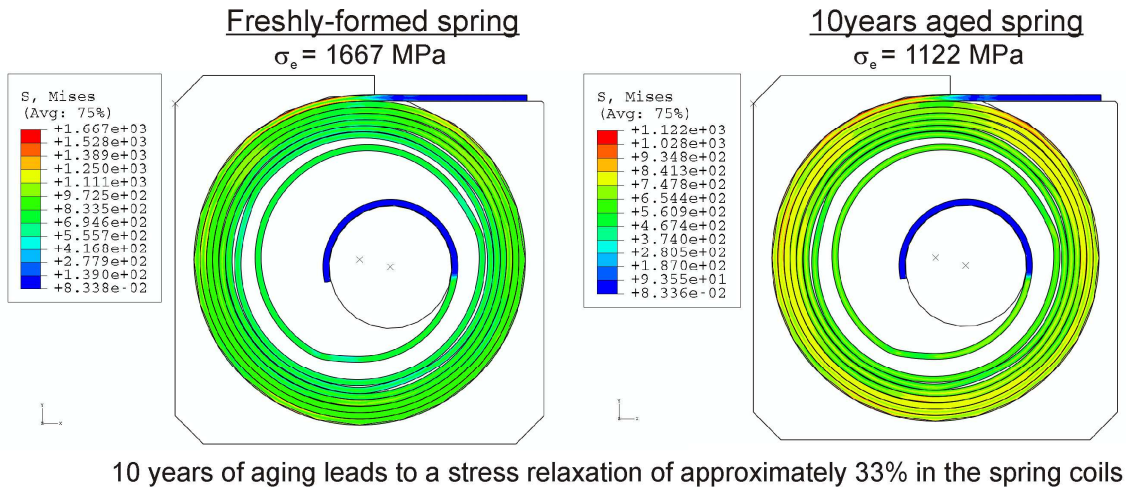

FIGURE 6.8: Comparison of the von Mises stress distributions in the spring before and after the process of 10 years of aging

Investigations were carried out to understand the influence of aging on the long-term torque-drop response of the spring system. The simulations for capturing the long-

term response of the aged springs uses the material-creep parameters of A = 2E-20 $MPa^{-2.8}S^{-1}$ and n = 2.8. The results obtained for the torque-drop are shown in Table 6.5.

TABLE 6.5: Torque-drop results from the second generation FE model for a spring aged for 10 years

Wind-up positions	Time (days)	Torque-drop results ΔT_{creep} (mN.mm)
1 revolution	1	0.12
	12	1.53
	365 (1 year)	45.4
2.25 revolutions	1	0.38
	12	4.56
	365 (1 year)	131

The results indicate a reduction in the torque drop by approximately 24%- for the wind-up of 1 revolution, and by approximately 18%- for the wind-up of 2.25 revolutions, as a result of the 10 years of aging. The model predicts an average rate of torque-drop of approximately 0.12 mN.mm/day for a pre-load of 1 revolution, and approximately 0.36 mN.mm/day for a pre-load of 2.25 revolutions- for a spring aged for 10 years.

Table 6.6 shows a comparison of the torque-drop results obtained from the finite element model over a period of 1 year of relaxation for a freshly-formed spring to that of a spring aged for 10 years. These results are also compared with the corresponding experimental data. From the table, it can be observed that the finite element results for the torque-drop are in a relatively better agreement with the experimental results, in comparison to the results of the first generation model.

TABLE 6.6: Comparison of the torque-drop results between the finite element model and the experimental data over a period of 1year of relaxation

Wind-up positions	Finite Element results for torque-drop (mN.mm) [for 1 year]		Experimental results for the torque-drop (mN.mm) [for 1 year]
	Freshly-formed springs	10 years aged springs	
1 revolution	59.6	45.4	≈ 20
2.25 revolutions	160	131	≈ 20

It is interesting to note that there still remains a somewhat smaller discrepancy in the comparison of the FE results with the experimental data for either levels of wind-up. However, the differences are brought down from the large multiples (numerical to experimental) of 12 - 18 times to relatively smaller multiples of 3 - 8 times for a freshly-formed spring, and from 6 - 16 times to a relatively lower range of 2 - 7 times for a spring aged for 10 years. The reasons behind the discrepancies between the numerical predictions and the experimental values may still be the uncertainties (although relatively smaller) in the determination of the material-creep parameters from the uniaxial tests, and/or the differences in the methodologies of measurements used in the experimental and numerical procedures (i.e., the experiments measure the rotational creep and converts the data to torque-drop, whereas the finite element model directly predicts the torque-drop).

The reasons behind the similarity in the torque-drop values from the experiments for either levels of wind-up were investigated earlier. The results of the investigation pointed to the presence of ‘geometric locking’ of the spring coils at higher levels of wind-up which prevented any further rotational movement of the arbor. In order to numerically investigate this aspect, one can modify the current finite element model so that it can be

used to capture the rotational creep of the arbor. This in turn would help in a better comparison with the experimental results.

6.3.5 Rotational creep of the spring

As mentioned in the previous chapters, the finite element model is analogous to the set up experienced by the spring during the actual application. It captures the long-term stress relaxation in the spring coils and the associated torque-drop at constant rotation. However, the experiments measure the long-term rotational creep of the arbor at a constant applied torque, and then convert it to an estimate for lost torque using a rigidity modulus. To determine the long-term response of the spring system more closely, it is important to replicate the experimental procedure. For this purpose, a new set of finite element simulations were carried out to compute the rotational creep of the spring system under a constant load. The constant torque that is applied for this purpose is approximately equal to the resisting torque obtained from the previous models at 1 revolution or 2.25 revolutions of the arbor. Table 6.7 shows the results obtained for the rotational creep of the freshly-formed spring over varying periods of time, at a pre-load of 1 revolution.

TABLE 6.7: Comparison of the rotational-creep values between the FE model and the experiments, at a pre-load of 1 revolution

Time (days)	Rotational creep at $T_{1\ revolution}$ (mrads)	Experimental results
1	34	16
12	44	30
365 (1 year)	368	132

From the table it can be observed that although the rotational creep predicted by the finite element simulations is higher than the experimental results, they are relatively closer to the experimental data in comparison with the results from the first generation model. For example, the rotational creep predicted by the second generation model at a pre-load of 1 revolution over a period of 1 year is approximately 3 times the corresponding experimental results, in comparison to 11 times predicted by the first generation model. Moreover, for a pre-load of 1 revolution, the new model predicts an average rotational-creep rate of about 1 mrad/day, in comparison to 3.88 mrads/day predicted by the earlier model (for a freshly-formed spring).

Investigation was also carried out to understand the influence of rotational creep at higher torque-loads. It is important to note that, in contrast to the case of the first generation model wherein the arbor was found to rotate only close to 2 revolutions on subjecting it to the constant torque- obtained from the wind-up application for 2.25 revolutions, for the second generation model the arbor was found to exactly rotate to 2.25 revolutions. The same trend was observed for the torque-load of 1 revolution as well. Table 6.8 shows a comparison of the rotational creep obtained from the second generation model at the pre-load of 1 revolution to the result at 2.25 revolutions over a period of 1 year of creep.

TABLE 6.8: Comparison of rotational-creep obtained at different pre-loads

Rotational creep over a period of one year (mrads)		
Torque loads à	$= T_{1\ \text{revolution}}$	$= T_{2.25\ \text{revolutions}}$
FE model- Freshly-formed spring	368	1228
Experiments	132	132

The results obtained from the new model at the higher torque-load were significantly different from the predictions of the older model as well as the findings from the experiments. As per the predictions of the new model, the rotational creep at the torque-load of 2.25 revolutions was found to be approximately 3 times higher than the creep at 1 revolution. The experiments and the first generation model had contrasting predictions towards this behavior. Figure 6.9 shows a comparison of the von Mises stress distributions in the torsional spring at the torque-load of 2.25 revolutions between the two models.

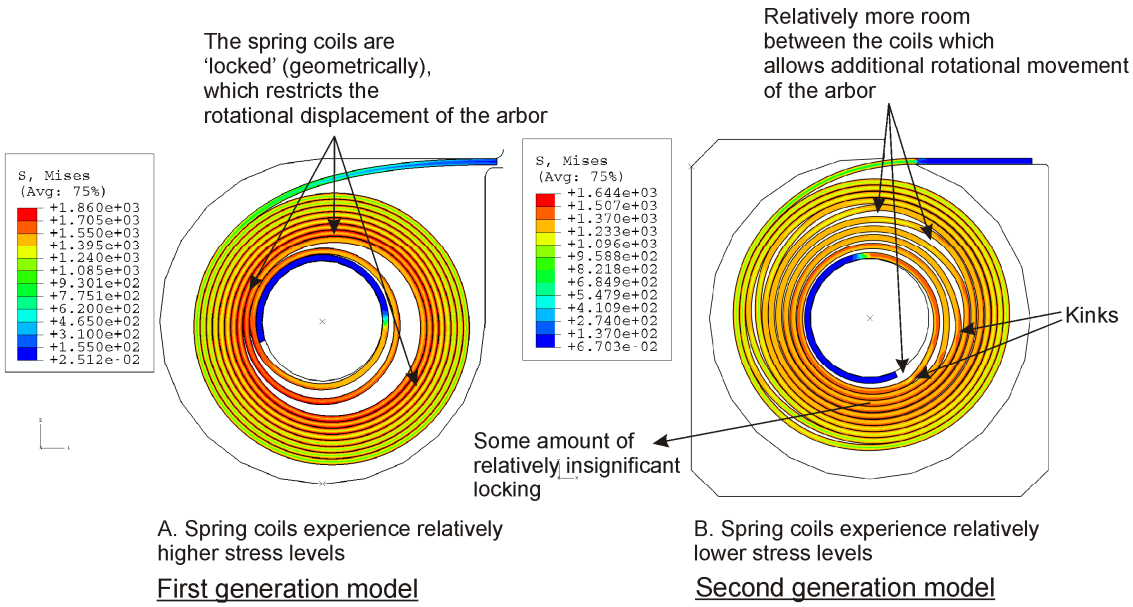

FIGURE 6.9: Comparison of the von Mises stress distributions at a torque-load of 2.25 revolutions for the two models

Further investigations were carried out to understand this phenomenon. The results suggest this phenomenon to be due to the absence of any significant 'geometric locking' between the spring coils at the higher torque loads. This may be attributed to the relatively low stress levels in the coils compared to the relatively higher stress levels

predicted by the first generation model. It was observed from the new model that at high torque loads of 2.25 revolutions, the spring coils were not excessively tightened and there was enough room between the coils which increases the possibility of additional rotational movement of the arbor during the process of creep. It can be observed from the above figure that the kinks may have a significant contribution towards creating the additional space between the coils.

The rate of average rotational creep predicted by the new model at a torque-load corresponding to 2.25 revolutions is 3.36 mrads/day compared to 1.97 mrads/day predicted by the earlier model.

6.4 Conclusions

A second generation finite element model is developed in order to address the discrepancies found with the original conceptual model in the comparison of the finite element results to the results of the experiments for the long-term response of the torsional spring. The attempt was to develop a model which would be an almost exact replica of the actual spring system incorporating even the minute details of the geometry. The results obtained for the initial winding stage of the spring forming process suggest approximately 195% more plastic deformations when compared to the predictions of the original model. The second generation model was observed to be a relatively better representation of the actual released profile of the spring compared to the original model. The results for the resisting torque obtained from the new model are in better comparison with the design specifications. The moment-rotation response obtained from the new model is observed to be consistent with the predictions of the earlier model in terms of the non-linearity of the response and the presence of the non-smooth behavior. However,

the predictions on the stress state of the spring coils at the wind-ups and the alignment of the coils are different compared to the predictions of the original model. The new model predicts the average stress levels in the spring coils to be approximately 12 – 16% lower than the stress levels predicted by the earlier model. The presence of 'kinks' or the regions of large plastic deformation are observed to have a significant role in the instantaneous moment-rotation response of the spring. It was found that the new model is capable of capturing the long-term relaxation response of the spring with relatively better accuracy when compared to the earlier model. The predictions for the torque-drop are observed to be about 70% lower than the earlier predictions for the pre-load of 1 revolution, and about 42% lower for the pre-load of 2.25 revolutions. The average rate of torque-drop predicted by the second generation model is in the range of 0.16 mN.mm/day – 0.44mN.mm/day, with the exact value depending on the magnitude of the pre-load. The magnitude of stress relaxation over a period of 1 year is predicted to be approximately 5% for either case of the wind-up. Based on the uncertainties in the determination of the creep parameters from the uniaxial tension tests, the average rate of torque drop is observed to vary between 0.16 mN.mm/day and 0.53 mN.mm/day. Aging was observed to have a relatively lower influence on the overall stress-state of the spring coils when compared to the predictions of the original model. The results indicate a reduction in the torque drop of approximately 24% for a pre-load of 1 revolution, and approximately 18% for 2.25 revolutions, as a result of 10 years of aging. The margin for the discrepancies in the comparison of the finite element results with the results of the experiments is found to be lowered extensively to about 2 – 8 times when compared to the earlier predictions. The average rate of rotational creep predicted by the new model varies between 1.00

mrad/day and 3.36 mrads/day depending on the magnitude of pre-load. The margin of discrepancies in the comparison of the numerical results to the experimental results for the rotational creep over a period of 1 year is lowered from 11 times to approximately 3 times. In contrast to the predictions of the earlier model, the spring coils were observed to have a relatively lower degree of 'geometric-locking' when subjected to a torque-load corresponding to 2.25 revolutions. As a result of this, the rotational creep at 2.25 revolutions was found to be much higher than the rotational creep at 1 revolution. This is in complete contrast to the earlier predictions.

To conclude, the second generation finite element model is capable of capturing the instantaneous moment-rotation response and the associated resisting torque of the spring with greater accuracy. In particular, the torque-drop predicted by the new model is in relatively better comparison to the experimental results when compared to the predictions of the earlier model. The margin of uncertainty has been reduced significantly when compared to the earlier predictions, although minor discrepancies still exists. The reasons for these minor discrepancies need to be investigated further.

BIBLIOGRAPHY

[1] Abaqus/Standard Analysis user's manual, SIMULIA Inc. 2007. Version 6.7: Chapters 7.1.1.

[2] Assefpour-Dezfuly M and Bonfield W. 1984. Strengthening mechanisms in elgiloy, Journal of Material Science. vol.19: pp. 2815-36.

[3] Assefpour-Dezfuly M and Bonfield W. 1985. Microplasticity in elgiloy, Journal of Material Science. vol.20: pp. 3018-26.

[4] Barnes S, Miller S, Rodgers S, and Bitsie F. March 2000. Torsional ratcheting actuating system, Inter. Conference paper on modeling and simulation of microsystems, San Diego, CA.

[5] Belytschko T, Liu WK, and Moran B. 2000. Nonlinear finite elements for continua and structures.

[6] Bose K. 2008. Graduate class notes on finite element analysis for Simpson's rule and Gauss-Lobatto methods of numerical integration.

[7] Carlson H. 1986. Simplified design of motor springs, Journal on Springs, v25: Issue.1, pp. 45-49.

[8] Chen N, Chen X, Wu YN, Yang CG, and Xu L. Dec 2005. Spiral profile design and parameter analysis of flexure spring, Journal on Cryogenics.

[9] Courtney TH. 2000. Mechanical behavior of materials (second edition).

[10] Dalder E. 2003, 2008. Tensile properties of elgiloy strip, U.C. Berkeley: Faxed data from Lawrence Livermore National Laboratory.

[11] Dykhuizen RC and Robino CV. 2004. Load relaxation of helical extension springs, Journal of Material Engineering Performance, vol. 13: pp. 151-7.

[12] Findley WN, Lai JS, and Onaran K. 1989. Creep and relaxation of nonlinear viscoelastic materials: with an introduction to linear viscoelasticity.

[13] Fish J and Belytschko T. 2007. A first course in finite elements.

[14] Henmi Z, Okada M, and Nagai T. Oct 1966. On the mechanism of age hardening in Elgiloy, Presented at the JIM annual meeting, Amagasaki.

[15] Hill R and Hill Rodney. 1950. The mathematical theory of plasticity.

[16] Hughes, TJR. 1987. The finite element method: linear static and dynamic finite element analysis.

[17] Johnson KL. 1985. Contact mechanics.

[18] Khan AS and Huang S. 1995. Continuum theory of plasticity.

[19] Kreyszig E. 1999. Advanced engineering mathematics.

[20] Laursen TA. 2002. Computational contact and impact mechanics: Fundamentals of modeling interfacial phenomena in non linear finite element analysis, Springer-Verlag, Berlin.

[21] Lawton KM, Lynn KC, and Ren D. 2007. The measurement of creep of elgiloy springs with a balanced interferometer, Journal of Precision Engineering, vol. 31: pp. 325-329.

[22] Lee Tae-Kyu and Morris Jr, JW. 2005. Image sent from Department of Materials Science and Engineering, University of California at Berkeley.

[23] Lubliner J. 1990. Plasticity theory.

[24] Nagtegaal JC, Parks DM, and Rice JR. 1974. On numerically accurate finite element solutions in the fully plastic range, Journal of Computer methods in Applied Mechanics and Engineering, vol. 4: pp. 153-77.

[25] Soutas-Little RW. 1999. Elasticity.